Synthesis and structural studies of NiS and PdS nanoparticles/nanocomposites from dithiocarbamates single source precursors

Nqombolo Azile

Department of Chemistry

Faculty of Science and Agriculture

University of Fort Hare

Together in Excellence

January 2016

Synthesis and structural studies of NiS and PdS nanoparticles/nanocomposites from dithiocarbamates single source precursors

By

AZILE NQOMBOLO (201004703)

B. Sc., B. Sc. (Honours) Chemistry (UFH)

Being a dissertation submitted to the Faculty of Science and Agriculture in fulfilment of the requirements for the award of the degree of

Master of Science in chemistry

of the

University of Fort Hare,

Supervisor: Professor P. A. Ajibade

January 2016

DECLARATION BY CANDIDATE ON PLAGIARISM

I Azile Nqombolo, declare that:

1. The research in this dissertation, except where otherwise indicated, is my original work.
2. This dissertation has not been submitted for any degree or examination at other university.
3. This dissertation does not contain any other person data unless specifically acknowledged as being sourced from them.
4. This dissertation does not contain any other persons' writing, unless specifically acknowledged as being sourced from other researchers. Where other written sources have been quoted, then:
    a. Their words have been re-written but the general information attributed to them has been properly referenced.
    b. In all instances where the exact words of other authors have been used, then their writing has been placed in italics and inside quotation marks, and referenced.
5. This dissertation does not contain text or graphics from the internet copied and pasted, unless specifically acknowledged, and the source being detailed in the dissertation and in the references section.

January 2016 _____ _____

Date Azile Nqombolo

CERTIFICATION

This is to certify that this research is a record of original work carried out by Azile Nqombolo under my supervision in the Inorganic Materials Research laboratory of the Department of Chemistry, University of Fort Hare in fulfilments of the requirements for the award of Master of Science degree in Chemistry.

_____ _____

Date

Supervisor

P. A. Ajibade

Professor of Inorganic Materials Chemistry

B. Sc (Hons), MSc (Ibadan);

PhD (UniZul); MRSC (London)

DEDICATION

THIS WORK IS DEDICATED TO MY LATE SISTER (LUNOTHANDO), MY FAMILY AND NONTLE FOR THEIR LOVE AND SUPPORT.

ACKNOWLEDGEMENTS

I thank God Almighty for the gift of life and strength He gave me in the course of this study. My appreciation to my supervisor, Prof. P. A. Ajibade for his constant instructions, support, motivation, encouragement throughout my research and for helping me to grow in the field of science, without him I would not be where I am today. His fatherly support and advices kept me going in the course of my research. I would like to express my appreciation to Mr T. Mcako and Mr K. Tshapu for their assistance with the instrumental analysis in the department.

I thank the Inorganic Materials Research Group for their love and support throughout the year. I also thank National Research Foundation (NRF) and Sasol Inzalo Foundation for their award of innovation MSc scholarship. I am grateful to my family and friends for their love, encouragement and support throughout the course of this work.

TABLE OF CONTENTS

LIST OF FIGURES

LIST OF TABLES

LIST OF SCHEMES

ABREVIATIONS AND SYMBOLS

CS_2	Carbon disulfide
DTC	Dithiocarbamate
EDS	Energy Dispersive Spectroscopy
FTIR	Fourier Transform Infrared
g	Gram
KOH	Potassium hydroxide
L	Litre
MLCT	Metal to ligand charge transfer
nm	Nanometer
PL	Photoluminescence
XRD	X-ray diffraction
SEM	Scanning electron microscope
TEM	Transmission electron microscopy
TOP	Trioctyl phosphine
HDA	Hexadecylamine
TOPO	Trioctyl phosphine oxide
UV-Vis	Ultra-violet visible

Eg	Band gap
mg	Milligrams
DMSO	Dimethylsulfoxide
NMR	Nuclear magnetic resonance spectroscopy

RESEARCH OUTPUTS

1. Peter A. Ajibade and Azile Nqombolo. Synthesis and characterization of NiS and PdS nanocrystals from imidazolyl dithiocarbamate single source precursors. *Journal of Materials Science in Semiconductor Processing*, (**Manuscript No.: MSSP-D-15-02323).**

2. Azile Nqombolo and Peter A. Ajibade. Synthesis and structural studies of nanocrystalline nickel sulfides and potato starch nanocomposites. *Journal of Physcis and Chemistry of Solid* (To be submitted).

3. Peter A. Ajibade and Azile Nqombolo. Optical and structural studies of PdS quantum dots. *Physica E: Low Dimensional Systems and Nanostructures* (To be Submitted)

ABSTRACT

The main aim of this research is to synthesize Ni(II) and Pd(II) dithiocarbamate complexes and use them as single source precursors for the synthesis of NiS and PdS nanoparticles and metal sulphides potato starch nanocomposites. Four dithiocarbamate ligands were synthesized and characterized using elemental analysis and spectroscopic techniques. The ligands were used to prepared homoleptic Ni(II) and Pd(II) complexes of the dithiocarbamate ligands. The metal complexes were characterized with elemental analysis, UV-Vis, FTIR and ^{1}H-NMR spectroscopic techniques.

Conductivity measurements indicate that all the complexes are non-electrolytes in solution and results from the electronic spectra studies confirmed the proposed 4-coordinate square planar geometry around the metal ions. The nickel complexes showed d-d transitions around 477 nm while in the palladium complexes, no d-d transitions were observed but the compounds showed strong metal to ligand charge transfer transitions. From the FTIR spectra studies, it can be confirmed that the complexes were successfully synthesised because all peaks of interest were observed at expected regions from the literature. The νC-N was observed around 1469-1495 cm^{-1}, νC=S around 1101-1188 cm^{-1} and νC-S around 738-1060 cm^{-1} for both Ni(II) and Pd(II) complexes. νNi-S was observed around 375-543 cm^{-1} and νPd-S around 529-545 cm^{-1}. The FTIR also confirmed that the dithiocarbamate ligands act as bidentate chelating ligands through the sulfur atoms.

The complexes were used as single source precursors and thermolysed in hexadecylamine (HDA) at 220 °C to prepare four HDA-capped nickel sulfide nanoparticles and four palladium sulfide nanoparticles. The as-prepared nanoparticles were studied with optical

absorption spectra, photoluminescence, powder X-ray diffraction (PXRD), transmission electron microscopy (TEM), scanning electron microscopy (SEM) and energy dispersive X-ray spectroscopy (EDS). The optical studies results showed that NiS have large band gaps that are greater than that of the bulk, therefore they are found to be blue shifted relative to the bulk, which shows that they have small particle size and thus confirming their quantum confinement effect. PL spectra reveal that the emission peaks are red shifted compared to the absorption band edges of the nanoparticles.

The XRD patterns confirmed the formation of cubic and rhombohedral phase for NiS nanoparticles and cubic phase for PdS nanoparticles. SEM images of both NiS and PdS show uniform surface morphology at low and high magnification with different shapes. EDS analyses confirmed the presence of Ni, S, and Pd in each of the spectrum indicating that the nanoparticles were successfully synthesized. TEM images showed that the synthesised nanoparticles have uniform and narrow size distribution with no agglomeration. The sizes of the NiS nanoparticles were found to be in the range of 12-38 nm for **NiS1**, 8-11 nm for **NiS2**, 9-16 nm for **NiS3** and 4-9 nm for **NiS4**. The TEM images for the as-prepared PdS nanoparticles showed that the average crystallite sizes are 6.94-9.62 nm for **PdS1**, 8-11 nm for **PdS2**, 9-16 nm for **PdS3** and 4-9 nm for **PdS4** respectively. The nanoparticles were used to prepare potato starch nanocomposites and SEM images indicate that the surface morphology of starch polymer nanocomposites compose of potato starch and few particles in between the pores of the matrix, this is due to the small ratio of nanoparticles used.

CHAPTER ONE

1.0. INTRODUCTION & LITERATURE REVIEW

1.1. Nanomaterial

Nanotechnology has attracted many research groups throughout the world due to its potential application in various industries. For the past decades, nanomaterials have gained more attention and are widely studied because of their different properties such as size and shape, physical, chemical and magnetic properties for their application in different fields [1,2]. Transition metal based material such as Ni, Co and Fe have attracted much attention for the synthesis of nanomaterials, since they have magnetic properties useful for different applications [1]. Quantum dots are particles or nanocrystals of semiconducting material within a range of 2-10 nm. They show distinctive electronic properties. Electrons in quantum dots are confined in a small space since they have small size. They can be synthesized from different types of semiconductor materials via colloidal synthesis or electrochemistry [2].

Poly(methyl methacrylate) (PMMA) is a vital thermoplastic which has the following properties: It is chemical resistant, protective against ultraviolet radiation and it has high strength [3]. A route of producing full PMMA/clay nanocomposites have been reported by Zhao *et al*. [4] this was done via in situ polymerization in s_cCO_2, the results showed that fluorinated modified clay can help in producing PMMA in large yields in s_cCO_2 by serving as a stabilizer [4]. Di(ethylene glycol) (DEG) have been used as a medium and p-TSA, P-toluene sulfonic acid have been used as end capping agents in the synthesis of ZnO nanorods at high concentration of the precursor using polyol method as reported by Anzlovar *et al*. [5]. The prepared polymer ZnO nanocomposites showed that the increase of storage modulus of

nanocomposites is as the result of ZnO nanorods at low concentration, the glass transition temperature (T_g) shifted towards higher temperature [5].

Researchers have reported their composites which they prepared by different strategies (i) *in situ* method, (ii) solution bleeding, and (iii) melt bleeding. From these three methods, the *in situ* method have an advantage of ease of handling, is a quick process and offers better performance for final procedure [6]. Nanoparticles are materials that have at least one dimension ranging from 1-100 nm. Nanocrystals are usually called single-down ultrafine particles or nanometer-sized single crystals. At present research on nanoparticles is an interesting scientific research owing to its wide-ranging of applications [7]. These particles are referred to as the bridge that separates molecular structures and bulk materials. Nanoparticles exhibit a number of special properties in relation to bulk material. Nanoparticles have a very high surface area to volume ratio. Liquid electrolytes have been used in the application of metal sulfide as active materials to lithium batteries [7, 8].

In the ninth century, nanoparticles were used by artisans for the generation effect on the surface of pots. With the use of lithium electrolytes, metal sulfide has been found to be applicable on lithium ion batteries. Nanoparticles are small enough to confine their electrons and also to yield quantum dots since they have unexpected optical properties [8]. The effects of metal sulfide deposits are complex and only partially understood. Catalytic performance is affected by these metal sulfide deposits in the following ways: (i) By chopping off their pore mouths and their access of reactants and should be limited to the interior catalyst surface, (ii) by covering the site where catalysis will occur, (iii) by plugging catalytic beds, (iv) by making new catalytic sites. Structures and properties of metal sulfide on catalysis strongly

depend on their preparation and treatment conditions. The resulting nanoparticles are characterized by TEM and XRD in order to determine their particle size and structure [9]. Nanoparticles have very small sizes and large specific surface area; this is due to their unusual electronic, chemical, optical, and magnetic properties which differentiate nanoparticles from bulk materials. Nanoparticles are used in various applications including catalysis, dyes, drug delivery, mechanical devices, electronic, optical, magnetic recording media and so forth [10]. Lin *et al*. [11] demonstrated the addition of 1-octadecanethiol at high temperatures on the kinetic pathway of palladium nanoparticle sulfidation process in order to perform palladium nanoparticle dispersion [11].

Since most palladium sulfide-based catalysts are used at high temperatures, the focus of the study was at elevated temperatures. The generation of discrete metal nanoparticles that are stabilized in the matrix of a polymer with or without solid support has been reported by Kalu *et al*. [12] using facile and thermally induced method. In this method, they used sample poly-vinyl-butyral (PVB) [12]. Nanoparticles were used by artisans in the ninth century for generating effect on the surface of pots. Nanoparticle often possesses unexpected optical properties as they are small enough to confine their electrons and produce quantum effect [13]. Metal nanoparticles are generally unstable; this is due to their large active surface area, so their self-aggregation should be prevented so that there is no drop in catalytic activity [14]. Organometallic chemistry and polymer chemistry have focussed in developing early and late transition metal used as catalyst for ethylene and propylene polymerization [15].

Liquid solid-solution phase transfer and separating strategy that has been reported by Wang *et al*. [16] is a unified approach in producing large variety of nanomaterials with different

properties, stoichiometries and low dispersity [16]. Nickel sulfide undergoes metal insulator, paramagnetic-antiferromagnetic phase change, and this result in showing interesting electronic properties [17]. Nanoparticles are known to have high surface to volume ratio which increase their efficiency when used for catalysis. They show absolutely new or improved properties based on specific characteristics such as morphology, size and distribution [18]. Nickel nanoparticles can form nanocomposite materials which have special structures that helps these nickel sulfide to achieve its availability in different fields [19].

Nickel sulfide has different stoichiometries which makes it more attractive and interesting but complicated to study. Nickel system is highly interesting because of its number of phases including α-NiS_4, NiS_2 and other forms of nickel sulfide [20]. Nickel sulfide undergoes a transition in terms of its magnetism (from paramagnetic to antiferromagnetic). At high temperature, for nickel sulfide spin freezing has been observed and at low temperature, superparamagnetism is observed [21]. Decrease in thermal analysis leads to increase in magnetism with decreasing temperature [22]. Among all metal sulfide, nickel sulfide have gained much attention due to their wide range of applications, catalysts and cathode materials for rechargeable lithium battery [23]. Composition of nickel-based nanoparticles depends on certain conditions such as pH, concentration of reagent, reaction time and temperature. Nickel sulfide display two phases: high temperature hexagonal (α-NiS) and low temperature rhombohedral (β-NiS) crystal structures.

Nickel has different application in many fields such as infrared detectors, hydro sulfurization catalysis, photoconductive material or solar storages [23, 24]. Nickel sulfide has an interesting electromagnetic property because it is able to form transition from paramagnetic

metal to antiferromagnetic semiconductors when cooled under transition temperature (T_t) which is approximately up to 379 °C [25]. Nickel sulfide has different stoichiometries which make it more attractive and interesting but complicated to study. Nickel system is highly interesting because of its number of phases including α-NiS_4, NiS_2 and other forms of nickel sulfide [26]. Nickel sulfide has important applications in hydrogenation catalysis especially in organic synthesis procedures. It has been reported that α-NiS and Ni_3S_2 are the only important catalytic compounds. In the past years, nickel catalysts were known to oligomerize ethylene and dimerize propylene and α-olefins since nickel metal was thought to prefer β-H elimination followed by reduction elimination [27].

1.2. Methods of synthesising nanoparticles

Synthesis of nanoparticles is achieved by the following methods: sputtering [28, 29], co-precipitation [30], sol gel method [31], micro emulsion [32], hydrothermal [33] or single source precursor [34]. Nanoparticles can be produced by using precipitation, gelation and hydrothermal treatment when using chemical synthetic approach called sol gel process.

1.2.1 Hydrothermal method

Hydrodynamic cavitation involves the generation of nanoparticles by creating and realising gas bubbles inside the sol-gel solution. The particle size of the synthesized nanoparticles is controlled by adjusting the pressure, and also the solution retention time in the cavitation chamber [33]. Metal nanoparticles have been prepared by methods such as physical and chemical inert supports and they were found to have large surface area which makes them to be good in heterogeneous catalysis [32, 33].

1.2.2 Impregnation method

This is the mostly used and studied method for preparing catalysts, here the carrier is purified, impregnated with a solution of metal precursor, it is dried, calcinated and then reduced in order to get nanoparticles dispersed on the support. The temperature used may be 300 °C or more than 300 °C so as to decompose the precursor salt [35]. In microwave radiation method, there is an introduction of microwave radiation in the reaction solution; synthesis of copper nanoparticles by microwave radiation method has become popular because it is simple to be used, ease of operation, it has short reaction period, increased product yield by comparing it with the conventional heating method [36]. The nanoprecipitation method which is also known as solvent displacement method, involves preformed polymer being precipitated from an organic solution then in the presence or absence of a surfactant, organic solution diffuses in the aqueous medium. The polymer used is dissolved in semi polar water miscible solvents including acetone or ethanol, then the organic solution is injected into the solution which contains stabilizer under magnetic stirring then nanoparticles are obtained [37].

1.2.3 Emulsion-diffusion method

Emulsion-diffusion method is a widely used method when preparing nanoparticles. Here, a partially water-miscible solvent is used to dissolve the polymer, and then it is saturated with water to confirm the initial thermodynamic equilibrium of liquids used. Emulsification of polymer water saturated solvent phase in aqueous solution which contains stabilizer, this leads to the diffusion of the solvent to the external phase, then nanoparticles or polymer nanocomposites are obtained. The solvent gets eliminated by filtration or evaporation [38]. Single source precursor method has been widely used to prepare metal sulfide and thin films

since they have an advantage of forming in one-step synthesis. In the control of deposition of thin films, single source precursor (SSP) plays the most important role [34, 39]. SSP method for the synthesis of nanocrystals and thin film has been an area of interest to many researchers [40].

1.2.4 Single source precursor (SSP) method

The use of single source precursors for the syntheses of thin films and nanocrystals has been an area of intense research [34, 41]. The use of SSP has served as efficient route to improve quality, crystalline monodispersed nanoparticles of semiconducting materials. Metal complexes of Schiff bases have been investigated with many metal ions. These ligands are attractive because of their simple modification of both steric and electronic effect [42]. Abdelhady *et al*. [43] have reported the use of iron(III) and Ni(II) thiobiuret complexes as single source precursor for the synthesis of iron sulfide and nickel sulfide nanoparticles, with nickel sulfide hollow nanosphere being synthesized via ϒ-irradiation, whereas micro emulsion system and others produce nickel sulfide nanoparticles [43]. Salavati-Niasari *et al*. [44] reported the synthesis of nickel sulfide nanoparticles; they used thio acetadiamide (TTA) as the organic capping agent, and sulfur source for microwave radiation [44].

Alagumuthu *et al*. [45] reported facile way of synthesising silver nanowires via solvothermal method. Silver nitrate was reduced with ethylene glycol, and n-butyl alcohol was used as appropriate media with TOPO as an adsorption agent [45]. Murugadoss *et al*. [46] reported a preparation method of TOPO-capped ZnS nanoparticles that are incorporated with Na_2S, $Zn(CH_3COO)_2$ as sulfur and ZnS sources through chemical precipitation. An organic capping agent (TOPO) was used for the prevention of particle agglomeration and stabilizing

nanocrystals [46]. Tong *et al*. [47] reported the use of dithiocarbamate derivatives as capping ligands to stabilize silver nanoparticles, and also the initial feed ratios of dithiocarbamate as well as silver salt concentration were controlling the average of particle core diameter that falls in the range of 2.5-5 nm [47]. Synthesis of zinc metalloporphyrin zinc dithiocarbamate and new disulfide with gold nanoparticles has been reported by Cormode *et al*. [48].

Alonso *et al*. [49] reported the synthesis and characterization of nickel nanoparticles that was used in hydrogenation transfer reaction where isopropanol was used as catalyst donor [49]. Tetrakis and mono-functionalised dithiocarbamate ligands that contain benzyl, alkyl and substituents of ruthenium(II) bipyridyl for the synthesis and characterization of gold nanoparticles have been reported by Vickers *et al*. [50]. Zeid [51] have synthesized cuprous sulfide (Cu_2S) nanocrystals via the thermal decomposition of a single-source molecular precursor, copper bisdiethyldithiocarbamate ($Cu(II)[S_2CNC_4H_{10}]_2$). The precursor used in the synthesis, copper bisdiethyldithiocarbamate is a volatile metal complex which exists primarily in a dimeric crystalline form [51].

1.3. LITERATURE REVIEW

1.3.1. Dithiocarbamates

Dithiocarbamates belong to a group of compounds called 1,1-dithiolate (Table 1.1). This class of compounds also have dithiophosphinates, dithiophosphates and dithiocarbimates [52]. In organic chemistry, a dithiocarbamate is a functional group that is the analogue of a carbimate where two sulfur atoms replace two oxygen atoms. They are strong complexing agents and give rise to large interesting complexes with metal ions [53]. For the synthesis of

metal sulfide nanoparticles, dithiocarbamate complexes have been used as precursors [54]. Dithiocarbamates are useful ligands that form metal dithiocarbamate complexes with most of the elements and are able to stabilize variety of oxidation states.

Table 1.1: Some types of 1,1-dithiolate ligands [52]

Composition	**Structure**	**Name**
$R_2NCS_2^-$	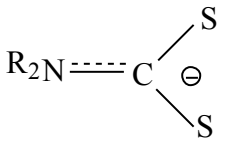	Dithiocarbamate
$RNCS_2^{2-}$	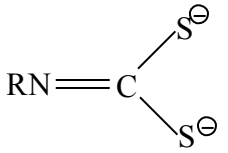	Dithiocarbimate
R_2PS_2	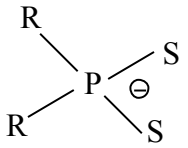	Dithiophosphinate
$(RO)_2PS_2$	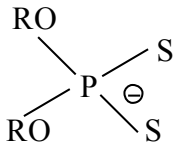	Dithiophosphate

Most dithiocarbamates are synthesized from secondary amines which are used as starting material when preparing dithiocarbamate compound. Dithiocarbamate salts are formed when

carbon disulfide reacts with either aromatic or aliphatic primary or secondary amines as shown below:

$2R_2NH + CS_2 \rightarrow [R_2NH_2]^+ + [R_2NCSS]^-$

Then when using alkali hydroxide as proton acceptor, dithiocarbamate salts may be obtained [55].

$R_2NH + CS_2 + MOH \rightarrow R_2NCSS^- M^+ + H_2O$

Dithiocarbamates have a very wide range of applications and uses and are therefore formed in large amounts worldwide [56]. Dithiocarbamates have application on medicinal chemistry and are also used for cancer treatment; tests have been done in their clinical trials for various indications such as HIV [57]. Dithiocarbamate ligands have complexing ability from the presence of sulfur donors, which delocalizes the positive charge towards the periphery from the metal centre [58].

1.4. Ni(II) and Pd(II) dithiocarbamate complexes

Ni(II) dithiocarbamates are diamagnetic due to their square planar geometries. Studies of dithiocarbamates based ligands have received much attention due to their strong metal binding property. Hogarth *et al*. [59] synthesized and characterized functionalized dithiocarbamate using elemental analysis, FT-IR, NMR [59]. Phosphines known as soft Lewis bases and nitrogenous ligands known as hard bases coordinate Ni^{2+} ions to form nickel(II) dithiocarbamates that have a planar NiS_4 chromophore that display remarkable variation in reactivity [60]. Square planar nickel(II) bis(dithiocarbamate) complexes exhibit a square planar arrangement, their maximum absorption in the UV-Vis region of the spectrum is about 330 nm, which is assigned to metal-ligand charge transfer transitions (MLCT) [61].

Coordination complexes based on dithiocarbamate have been thoroughly studied because they have an ability to coordinate many common metal ions with different binding modes as shown [62].

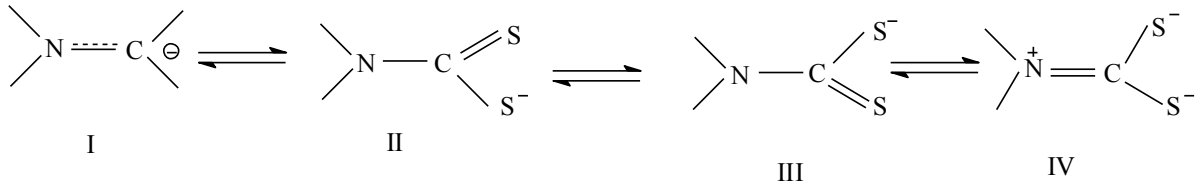

Scheme 1.1: Resonance structure of dithiocarbamates

Transition metal dithiocarbamates can be prepared by oxidative addition of carbon disulfides to metal centres. Transition metal dithiocarbamate complexes have also been formed from the reaction of secondary or primary amines with metal-bound xanthates [63]. Synthesis and structural studies of two salts of nickel complexes from dithiocarbamates that are derived from sulphonamide have been described by many researchers [64]. Transition metal dithiocarbamate complexes were first reported in the early 1900 and since that time, these complexes have been widely studied [65].

Most metals of transition or non-transition metals show coordinating affinity towards dithiocarbamate moiety. One of dithiocarbamate ligand property is its ability to accommodate metal ions in unusual oxidation states [66]. For Pd(II) complexes, only bidentate ligands are found to be active, complexes with monodentate ligands quickly isomerise to the inactive trans geometry. This inactivity of Pd(II) complexes has been assumed to be related to a low stability of the Pd/DNA adducts and to their rapid reaction kinetics, when compared to Pt(II)

compounds, leading to deactivation by reaction with several biochemicals other than DNA [67]. New xanthate complexes and dithiocarbamate complexes of nickel(II) with iminophosphine have been synthesized by Serrano *et al*. [68]. From their results they found out that complexes of nickel(II) containing hemi labile ligands were found to be active against catalytic reactions [69]. Stephenson *et al*. [70] reported catalyst of Ni(II)phenoxyiminato that contain remote ligand $–SO_2-$ group shows enhanced activity on thermal stability and alkene polymerization, also produces high molecular weight polyethenes that have remarkably high levels of chain branching compared to $–CH_2-$ control [70]. Tsuchida *et al*. [71] reported their preparation of dithiocarbamate complexes of nickel(IV) that have three ferrocenyl subunits where by each ferrocenyl group is linked covalently to the central metal and its convenient electro synthesis by use of nickel(II) analogue bearing two ferrocenyl subunits [71]. Ekennia *et al*. [72] synthesized, characterized and did antibacterial application on nine mixed ligand complexes of aryl dithiocarbamate and salycylaldehyde moiety, in order to produce lead compounds for the production of selective bactericides **1** [72].

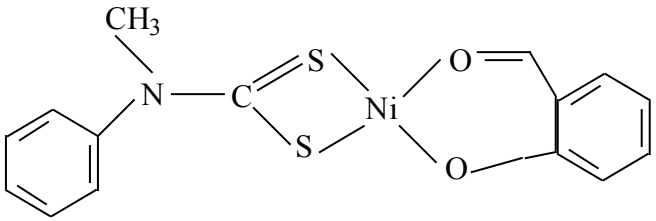

(1)

Yoon *et al*. [73] synthesized new cadmium sulfide based precursors with high purity and also high yields. These cadmium sulfide thin films were deposited successfully through the metal organic chemical vapour deposition (MOCVP) or different substrate which includes glass or TiO_2/ITO/glass [73]. Chae *et al*. [74] reported synthesis of two new derivatives of

selenocarbamates that contain asymmetric cyclic or aliphatic ligand: Cd(N,N-ethyl butyldiselenocarbamate)$_2$ as well as Cd(2-ethylpiperidinediselenocarbamate)$_2$, precursors that contain diselenocarbamate ligands with dialkyl groups that are asymmetrical and some interesting compounds because they have been discovered to have relatively lower decomposition or melting temperatures than those of symmetric ones [74].

Dawood *et al*. [75] have synthesized and characterized complexes of nickel(II) of mixed ligands {benzilbis-(semicarbazone)-SCH_2 **4** and ammonium indolenedithiocarbamate-Indtc **5**, ammonium pyrrolidenedithiocarbamate-Pyrdtc **6**}. They concluded that SCH_2 ligand acted as tetradentate or tridentate chelating ligands joint to nickel(II) ion through the oxygen and nitrogen atoms. From the prepared complexes in neutral molecule and in basic medium the ligand acted as anion (-1 or -2) owing to their deprotonation process that occurs in enol of the ligand [75].

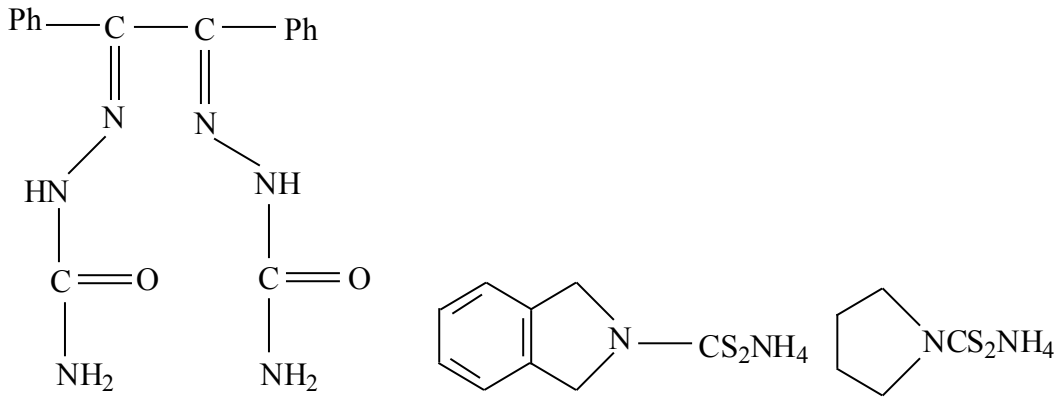

Figure 1: Structures of ligands and dithiocarbamates (labelled 4, 5 and 6)

The first report on transition metal dithiocarbamate complexes was published in early 1900 and since then these complexes have been widely studied [76]. Separation strategy and phase transfer of liquid-solid solution have been used in producing large variety of nanocrystals that have different properties and also low dispersity were reported by Wang *et al*. [77]. The

particle shape and size of selenide nanorods, were successfully controlled by Puntes *et al*. [78]. In previous research a new dithiocarbamate compound was synthesized and characterized using elemental analyses, FT-IR, NMR [79]. In general, studies on nanotechnology are expected to have extreme impact on the development of new catalysts, because the detailed understanding of chemistry of catalytic materials in the nanometer-scale and the ability to control their preparation lead to rational and cost-efficient catalyst design [80].

1.5. Catalysis

Nickel-based catalysts have been known for several years and are valued commercially since they oligomerize or dimerize α-olefins. Ni and Pd are under homogeneous catalysts. These catalysts give access to polyolefin with a large choice of properties and this increases production of polymers for special-purpose applications [81]. Late transition metal based catalyst have been found to be the best catalysts to be used in polymerization of olefins since their oxophilicity is reduced. Late transition metal system polymerizes ethylene to high molecular weights, but there are no systems that convert α-olefins to polymer with high molar mass [82]. Nickel sulfides have important applications in hydrogenation catalysis especially in organic synthesis procedures. It has been reported that α-NiS and Ni_3S_2 are the only important catalytic compounds [83].

In the past years, nickel catalysts were known to oligomerize ethylene and dimerize propylene and α-olefins since nickel metal was thought to prefer β-H elimination followed by reduction elimination [84]. Normally, a catalyst used in olefin polymerization has these four catalyst components: (i) a ligand, (ii) transition metal, (iii) alkyl, and (iv) catalyst. Ligand is

the most component that play a significant part in polymerization process and when it comes to catalyst design, ligand design is essential [85]. Catalyst based on cationic Ni(II) and Pd(II) derived from substituted α -diimines have been reported in 1995 to convert ethylene and α -olefins to polyolefin with high molecular weight [86]. Complexes of late transition metals are more functional-group when compared to those of early transition metal catalysts due to their less oxophilicity nature. Research on industrial and academic have recently focused on olefin oligomerization and polymerization catalysed by late transition metal complexes [87].

For different reactions in the past years, catalysts have been used owing to their excellent chemical and physical properties [88]. Partially crystalline and crystalline sulfide have been recently studied because they have potential application as catalyst for solid lubricant, solar cell devices, coal liquefaction, rechargeable batteries, and coatings for microwave shield [89]. The activity and dispersity of the catalyst is determined by the size of the particle used and the range of the optimum size is within 10-20 nm, therefore the size of sulfide particle is very important [90]. Since the discovery of Ni(II) and Pd(II)-based catalysts by Brookhart, alkene polymerization catalyst have gained much attention on α-diimine catalyst and Grubbs discovered neutral nickel phenoxyiminato catalysts [91].

1.6. Rationale and motivation

Single source precursor method is the recently used method in the synthesis of metal sulfide nanoparticle. The precursor needs to be well capped during synthesis so as to obtain nanoparticles with uniform size distribution and to minimise agglomeration. Complex decomposition can be done at different temperatures with resultant different sizedistribution products that may find applications in different fields due to their varying properties.

1.7. Problem statement

Different methods have been used in the preparation of nanoparticles but they have problems which includes agglomeration of particles that is caused by the annealing temperature, and also the large particle size. SSP has been used as an appropriate method for the preparation of nanoparticles with small particle size, because of the organic capping agent used. In this study very small sizes of nanoparticles will be of great results as it will find usefulness in catalysis reactions because the smaller the particle sizes the larger the surface area of the particle which is efficient for catalysis. Industries need effective catalysts that will be used in olefin polymerization catalysis. Late transition metal system has been found to polymerize ethylene to high molecular weights, but there are no systems that convert α-olefins to polymers with high molar mass.

1.8. Aims and objectives

1.8.1 Aim

The main aim of this research is to synthesize Ni(II) and Pd(II) dithiocarbamate complexes and use them as single source precursors for the synthesis of NiS and PdS nanoparticles/ starch nanocomposites.

1.8.2 Objectives

- To synthesize four different dithiocarbamate ligands.
- To synthesize the Ni(II) and Pd(II) complexes of the different dithiocarbamate ligand
- To characterize all synthesized ligands and complexes using analytical and spectroscopic techniques.

- To use the Ni(II) and Pd(II) dithiocarbamate complexes as single source precursor for the synthesis of HDA capped NiS and PdS nanoparticles.
- To synthesize NiS and PdS/potato starch nanocomposites
- To study the optical and structural properties of the metal sulfide nanoparticles/ potato starch nanocomposites.

References

1. Libor, Z.; Zhang, Q. The synthesis of nickel nanoparticles with controlled morphology and SiO_2/Ni core-shell structures. *Mater*. *Chem*. *Phys*. **2009**, 114, 902-907.

2. Pal, S.L.; Jana, U.; Mana, P.K.; Mohanta, G.P.; Manavalan, R. Nanoparticles: An overview of preparation and characterization. *J*. *Appl*. *Pharm*. *Sci*. **2011**, 01(06), 228-234.

3. Brostow, W.; Dutta, M.; Souza, J.R.; Rusek, P.; Medeiros, A.M.; Ito, E.N. Nanocomposites of poly(methyl methacrylate) (PMMA) and mantmorillonite (MMT) Brazilian clay: A tribological study. *Expr*. *Polym*. *Lett*. **2010**, 4, 570-575.

4. Zhao, O.; Samulski, E.T.A comparative study of poly(methyl methacrylate) and polystyrene/clay nanocomposites prepared in supercritical carbon dioxide. *Polymers*, **2006**, 47, 663-671.

5. Anzlovar, A.; Orel, Z.C.; Kogej, K.; Zigon, M. Polyol-mediated synthesis of zinc oxide nanorods and nanocomposites with poly(methyl methacrylate). *J*. *Nanomat*. **2012**.

6. Yang, F.; Nelson, G.L. PMMA/silica nanocomposite studies: Synthesis and properties. *J*. *Appl*. *Sci*. **2004**, 91, 3844-3850.

7. Banerjee, M.; Chongad, L.; Sharma, A. Structural and optical properties of pure and copper doped NiS nanoparticles. *Res*. *J*. *Recent*. Sci. **2013**, 2, 326-329.

8. Xu, W.; Wang, Y.; Xu, R.; Liang, S,; Zhang, G.; Yin, D. Synthesis and fluorescence spectrum analysis of CdS nanocrystals, *J*. *Mater*. *Sci*. **2007**, 42, 6942–6945.

9. Morozov, Yu. G.; Belovsova, O.V.; Kuznetsov, M.V. Nickel nanoparticles for catalytic applications, *Yug*. *Mater*. *Sci*. *Soc*. *Conf*. **2009**, 56, 231-234.

10. Wang, X.; Zhuang, J.; Peng, Q.; Li, Y. A general strategy for nanocrystal synthesis. *Nature* Sci. **2005**, 437, 121–124.

11. Lin, X.; Sun, C.; Bolin, T.; Wu, T.; Liu, Y.; Sternberg, M.; Sun, S. Kinetic Pathway of Palladium Nanoparticle Sulfidation Process at High Temperatures. *Nano*. *Lett*. **2013**, 13, 4893-4901.

12. Kalu, E.E.; Daniel, M.; Bockstaller, M. R. Synthesis, characterization, electro catalytic and catalytic activity of thermally generated polymer-stabilized metal nanoparticles. *Int*. *J*. *Electrochem*. *Sci*. **2012**, 7, 5297-5313.

13. Wang, S.; Yang, S. Surfactant-assisted growth of crystalline copper sulphide nanowire arrays. *Phys*. *Lett*., **2000**, 322, 567- 571.

14. Schmidt, W. nanoparticles by chemical synthesis, processing to materials and innovative applications. *Appl*. *Organomet*. *Chem*. **2001**, 15, 331-343.

15. Ruhland, T.M.; Lang, J.R.V.; Alt, H.G.; Muller, A.H.E. Magnetic Core-Shell Nanoparticles as Carriers for Olefin Dimerization Catalysts. *Eur*. *J*. *Inorg*. *Chem*. **2013**, 2146-2153.

16. Wang, H.; Zhang, J.R.; Shao, X.N.; Xu, S.H.; Zhu, J.J. Preparation of copper monosulfide and nickel monosulfide nanoparticles by sonochemical method. *Mater*. *Lett*. **2002**, 55, 253–258.

17. Tilley, R.D.; Jefferson, D.A. The synthesis of nickel nanoparticles on Graphite carbon supports. *J*. *Phys*. *Chem*. **2002**, 106, 10895-10901.

18. Raevskaya, A.E.; Stroyuk, A.L. Catalytic activity of CuS nanoparticles in hydrosulfide ions air oxidation. *J*. *Mol*. *Catal*. *A*, **2003**, 212, 259-265.

19. Barman, M.; Paul, S.; Sarkar, A. A study of magnetic properties in confined sol-gel synthesized nickel sulfide nano-clusters. *J. Am. Chem. Soc.* **2013**, 4, 343-349.

20. Aso, K.; Kitaura, H.; Kayashi, A.; Tatsumisago, M. Synthesis of nanosized nickel sulfide in high-boiling solvent for all-solid-state lithium secondary batteries. *J. Mater. Chem.* **2011**, 21, 2987-2990.

21. Fazli, Y.; Mahdi, S.P.; Kohsari, I.; Sadeghpur, M. Electrochemical synthesis and structure characterization of nickel sulfide nanoparticles. *Mat. Sci. Semicon. Proc.* **2014**, 27, 362-367.

22. Libor, Z.; Zhang, Q. The synthesis of nickel nanoparticles with controlled morphology and SiO_2 /Ni core-shell structures. *Chem. Mater.* **2008**, 114, (2-3), 902-907.

23. Chen, D.H.; Wu, S.H. Synthesis of nickel nanoparticles in water-in-oil microemulsions. *Chem. Mater.* **2000**, 12, 1354-1360.

24. Monohar, A.; Ramalingam, K.; Karpagavel, K. Mixed ligand complexes involving bis(dithiocarbamato) nickel(II) and phosphorus donors: Synthesis, spectral, thermal studies and BVS investigations. *J. Chem. Tech. Res.* **2012**, 4(4), 1383-1391.

25. Atay, F.; Kose, S.; Bilgin, V.; Akyuz, I. Electrical, optical, structural and morphological properties of NiS films. *Turk. J. Phys.* **2003**, 27, 285-291.

26. Wang, R.; Wang, H.; Feng, H.J.S. Palladium decorated nickel nanoparticles supported on carbon for formic acid oxidation. *Int. J. Electrochem. Sci.* **2013**, 8, 6068-6076.

27. Baogen, D.; Xiao Zhen, Y.; Xiong Feri, Z.; Ling, H.S.; Wen Hua, S. Catalytic activity correlation of Ni(II), Co(II) and Pd(II) complexes to metal atom net charge. *Sci China Se*r-*B-Chem*. **2008**, 1-8.

28. Nie, M.; Kai Sun, K.; Meng, D.D. Formation of metal nanoparticles by short-distance sputter deposition in a reactive ion etching chamber. *J. Appl. Phys*. **2009**, 106, 054314.

29. Cha, I.Y.; Ahn, M.; Yoo, S.J.; Sung, Y. Facile synthesis of carbon supported metal nanoparticles via sputtering onto a liquid substrate and their electrochemical application, *RSC. Adv*. **2014**, 4, 38575-38580.

30. Ahn, T.; Kim, J.H.; Yang, H.M.; Lee, J.W.; Kim, J.D. Formation pathways of magnetic nanoparticles by coprecipitation method. *J. Phys. Chem. C*. **2012**, 116(10), 6069-6076.

31. Alwan, R.M.; kadhim, Q.A.; Sahan, K.M.; Ali, R.A.; Mahdi, R.J.; Kassim, N.A.; Jassim, A.N. Synthesis of zinc oxide nanoparticles via sol-gel route and their characterization. *Nanosci. Nanotech*. **2015**, 5(1), 1-6.

32. Malik, M.A.; Wani, M.Y.; Hashim, M.A. micro emulsion method: A novel route to synthesize organic and inorganic materials. *Arab. J. Chem*. **2012**, 5(4), 397-417.

33. Hasashi, H.; Hakuta, Y. Hydrothermal synthesis of metal oxide nanoparticles in supercritical water. *Materials*, **2010**, 3, 3794-3817.

34. Ramasamy, K.; Malik, M.A.; Raftery, J. Metal complexes of thiobiurets and dithiobiurets: Novel single source precursors for metal sulfide thin film nanostructures. *Dalton. Trans*, **2010**, 39, 1460-1463.

35. Umer, A.; Naveed, S.; Ramzon, N. Selection of a suitable method for the synthesis of copper nanoparticles. *World Sci. J*. **2012**, 7(5), 18 pages.

36. Hou, Y.; Kondoh, H.; Ohta, O.; Gao, S. Size-controlled synthesis of nickel nanoparticles. *Appl. Surf. Sci* **2005**, 241, 218-222.

37. Yadav, H.K.S.; Nagavarma, B.V.N.; Ayaz, A.; Vasudha, L.S.; Shivakumar, H. G. Different techniques for preparation of polymeric nanoparticles for preparation of polymeric nanoparticles –A review. *Asian*. *J*. *Pharm*. *Clin*. *Res*; **2012**, 5, 16-23.

38. Sailaja, A.K.; Amareshwar, P; Chakravarsity, P. Different techniques used for the preparation of nanoparticles using natural polymers and their application. *Int*. *J*. *Pharm*. *Pharm*. *Sci*. **2011**, 3, 45-50.

39. Cumberland, S.L.; Hanif, K.M.; Javier, A,; Khitrovig, A.; Strouse, G.F.; Woessner, S.M.; Yun, C.S. Inorhanic cluster as single source precursors for preparation of CdSe, ZnSe, and CdSe/ZnS nanomaterials. *Chem*. *Mater*. **2002**, 14, 1576-1584.

40. Bochmann, M. Metal chalcogenide materials: Chalcogenolato complexes as "single-source" precursors. *Chem*. *Vap*. *Dep*. **1996**, 2(3), 1-12.

41. Jain, V.K. Synthesis and characterization of single-source molecular precursors from the preparation of metal chalcogenides. *J*. *Chem*. *Sci*. **2006**, 118(6), 547-552.

42. Abdelhady, A.L.; Malik, M.A.; O'Brien, P.; Tuna, F. Nickel and iron sulfide nanoparticles from thiobiurets. *J*. *Phys*. *Chem*. *C*. **2012**, 116, 2253-2259.

43. Salavati-Niasari, M.; Banaiean-Monfare, M.; Emadi, H.; Emhessari, M. Synthesis and characterization of nickel sulfide nanoparticles via cyclic microwave radiation. *C*. *R*. *Chimie*, **2013**, 16, 929-936.

44. Alagumuthu, G.; Kirubha, R. Synthesis and characterization of silver nanoparticles in different medium. *J*. *Synth*. *Theo*. *Appl*. **2012**, 1, 13-17.

45. Murugadoss, G.; Rajamannan, B.; Ramasamy, V. Photoluminescence properties of monodispersed Mn^{2+} doped ZnS nanoparticles prepared in high temperature. *J*. *Mol*. *Struc*. **2011**, 991, 202-206.

46. Tong, M.C.; Chen, W.; Sun, J.; Ghosh, D.; Chen, S. Dithiocarbamate-capped silver nanoparticles. *J. Phys. Chem*. B, **2006**, 110, 19238-19242.

47. Cormode, D.P.; Davis, J.J.; Beer, P.D. Anion sensing porphyrin functionalized nanoparticles. *J. Inorg. Organomet. Polym*. **2008**, 18, 32-40.

48. Alonso, F.; Riente, P.; Sirvent, J. A.; Yus, M. Nickel nanoparticles in hydrogen-transfer reductions: Characterization and nature of the catalyst. *Appl. Catal*. A: Gen **2010**. APCATA-12428; No. of Pages 10

49. Vickers, M.S.; Beer, P.D.; Cookson, J.; Bishop, P.J.; Thiebaut., B. Dithiocarbamate ligand stabilised gold nanoparticles. *J. Matter. Chem*. **2006**, 16, 209-215.

50. Zeid, T.W.; Mokari, T.; Plante, I.J.; Yang, P. Synthesis of metal sulfide nanomaterials via thermal decomposition of single-source precursors. *J. Mater. Chem*. **2012**, 20, 6612-6617.

51. Amim, R.S.; Oliveira, M.R.L.; Perpetuo, G.J.; Janczack, J.; Miranda, L.D.L. Synthesis, crystal structure and spectroscopic characterization of new platinum(II) dithiocarbamato complexes. *Polyhedron*, **2008**, 27, 1891-1897.

52. Price, D.J.; Wali, M.A.; Bruce, D.W. Mesomorphic dithiocarbamate complexes. *Polyhedron* 16(2), **1996**, 315-320.

53. Kanchi, S.; Singh, P.; Bisetty, K. Dithiocarbamates as hazardous remediation agent: A critical review on progress in environmental chemistry for inorganic species studies of 20th century. *Arab. J. Chem*. **2014**, 7, 11-25.

54. Rani, P.J.; Thirumaran, S.; Ciattini, S. Synthesis and characterization of Ni(II) and Zn(II) complexes of (furan-2-yl)methyl(2-(thiophen-2-yl)ethyl) dithiocarbamate (ftpedtc): X-ray structures [Zn(ftpedtc)$_2$ (py)] and [Zn(ftpedtc)Cl(1,10-phen)] *Spectrochim. Acta Part A*, **2015**, 137, 1164-1173.

55. Donzell, A.; Potvin, P.G. Dithiocarbamate complexes of Ti(IV) Alkoxides: Synthesis, characterization and electrochemistry. *Inorg*. *Chem*. **2009**, 8, 4171-4178.

56. Khan, H.; Badshah, A.; Rehman, Z.; Said, M.; Murtaza, G.; Shah, A.; Butler, I.S.; Ahmed, S.; Fontaine, F. New dimeric and supramolecular mixed ligand palladium(II) dithiocarbamates as potent DNA binders. *Polyhedron*, **2012**, 39, 1-8.

57. Matthews, V.S.; James, C.; Paul, D.B.; Peter, B.T.; Thiebaut, B. Dithiocarbamate ligand stabilised gold nanoparticles. *J*. *Mater*. *Chem*. **2006**, 16, 209-215.

58. Pastorek, R.; Kamenick, J.; Pavlicek, M.; Husarek, J.; Sindelar, Z.K.; Zak, Z. Dithiocarbamate complexes of nickel(II) with 1,1'-bis(diphenylphosphino) Ferrocene. *J*. *Coord*. *Chem*. **2010**, 55(11), 1301-1308.

59. Hogarth, G.; Rainford-Brent, E-J.C-R.C.R.; Kabir, S.E.; Richards, I.; Wilton-Ely, J.D.E. T.; Zhang, Q. Functionalized dithiocarbamate complexes: Synthesis and molecular structures of 2-diethylaminoethyl and 3-dimethylaminopropyl dithiocarbamate complexes [M{$S_2CN(CH_2CH_2NEt_2)_{(2)}$}(n)] and [M{$S_2CN(CH_2CH_2CH_2NMe_2)$(n)] (n=2, M= Ni, Cu, Zn, Pd; n=3, M= Co). *Inorg*. *Chim*. *Acta*, **2009**, 362, 2020-2026.

60. Husarek, J.; Pastorek, R.; Malon, M.; Sindala, Z.; Pavlicek, M. Nickel(II) cyclohexylethyldithiocarbamate complexes with monodantate P-donor ligands in the coordination sphere. *J*. *Serb*. *Chem*. **2004**, 69(120), 1053-1061.

61. Mahmoud, A.M.; Garlyyev, B.; El-Sayed, M.A. Controlling the catalytic efficiency on the surface of hollow gold nanoparticles by controlling an inner thin layer of platinum or palladium. *J*. *Phy*. *Chem*. *Lett*. **2014**, 5, 4088-4094.

62. Oliveira, M.R.L. Preparation of novel cobalt(III) complexes with dithiocarbamates derived from sulfonamides. *Trans*. *Met*. *Chem*. **1999**, 24, 127-130.

63. Leka, Z.; Kosovic, M.; Vojta, D.; Latinovic, V.; Dakovic, M.; Visnjevac, A. Synthesis, structural and antifungal activities of novel Co, Mo and Pt complexes with triammonium N,N-diacetatedithiocarbamate. *Polyhedron*, **2014**, 80, 233-242.

64. Oliveira, M.R.L.; Diniz, R.; De Bellis, V. M.; Fernandes, N. G. Nickel(II) complexes of dithiocarbamates from sulphonamides: Synthesis and crystal structures. *Polyhedron*, **2003**, 22, 1561-1566.

65. Sarwa, N.; Ahmad, S.; Ali, S.; Awan, S. A. Copper(II) complexes of pyrrolidine dithiocarbamate, *Trans*. *Met*. *Chem*. **2007**, 32(2), 199-203.

66. Trevisan, A.; Marozano, C.; Cristofori, P.; Borella, V.M.; Giovagnini, Li.; Fregona, D. Synthesis of a palladium(II)-dithiocarbamate complex: Biological assay and nephrotoxicity in rats. *Arch*. *Toxicol*. **2002**, 76, 262-268.

67. Mahapatra, B.; Panda, D. Anionic mixed ligand complexes of cobalt(II) and copper(II). *J*. *Indian*. *Chem*. *Soc*. **1998**, 63, 792-793.

68.Serano, A.; Ma, C.; Cristofori, P.; Venturini, M.B.; Giovagnini, L.; Fregona, D. Synthesis of a palladium(II)-dithiocarbamate complexes: Biological assay and nephrotoxicity in rats. *Arch*. *Toxicol*. **2002**, 76, 262-268.

69. Stephenson, C.J.; McInnis, J.P., Chen, C; Weberski, M.P.; Delferro, M.; Motta, A.; Marks, T.J. Ni(II) phenoxyiminato olefin polymerization catalysis: Striking coordinative modulation of hyper branched polymer microstructure and stability by a proximate sulfonyl group. *J*. *Amer*. *Chem*. *Soc*. **2014**, 4, 999-1003.

70. Tsuchida, E.; Oyaizu, K.; Ishii, Y.; Yamamoto, K. Synthesis and characterization of nickel dithiocarbamate complexes bearing ferrocenyl subunits. *Chem*. *Eur*. *J*. **1999**, 5(11), 3193-3201.

71. Ekennia, A.C. Antibacterial application of novel mixed ligand dithiocarbamate complexes of nickel(II). *J. Appl. Chem*. **2013**, 5, 36-39.

72. Yoon, S.H.; Lee, S.S.; Seo, K.W.; Shim, W. Preparation of CdS Thin Films through MOCVD Method Using Cd-S Single-source Precursors. *Bull. Korean. Chem*. **2006**, 27(12) 2071-2073.

73. Chae, D.Y.; Seo, K.W.; Lee, S.S.; Yoon, S.H.; Shim, W. CdSe Thin Films Grown by MOCVD Method Using New Single-source Precursors. *Bull. Korean. Chem*. Soc. **2006**, 27(5), 762-764.

74. Dawood, Z.F.; Mohammed, T.J.; Sharif, M.R. New nickel(II) complexes with benzilbis (semicarbazone) and dithiocarbamate ligands. *Iraqi Journal of Veterinary Science*, **2009**, 23, 135-141.

75. Wang, G.Y.; Zhang, Y.C.; Hu, X.Y. Solvothermal synthesis of hexagonal CdS nanostructures from a single-source molecular precursor, *J. Alloy. Comp*. **2007**, 437, 47-52.

76. Puntes, V.F.; Krishnan, K.M.; Alivisatos, A.P. Colloidal nanocrystal shape and size control: The case of cobalt. *Sci*. **2001**, 291, 2115–2117.

77. Manav, N.; Mishra, A.K.; Kaushik, N.K. Triphenyl phosphine adducts of platinum(IV) and palladium(II) dithiocarbamates complexes: A spectral and in vitro study. *Spectrochem. Acta Part A*, **2004**, 60, 3087-3090.

78. Nabipouri, H.; Ghammamy, S.; Ashuri, S.; Aghbolagh, Z.S. Synthesis of new dithiocarbamate compound and study of its biological properties. *Org. Chem. J*. **2010**, 2, 75-80.

79. Polo-Ceron, D.; Gomez-Ruiz, S.; Torres, J.C.; Prashar, S.; Fajardo, M.; Reyes, M.I. Synthesis and structural characterization of novel three carbon atom bridged ansa-

bis(indenyl)zirconocene complexes: Application in ethylene polymerization. *Polyhedron*. **2014**, 80, 129-133.

80. Varnoosfaderani, M.; Pourmandian, S.; Tarami, F. High performance bulky α-diimine nickel(II) catalysts for ethylene polymerization. *J. Iran Poly*. **2011**, 20(11), 897-912.

81. Braunstein, P.; Speiser, F.; Sausage, L. Catalytic ethylene dimerization and oligomerization: Related developments with nickel complexes containing P,N-chelating ligands. *Acc*. *Chem*. *Res*. **2007**, 38, 784-793.

82. Narayanan, R.; El-Sayed, M.A. Effect of catalysis on the stability of metallic nanoparticles: Suzuki reaction catalysed by PVP-palladium nanoparticles. *J*. *Am*. *Chem*. *Soc*. **2003**, 125, 8340–8347.

83. Bateman, S.A.; Wu, D.Y. Sulfonyl azides: An alternative route to polyolefin modification. *J*. *Appl*. *Polym*. *Sci*. **2002**, 84, 1395－1402.

84. Gomez, M.; Favier, I.; Schmidt, G.; Toshima, N. Metal nanoclusters in catalysis and material science. *J*. *Mater*. *Sci*. **2008**, 14, 451-457.

85. Haung, Y.; Jia, W.; Jin, G. Synthesis, characterization and olefin polymerization of nickel catalysts supported by [N, S] ligands. *J*. *Organomet*. *Chem*. 694, **2009**, 86-90.

86. Long, B. K.; Rhinehart, J.; Brown, L.A.A robust Ni(II) α-diimine catalysts for high temperature ethylene polymerization. *J*. *Am*. *Chem*. *Soc*. **2013**, 135, 16316-16319.

87. Novak, B.M.; Boyle, P.T.; Nodom, M. Ethylene polymerization catalysed by neutral nickel(II) complexes with OˆN-chelating ligand. *Polym*. *J*. **2004**, 36(2), 140-145.

88. Liu, F.S.; Hu, H.B.; Guo, L.H.; Zai, S, B.; Song, K.M.; Gao, H.Y.; Zhang, L.; Zhu, F.M.; Wu, Q. Thermostable α-diimine nickel(II) catalyst for ethylene polymerization: Effects of the

substituted backbone on catalytic properties and branching structure of polyethylene. *Macromolecules*, **2009**, 42, 7789-7796.

89. Grubbs, R.H.; Wang, C.; Friedrich, S.; Younkin, T.R.; Li., R.T.; Bansleben, D.A.; Day, M. W. Neutral nickel(II)-based catalysts for ethylene polymerization. *Organometallics*, **1998**, 17(15), 3149-3151.

90. Collins, S. Polymerization catalysis with transition metal amidinate and related complexes. *Coord*. *Chem*. *Rev*; **2011**, 255, 118-138.

91. Schmidt, H. Nanoparticles by chemical synthesis processing to materials and innovative applications. *Appl*. *Organometal*. *Chem*. **2011**, 15, 331-343.

CHAPTER TWO

2.0 EXPERIMENTAL

This chapter provides the list of all chemicals used, experimental methods that have been used and the physical measurements used to characterize all the compounds in trying to achieve the aim and objectives of the study.

2.1. Reagents and solvents

Anisidine, dibenzylamine, butylamine, imidazole, carbon disulfide, potassium hydroxide, ethanol, methanol, diethyl ether, nickel(II) chloride, palladium(II) chloride, acetonitrile, and acetone were all obtained from Sigma-Aldrich or Merck and used as obtained without further purification.

2.2. Physical measurements

2.2.1. Melting points

The melting point and decomposition of both ligands and complexes were recorded on the Stuart SMP 11 apparatus.

.

2.2.2. Conductivity measurements

The molar conductance of all compounds have been determined using EC-Meter Basic 30^{+} at 25 °C, while all the four ligands were dissolved in water, nickel(II) complexes were dissolved in methanol and palladium(II) complexes in acetone.

2.3. Spectroscopic techniques

2.3.1. Infrared Spectroscopy

Infrared spectra of all ligands and complexes were collected on Perkin Elmer Paragon 2000 FTIR spectrophotometer as KBr pellet, in the range of 4000-400 cm^{-1}.

2.3.2. UV-Vis spectroscopy:

The electronic spectra of the compounds in solution were ran in the range 180-1100 nm on Perkin Elmer 25 spectrophotometer. All ligands and complexes were dissolved in different solvents. 2 mg of each ligand was dissolved in 4 mL of distilled water and then they were transferred into a quartz cell and the UV data was recorded in nanometres (nm). The complexes were dissolved in dichloromethane.

2.3.3. NMR spectroscopy

Bruker ultra shield 400 NMR spectrometer was used to determine number of protons and carbons in each compound at 400.1 MHz for ^{1}H and 100.6 MHz for ^{13}C nuclei. 2 mg of each of the dithiocarbamate ligand was dissolved in 2 mL of dichloromethane and complexes were dissolved in DMSO. Each solution was then transferred into a thin glass NMR tube for determination.

2.4 Synthesis of dithiocarbamate ligands [1]

2.4.1. Synthesis of potassium salt of anisidine dithiocarbamate (L^1)

6.16 g (5 mmol) of anisidine was dissolved in 10 mL of deionised water; 2.18 g (5 mmol) of potassium hydroxide was dissolved in 10 mL of water in a conical flask and placed in ice water. Anisidine solution was added to the potassium hydroxide solution and stirred, after which 3 mL of cold carbon disulfide was added drop wise. The reaction was done at temperature less than 4 ºC for about 3-4 hours. The resulting product was filtered, washed with diethyl ether to remove impurities, then recrystallized in acetonitrile and dried.

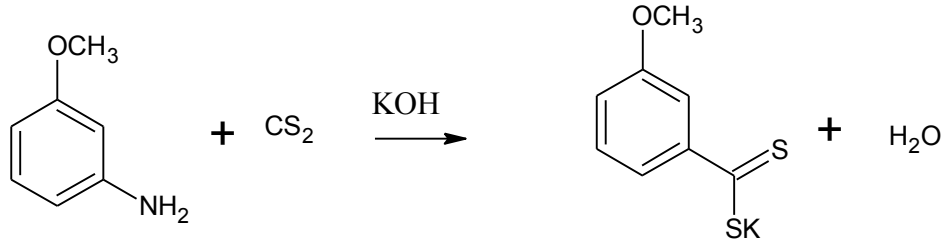

Scheme 2.1: Synthesis of potassium salt of anisidine dithiocarbamate (L^1)

2.4.2. Synthesis of potassium salt of dibenzyl dithiocarbamate (L^2)

10 mL of dibenzylamine was reacted with a solution of 2.81 g (5 mmol) of potassium hydroxide dissolved in 10 mL of water. 3 mL of cold carbon disulfide was added drop wise to the solution while stirring. The reaction was stirred for 3-4 hours then the precipitate obtained was filtered, washed and recrystallized in acetonitrile.

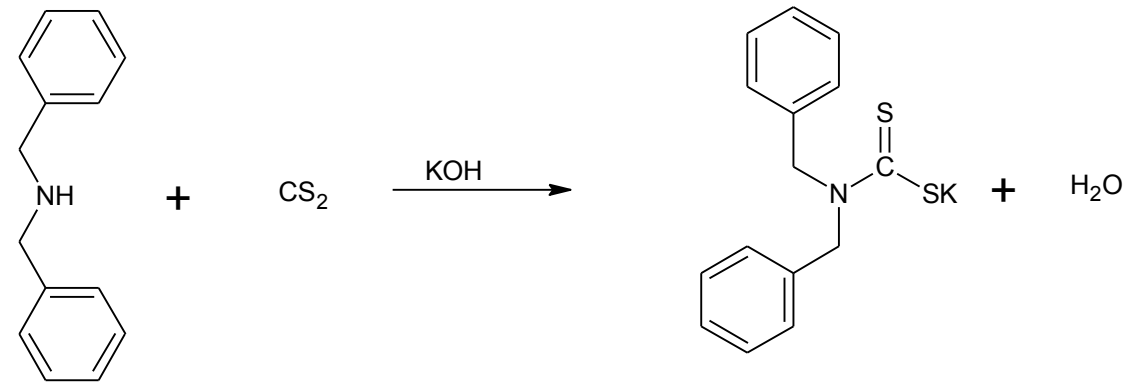

Scheme 2.2: Synthesis of potassium salt of dibenzyl dithiocarbamate (L^2)

2.4.3. Synthesis of potassium salt of butyl dithiocarbamate (L^3)

5 mL of butylamine reacted with a solution of 2.81 g (5 mmol) of potassium hydroxide dissolved in 10 mL of water. 3 mL of cold carbon disulfide was added drop wise to the solution while stirring for about 3-4 hours. The product formed was filtered, washed and recrystallized in acetonitrile.

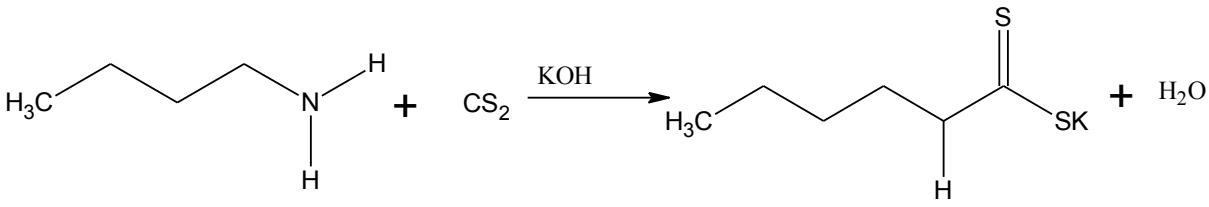

Scheme 2.3: Synthesis of potassium salt of butyl dithiocarbamate (L^3)

2.4.4. Imidazolyl dithiocarbamate (L^4)

3.4 g (5 mmol) of imidazole was dissolved in 10 mL of deionised water; 2.18 g (5 mmol) of potassium hydroxide was dissolved in 10 mL of water in a conical flask and placed in ice water. Imidazole solution was added to the potassium hydroxide solution in the conical flask and stirred, while stirring 3 mL of cold carbon disulfide was added drop wise. The reaction

was done at temperature less than 4 ºC for about 3-4 hours. The resulting product was filtered, washed with diethyl ether, and then recrystallized in acetonitrile.

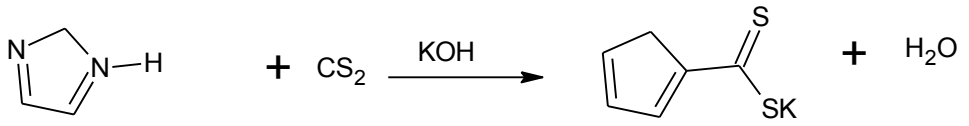

Scheme 2.4: Synthesis of potassium salt of imidazolyl dithiocarbamate (L^4)

2.5 Synthesis of dithiocarbamate complexes [2]

2.5.1 Synthesis of Ni(II) anisidine dithiocarbamate complex $[Ni(L^1)_2$

0.45 g (5 mmol) of anisidine dithiocarbamate ligand was dissolved in 10 mL of methanol in a beaker. 0.59 g (2.5 mmol) of $NiCl_2$ was dissolved in a separate beaker. The two solutions were mixed and stirred immediately. The reaction occurred at room temperature for 1-3 hours. The resulting product was filtered and washed with water followed by diethyl ether and dried.

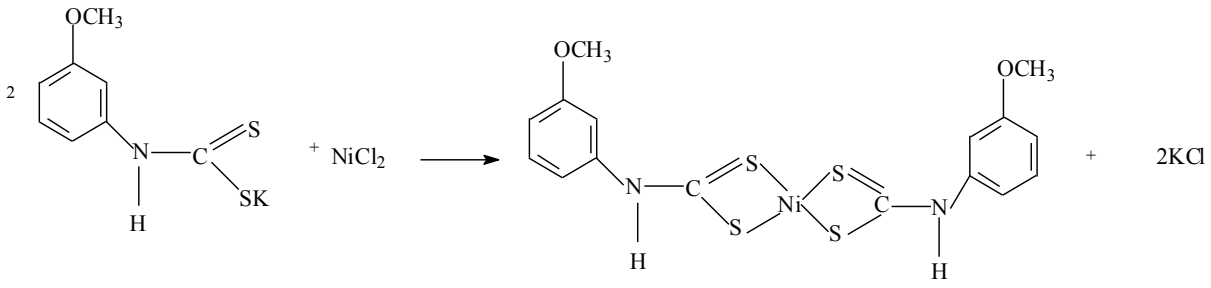

Scheme 2.5: Synthesis of nickel(II) anisidine dithiocarbamate

2.5.2 Synthesis of bis(acetonitrile)palladium(II) [3]

2 g of palladium chloride reacted with 40 mL of acetonitrile at 60 °C for 30 minutes, product was then evaporated using a rotatory evaporator, filtered, washed and then dried.

$$PdCl_2 + CH_3CN \xrightarrow[\text{at } 60\ ^0C]{\text{Acetonitrile}} PdCl_2(CH_3CN)_2$$

Scheme 2.6: Synthesis of bis(acetonitrile) palladium(II)

2.5.3 Synthesis of palladium(II) anisidine dithiocarbamate complex [$Pd(L^1)_2$]

0.4 g (2.5 mmol) of the precursor (palladium acetonitrile) was dissolved in 80 mL of acetone; 0.45 g (5 mmol) of the ligand was dissolved in 50 mL acetone and refluxed at 60 °C for four hours after which it was left at room temperature for six hours. The resulting product was evaporated, washed with water followed by diethyl ether and dried [4].

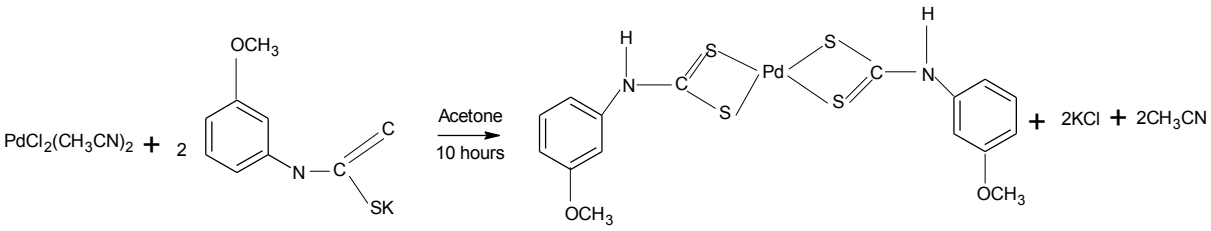

Scheme 2.7: Synthesis of palladium(II) anisidine dithiocarbamate complex

2.5.4 Synthesis of nickel(II) dibenzyl dithiocarbamate complex [$Ni(L^2)_2$]

0.57 g (5 mmol) of dibenzyl dithiocarbamate ligand was dissolved in 10 mL of methanol in a beaker. 0.59 g (2.5 mmol) of $NiCl_2$ was dissolved in a separate beaker. The two solutions

were mixed and stirred immediately. The reaction occurred at room temperature for 1-3 hours. The resulting product was filtered, washed and dried.

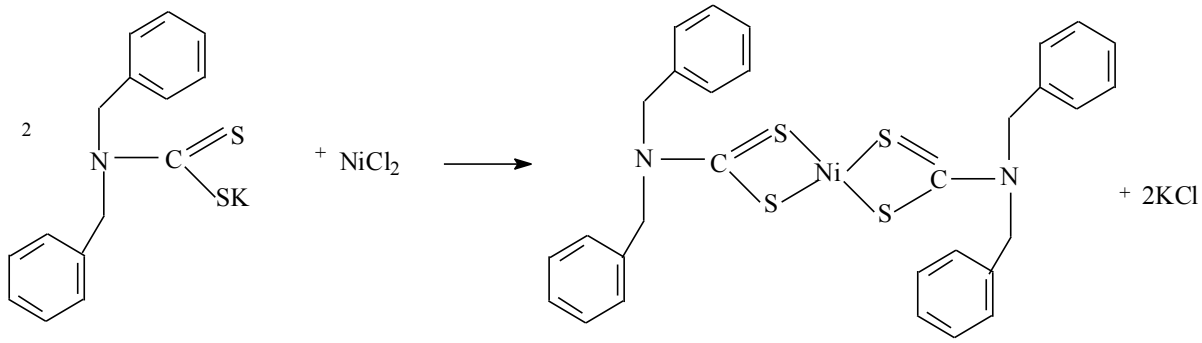

Scheme 2.8: Synthesis of nickel(II) dibenzyl dithiocarbamate complex

2.5.5 Synthesis of palladium(II) dibenzyl dithiocarbamate complex [Pd(L^2)$_2$]

0.4 g (2.5 mmol) of palladium acetonitrile was dissolved in 80 mL of acetone; 0.45 g (5 mmol) dibenzyl dithiocarbamate was dissolved in 50 mL acetone, refluxed for 4 hours at 60 °C and then stirred for 6 hours at room temperature. The product was evaporated using rotatory evaporator, washed with water followed by diethyl ether and dried.

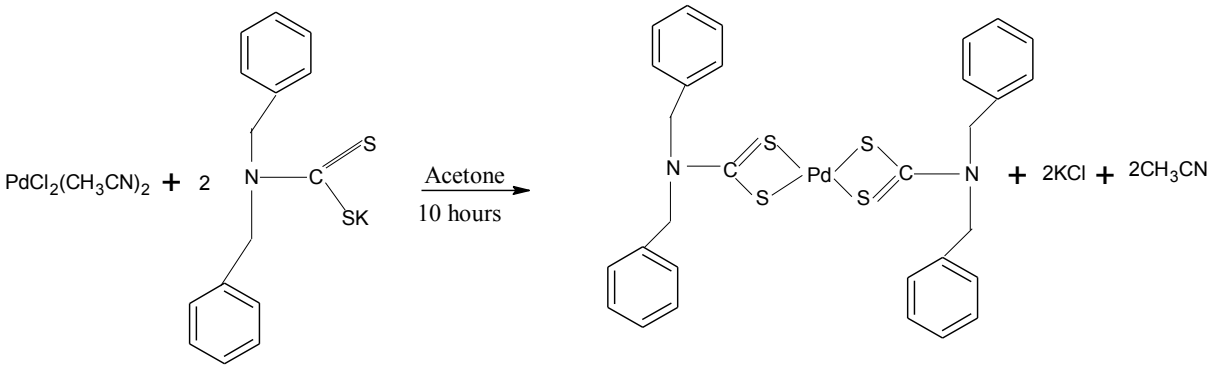

Scheme 2.9: Synthesis of palladium(II) dibenzyl dithiocarbamate complex

2.5.6 Synthesis of nickel(II) butyl dithiocarbamate complex [Ni(L^3)$_2$]

0.43 g (5 mmol) of butyl dithiocarbamate ligand was dissolved in 10 mL of methanol in a beaker. 0.59 g (2.5 mmol) of $NiCl_2$ was dissolved in a separate beaker. The two solutions were mixed and stirred, the reaction occurred at room temperature for 1-3 hours. The resulting product was filtered, washed and dried.

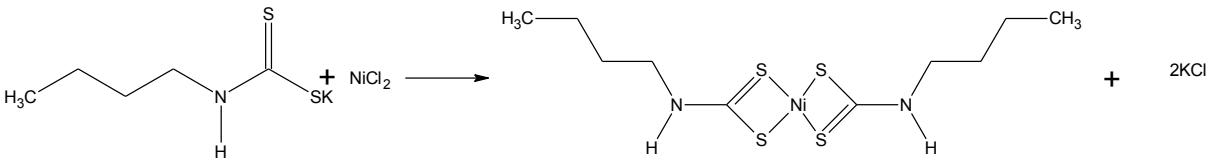

Scheme 2.10: Synthesis of nickel(II) butyl dithiocarbamate complex

2.5.7 Synthesis of palladium(II) butyl dithiocarbamate complex [Pd(L^3)$_2$]

0.4 g (2.5 mmol) of palladium acetonitrile and 0.43 g (5 mmol) of butyl dithiocarbamate were refluxed in acetone at 60 °C for 4 hours and stirred for 6 hours at room temperature. The product was filtered, washed with water and diethyl ether then dried.

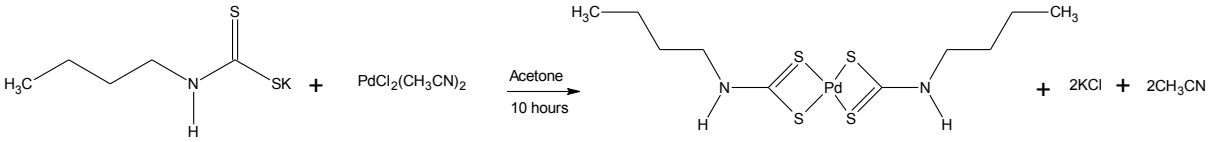

Scheme 2.11: Synthesis of palladium(II) butyl dithiocarbamate complex

2.5.8 Synthesis of nickel(II) imidazolyl dithiocarbamate complex [Ni(L^4)$_2$]

0.53 g (5 mmol) of imidazole dithiocarbamate ligand was dissolved in 10 mL of methanol in a beaker. 0.59 g (2.5 mmol) of $NiCl_2$ was dissolved in a separate beaker. The two solutions were mixed and stirred immediately. The reaction occurred at room temperature for 1-3

hours. The resulting product was filtered, washed with deionised water followed by diethyl ether and dried.

Scheme 2.12: Synthesis of nickel(II) imidazolyl dithiocarbamate complex

2.5.9 Synthesis of palladium(II) imidazolyl dithiocarbamate complex $[Pd(L^4)_2]$

0.4 g (2.5 mmol) palladium acetonitrile was dissolved in 80 mL of acetonitrile, 0.53 g (5 mmol) of imidazole dithiocarbamate was dissolved in 50 mL of acetone and refluxed at 60 °C for 4 hours and then stirred at room temperature for 6 hours. The precipitate was filtered and washed with water followed by diethyl ether and dried.

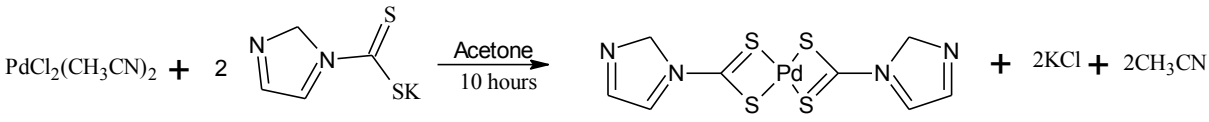

Scheme 2.13: Synthesis of palladium(II) imidazolyl dithiocarbamate complex

References

1. Ekennia, A.C. Antibacterial application of novel mixed ligand dithiocarbamate complexes of nickel(II). *J. Appl. Chem*. **2013**, 5, 36-39.

2. Tsuchida, E.; Oyaizu, K.; Ishii, Y.; Yamamoto, K. Synthesis and characterization of nickel dithiocarbamate complexes bearing ferrocenyl subunits. *Chem. Eur. J.* **1999**, 5(11), 3193-3201.

3. Bego, A.M.; Frem, R.C.G.; Netto, A.V.G.; Mauro, A.E.; Ananias, S.R.; Carlosb, I.Z.; Rochab, M.C. Immunomodulatory effects of palladium(II) complexes of 1,2,4-triazole on murine peritoneal macrophages. *J. Braz. Chem. Soc*. **2009**, 20(3), 437-444.

4. Hadizadeh, S.; Mazani, M.; Najafzadeh, N.; Niapour, A.; Amani, M.; Monsouri-Torshizi, H. Cytotoxic effects of newly synthesized palladium(II) complexes of diethyldithiocarbamate on gastrointestinal cancer cell lines. *Biochem. Res. Int*. **2014**, 1-9.

CHAPTER THREE

3.0. CHARACTERIZATION OF THE DITHIOCARBAMATE LIGANDS AND NI(II) AND PD(II) COMPLEXES

3.1. Introduction

This chapter provides the findings or results obtained using different physical measurements and spectroscopic techniques. It also describes the physiochemical results of all synthesized ligands and complexes. Dithiocarbamates belong to a large group of compounds called 1,1-dithiolates and this group have other compounds such as dithiophosphinates, dithiocarbimates, xanthates and so forth [1]. Dithiocarbamates have been widely studied because of their properties [2]. Most studies have been conducted in complexing these dithiocarbamate ligands with transition metals and use them in different fields [3-5].

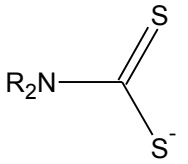

Figure 3.1: General formula of dithiocarbamate [4].

Dithiocarbamates can act as monodentate, bidentate chelating or bidentate bridging as shown below:

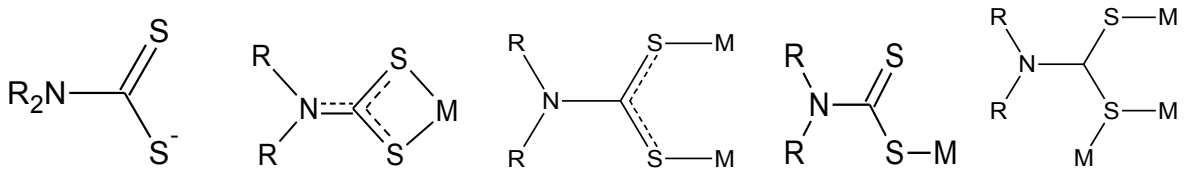

Figure 3.2: Different binding modes of dithiocarbamates [5].

Nickel complexes are green in colour and palladium complexes are brown, they are highly stable at room temperature. They are insoluble in water and soluble in most organic solvents.

3.2. Synthesis

The complexes were synthesised following the literature procedure [6, 7]. Dithiocarbamates are prepared by the reaction of primary or secondary amine with carbon disulfide in the presence of a strong base (KOH) as shown in scheme 2.1 to 2.4. Dithiocarbamate complexes are formed by reacting 2 moles of each dithiocarbamate ligand with 1 mole of $NiCl_2$ or $[PdCl_2(CH_3CN)_2]$. The compounds are formulated as four coordinate species in which the dithiocarbamate acts as bidentate chelating ligands as shown in scheme 2.5 to 2.13. The elemental analytical data are presented in Table 3.1 while their solubility is presented in Table 3.2.

Table 3.1: Elemental analysis

Compounds	Formula	Molecular weight (g/mol)	C Found (Cal)	H Found (Cal)	N Found (Cal)	S Found (Cal)
$L^1 \cdot 3H_2O$	$C_8H_8KNS_2(H_2O)_3$	221.38	28.2 (32.97)	4.03 (4.84)	4.12 (4.81)	20.54 (22.00)
$L^2 \cdot 3H_2O$	$C_{14}H_{13}KNS_2(H_2O)_3$	365.55	47.96 (49.28)	5.44 (5.51)	3.73 (3.83)	17.68 (17.54)
$L^3 \cdot 3H_2O$	$C_5H_{10}KNS_2(H_2O)_3$	241.41	25.92 (24.88)	7.53 (6.68)	6.06 (5.80)	27.77 (26.56)
$L^4 \cdot 3H_2O$	$C_4H_4KNS_2(H_2O)_3$	237.35	29.91 (20.30)	3.32 (4.25)	16.83 (11.80)	20.38 (27.01)
$[Ni(L^1)_2] \cdot 3H_2O$	$C_{16}H_{16}N_2NiO_2S_4(H_2O)_3$	509.31	33.28 (37.73)	2.23 (4.35)	4.89 (5.50)	23.22 (25.80)
$[Ni(L^2)_2] \cdot 3H_2O$	$C_{30}H_{28}N_2NiS_4(H_2O)_3$	657.56	37.41 (54.80)	3.53 (5.21)	2.96 (4.26)	13.17 (19.51)
$[Ni(L^3)_2] \cdot 3H_2O$	$C_{10}H_{20}N_2NiS_4(H_2O)_3$	409.28	31.7 (29.35)	6.14 (6.40)	7.41 (6.84)	34.38 (31.34)
$[Ni(L^4)_2] \cdot 3H_2O$	$C_8H_8N_4NiS_4(H_2O)_3$	401.18	20.66 (23.98)	2.08 (3.52)	10.4 (13.97)	21.53 (31.97)
$[Pd(L^1)_2] \cdot 3H_2O$	$C_{16}H_{16}N_2PdO_2S_4(H_2O)_3$	557	20.32 (34.50)	1.62 (3.98)	2.99 (5.03)	16.13 (23.02)
$[Pd(L^2)_2] \cdot 3H_2O$	$C_{30}H_{28}N_2PdS_4(H_2O)_3$	705.27	46.72 (51.09)	3.75 (4.86)	3.72 (3.97)	17.43 (18.19)
$[Pd(L^3)_2] \cdot 3H_2O$	$C_{10}H_{20}N_2PdS_4(H_2O)_3$	457.00	29.7 (26.28)	5.63 (5.00)	6.92 (6.13)	33.21 (28.07)
$[Pd(L^4)_2] \cdot 3H_2O$	$C_8H_8N_4PdS_4(H_2O)_3$	448.90	14.68 (21.40)	1.05 (3.14)	6.83 (12.48)	24.47 (28.57)

Table 3.2: Solubility test results

Compounds	**Water**	**Methanol**	**DCM**	**CHL**	**Acetone**	**Hexane**	**DMSO**
L^1	Yes	Yes	Yes	No	Yes	No	Yes
L^2	Yes	Yes	Yes	Yes	Yes	No	Yes
L^3	Yes	Yes	Yes	No	Yes	No	Yes
L^4	Yes	Yes	Yes	No	Yes	No	Yes
$[Ni(L^1)_2]$	No	Yes	Yes	Yes	Yes	Yes	Yes
$[Ni(L^2)_2]$	No	Yes	Yes	Yes	Yes	Yes	Yes
$[Ni(L^3)_2]$	No	Yes	Yes	Yes	Yes	No	Yes
$[Ni(L^4)_2]$	No	Yes	Yes	Yes	Yes	No	Yes
$[Pd(L^1)_2]$	No	Yes	Yes	No	Yes	No	Yes
$[Pd(L^2)_2]$	No	Yes	Yes	Yes	Yes	Yes	Yes
$[Pd(L^3)_2]$	No	Yes	Yes	Yes	Yes	Yes	Yes
$[Pd(L^4)_2]$	No	Yes	Yes	No	Yes	No	Yes

Table 3.3: Physiochemical properties of ligands and metal complexes

Compounds	**Melting point (°C)**	**Conductivity (µs/cm)**	**Colour**	**Actual yield (g)**	**Percentage yield (%)**
L^1	94	48.6	White	3.4899	97
L^2	98	39.7	White	3.905	91
L^3	67	162.1	White	8.321	90
L^4	69	190.9	Yellow	3.2156	75
$[Ni(L^1)_2]$	201	12.97	Dark green	1.35	49
$[Ni(L^2)_2]$	200	40.7	Green	1.48	60
$[Ni(L^3)_2]$	139	9.23	Dark green	4.36	49
$[Ni(L^4)_2]$	124	76.9	Green	6.33	44
$[Pd(L^1)_2]$	230	3.28	Brown	0.34	48
$[Pd(L^2)_2]$	260	1.81	Brown	0.28	67
$[Pd(L^3)_2]$	180	2.45	Brown	0.45	51
$[Pd(L^4)_2]$	185	1.43	Brown	0.421	67

All compounds and their percentage yields are presented in Table 3.3, from the results the yields of dithiocarbamate ligands are high because the ligands were purely synthesized and recrystallized to give a crude product and the actual mass weighed is not too far from theoretical mass that is calculated. Purity of all synthesised ligands and complexes has been determined by melting point, the obtained results are presented in Table 3.3. All ligands melt in the range of 67-98 °C. For the four synthesized nickel(II) complexes, $[Ni(L^3)_2]$ and $[Ni(L^4)_2]$ melt around 124-139 °C, $[Ni(L^1)_2]$ and $[Ni(L^2)_2]$ around 200 °C. For palladium(II) complexes, $[Pd(L^1)_2]$ and $[Pd(L^2)_2]$ decompose at 230 °C and 260 °C respectively, while

$Pd(L^3)_2$ and $Pd(L^4)_2$ melted around 183-185 °C. Results for conductivity measurement are presented on Table 3.3, and from the results all compounds were found to be non-electrolytes [8].

3.3. FTIR spectra studies of the ligands and metal complexes

FTIR is used as a fingerprint in determining the chemical nature of compounds and the structure looking at the major functional groups present in each compound [9]. In dithiocarbamate compounds there are four peaks of interests that are expected from the FTIR spectra, νN-H, νC-N, νC=S, νC-S. N-H for primary amines differs from that of secondary amines; primary amines are in the range of 3200-3400 and secondary amine around 3300-3400 [9, 10]. The summarized FTIR data are shown in Table 3.4.

Table 3.4: Selected FTIR spectra data for ligands and metal complexes

Compounds	**νN-H (cm^{-1})**	**νC-N (cm^{-1})**	**C-S (cm^{-1})**	**C=S (cm^{-1})**	**Ni-S/ Pd-S (cm^{-1})**
L^1	3574	1509	915	1178	-
L^2	3510	1474	761	1164	-
L^3	3495	1472	739	1164	-
L^4	3235	1473	739	1188	-
$[Ni(L^1)_2]$	3398	1469	824		375
$[Ni(L^2)_2]$	3420	1472	758		481
$[Ni(L^3)_2]$	3233	1595	738		384
$[Ni(L^4)_2]$	3391	1493	726		543
$[Pd(L^1)_2]$	3310	1558	1036		529
$[Pd(L^2)_2]$	-	1564	792		545
$[Pd(L^3)_2]$	3510	1595	1060		-
$[Pd(L^4)_2]$	-	1474	-	1101	545

3.3.1 FTIR spectra studies of anisidine dithiocarbamate and Ni(II) and Pd(II) complexes

FTIR spectra of anisidine dithiocarbamate and its corresponding complexes ($[Ni(L^1)_2$ and $[Pd(L^1)_2$) are presented in Figure 3.5. For anisidine dithiocarbamate (**L^1**), the νC-N appeared at 1421 cm^{-1}, νC=S at 1187 cm^{-1} and νC-S at 928 cm^{-1}. All peaks of interest were present in the FTIR spectrum of **L^1**, the shift in νC-N stretch to higher frequency from that of ligand was observed in both complexes, from 1421 cm^{-1} to 1466 cm^{-1} for $[Ni(L^1)]$ and to 1553 cm^{-1}

for $[Pd(L^1)_2]$ is due to the increase in the single bond character of νC-N. Also the shift in νC-S to lower frequency which can be ascribed to the decrease in the double bond character of νC=S in the formation of the complexes [10]. At 375 cm^{-1} the stretching vibration was observed and this confirms that the Ni ion is bonded to the dithiocarbamate through the sulfur atom, and Pd-S was observed at 560 cm^{-1}[11].

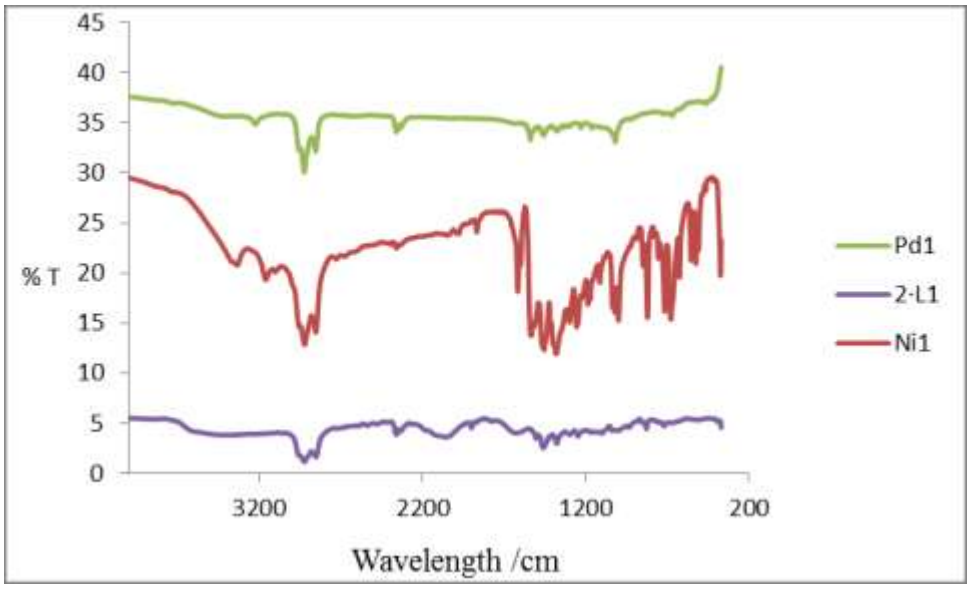

Figure 3.3: FTIR spectra of anisidine dithiocarbamate and Ni(II) and Pd(II) complexes

3.3.2 FTIR spectra studies of dibenzyl dithiocarbamate and Ni(II) and Pd(II) complexes

All relevant peaks of interest were assigned from the spectra of the compound shown in Figure 3.6 and the νC-N stretch is observed at 1461 cm^{-1}, νC=S at 1000 cm^{-1} and νC-S at 832 cm^{-1}. These are the three important peaks of interest in the dithiocarbamate compounds. There is a sharp peak in both complexes around 761 cm^{-1} and is attributed to νC-S, and confirms that dithiocarbamates are bidentately coordinated to the metal ions. There is a shift in the νC-N stretching vibrations to higher frequency as compared to that of the ligand, and

this is due to the increasing single bond character of νC-N. The νNi-S peak appeared at 473 cm^{-1} which confirms the formation of the metal complex [12].

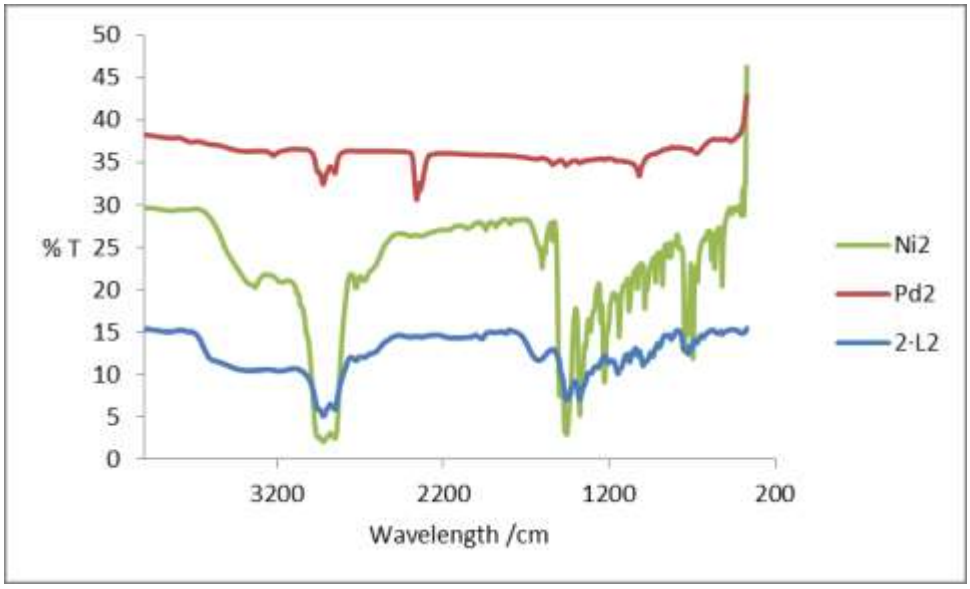

Figure 3.4: FTIR spectra of Ni(II) and Pd(II) dibenzyl dithiocarbamate complexes

3.3.3 FTIR spectra of butyl dithiocarbamate and its Ni(II) and Pd(II) complexes

The FTIR spectra of butyl dithiocarbamate and its metal complexes are shown in Figure 3.7. Butyl dithiocarbamate have all the peaks of interest, νC-N at 1461 cm^{-1}, νC=S at 1166 cm^{-1} and νC-S at 1012 cm^{-1}. $[Ni(L^3)_2]$ have νC-N at 1471 cm^{-1} which shifted a little bit to higher frequency from that of the ligand, νC-S is observed at 721 cm^{-1}, this shifted to lower frequency and can be attributed to the decrease in the double bond character of C=S. The νNi-S stretching vibration appeared at 383 cm^{-1} and νPd-S at 625 cm^{-1} which indicates that the metal ions are coordinated to the butyl dithiocarbamate through the sulfur atoms [13].

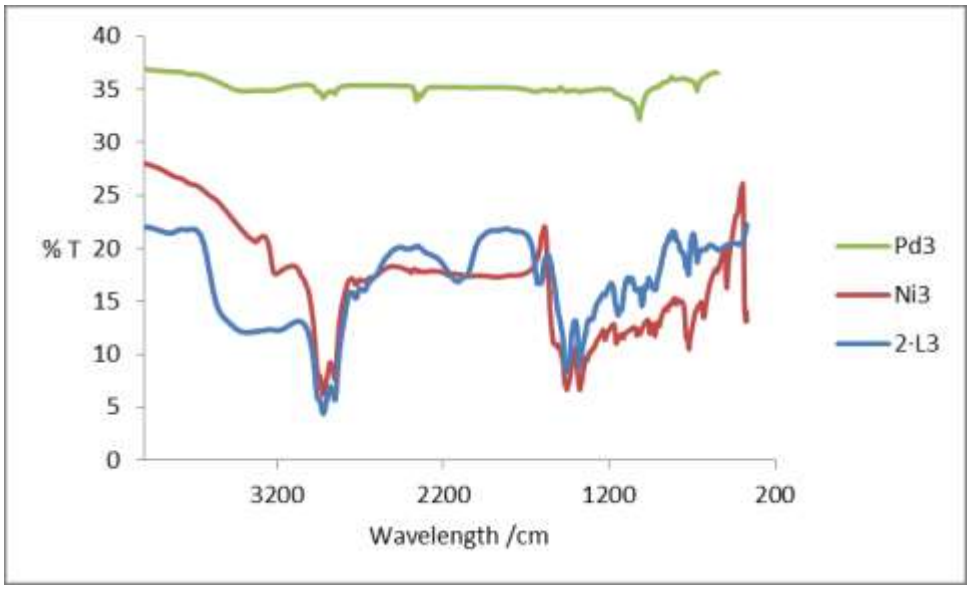

Figure 3.5: FTIR spectra of Ni(II) and Pd(II) butyl dithiocarbamate complexes

3.3.4 FTIR spectra of imidazolyl dithiocarbamate and Ni(II) and Pd(II) complexes

Imidazolyl dithiocarbamate has νC-N stretch at 1472 cm^{-1}, in the complexes, the νC-N stretching vibrations shifted to 1490 cm^{-1} in $[Ni(L^4)_2]$ and 1544 cm^{-1} in $[Pd(L^4)_2]$ (Figure 3.8). The νC=S that appeared as two bands at 1171 and 732 cm^{-1} in the ligand occurred as single sharp bands at 1096 cm^{-1}in $[Ni(L^4)_2]$ and 1048 cm^{-1} in $[Pd(L^4)_2]$. This confirms that the ligand is bidentately coordinated to the metal ion. The absence of N-H stretch is due to the deprotonating strong base (KOH). The νNi-S is observed at 551 cm^{-1} and νPd-S at 566 cm^{-1}, these two peaks confirms that the ligand used sulfur atom to bond itself to the metal centres.

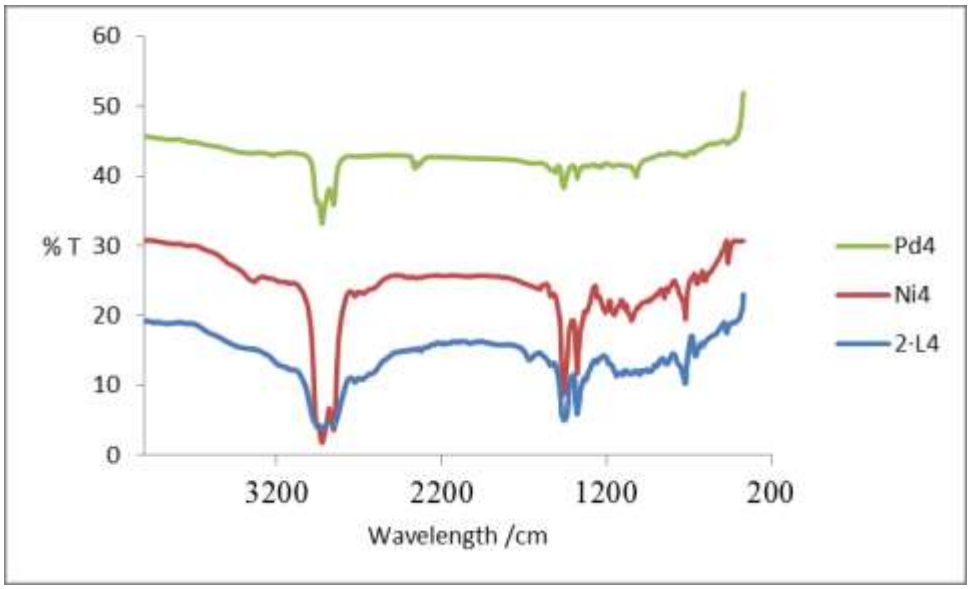

Figure 3.6: FTIR spectra of imidazolyl dithiocarbamate and Ni(II) and Pd(II) complexes

3.4. Electronic spectra studies of ligands and complexes

3.4.1. Electronic spectra of anisidine dithiocarbamate and Ni(II) complex

In the electronic spectra studies of the dithiocarbamates, there are three intraligand charge transfer transitions that are expected [15-17]. The electronic spectra of anisidine dithiocarbamate and Ni(II) complex is shown in Figure 3.9. Anisidine dithiocarbamate has an absorption band at 297 nm which is for π→π* transitions of N-C-S; the second one is at 303 nm which is assigned to π→π* transitions of S-C-S of dithiocarbamate moiety, and the last one is at 305 nm for n→π* bonding which is located on sulfur. In the Ni(II) anisidine dithiocarbamate, the intraligand charge transfer transitions occurred at 324 nm which is assigned to π→π* bonding of dithiocarbamate moiety. $[Ni(L^1)_2]$ also have an absorption band at 418 nm which is assigned to the d-d transition due to the excitation of the metal ions and this shows that the complex is a square planar [15].

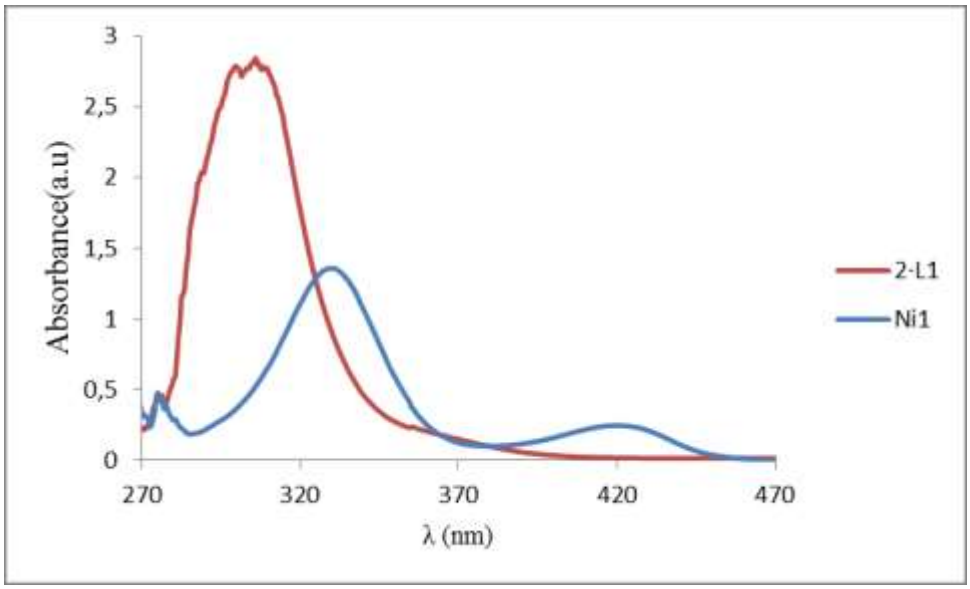

Figure 3.7: Electronic spectra of anisidine dithiocarbamate and Ni(II) complex

3.4.2. Electronic spectra of dibenzyl dithiocarbamate and Ni(II) complex

The electronic spectra of dibenzyl dithiocarbamate and Ni(II) complex is shown in Figure 3.10. Dibenzyl dithiocarbamate has intraligand charge transfer transitions at 295 nm, $[Ni(L^2)_2]$ also have intraligand charge transfer transitions but it shifted to higher wavelength at 332 nm and another band at 391 which is due to metal ligand charge transfer transitions. At 430 nm there is a small band for d-d transition observed in the Ni(II) complex. Baja reported nickel complexes with d-d transitions in the range of 410-453 and the second one ranging from 622-668 nm confirming the proposed square planar geometry around the Ni^{2+} ion [16, 17].

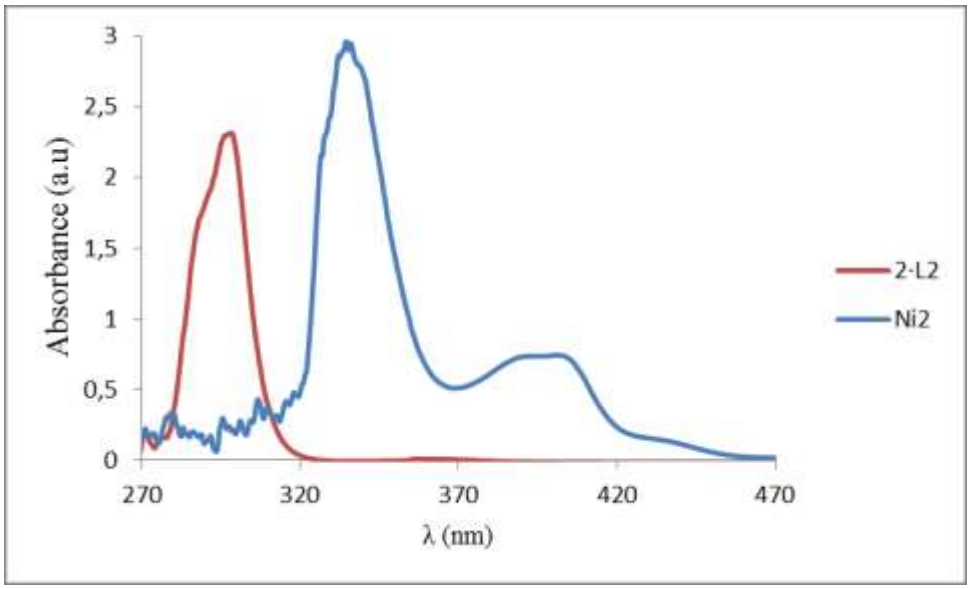

Figure 3.8: Electronic spectra of dibenzyl dithiocarbamate and Ni(II) complex

3.4.3. Electronic spectra of butyl dithiocarbamate and Ni(II) complex

The electronic spectra of the ligand and Ni(II) complex is shown in Figure 3.11. Butyl dithiocarbamate has a band at 291 nm, which is assigned to the $\pi \rightarrow \pi^*$ transition of the dithiocarbamate moiety. The $[Ni(L^3)_2]$ show a broad absorption band at 397 nm assigned to the MLCT. At 418 nm, there is a small band assigned to the d-d transition [15, 16]. This indicates the complex is a four coordinate square planar species [15, 16].

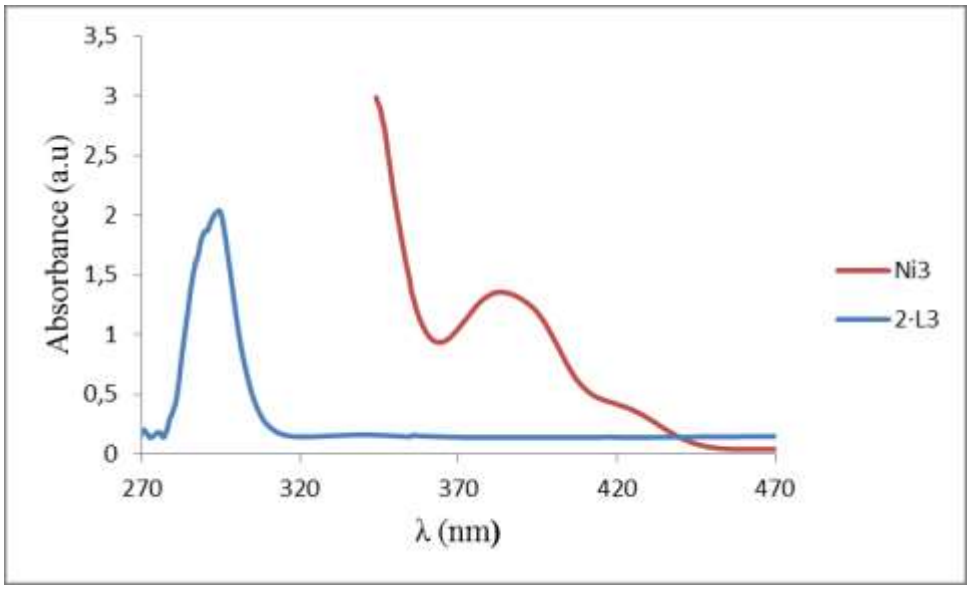

Figure 3.9: Electronic spectra of butyl dithiocarbamate and Ni(II) complex

3.4.4. Electronic spectra studies of imidazolyl dithiocarbamate and Ni(II) complex

The electronic spectra of the ligand and Ni(II) complex is presented in Figure 3.12. From the spectra, **L^4** have an absorption band at 301 nm, $[Ni(L^4)_2]$ has a band at 331 which is also intraligand charge transfer transition of the dithiocarbamate moiety. From the reported nickel imidazole dithiocarbamate complex there are two d-d transitions obtained at 408 nm and 472 nm [16, 17]. This complex had d-d transitions with λ_{max} at 477 and 410 nm, in addition to its higher energy charge transfer transition (LMCT) absorption at 304 nm and 375 nm. The reported imidazole had one broad d-d transition around 467 nm and two intense ligand charge transfer bands at 211 and 288 nm, and it was confirmed to be a four coordinate square planar complex [17].

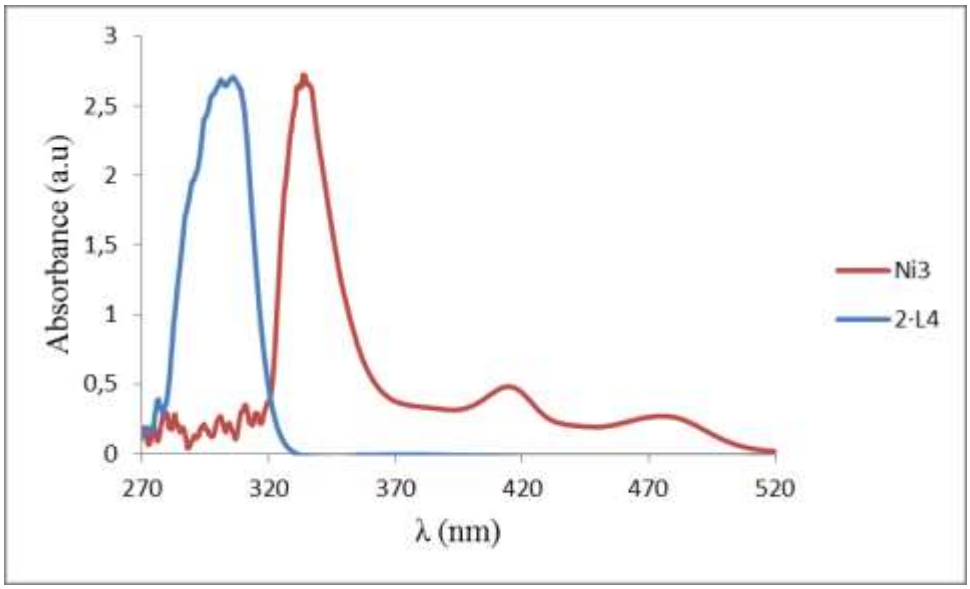

Figure 3.10: Electronic spectra of imidazolyl dithiocarbamate and Ni(II) complex

3.4.5. Electronic spectra of anisidine dithiocarbamate and Pd(II) complex

The electronic spectra of anisidine dithiocarbamate and Pd(II) complex is presented in Figure 3.13. Anisidine dithiocarbamate has an absorption band at 297 nm, 300 nm, and 304 nm which can be attributed to $\pi \rightarrow \pi^*$ transition of N-C-S, $\pi \rightarrow \pi^*$ associated with the S-C-S of dithiocarbamate moiety and $n \rightarrow \pi^*$ located on sulfur respectively. Palladium(II) anisidine dithiocarbamate display very strong charge transfer transitions at 328 nm, since palladium is diamagnetic, it does not have d-d transition because all electrons are paired up.

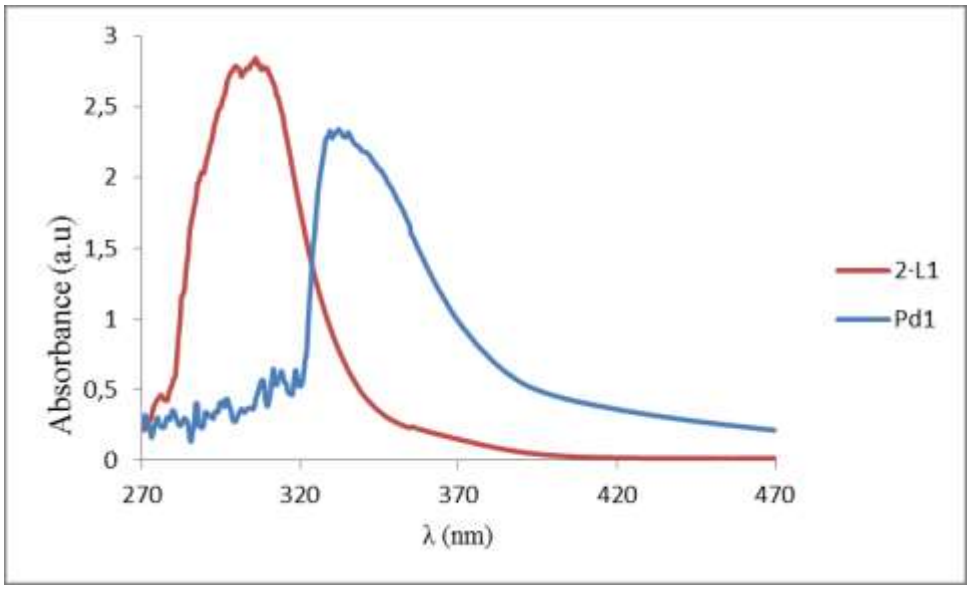

Figure 3.11: Electronic spectra of anisidine dithiocarbamate and Pd(II) complex

3.4.6. Electronic spectra of dibenzyl dithiocarbamate and Pd(II) complex

The electronic spectra of the ligand and complex are shown in Figure 3.14. Dibenzyl dithiocarbamate has a band at 294 nm which is attributed to $\pi \rightarrow \pi^*$ transition of the dithiocarbamate group. In the complex spectrum, there is a strong broad band starting at about 350 nm that could be ascribed to the MLCT due to the coordination of the ligand to the Pd^{2+} ion. This confirms the square planar geometry around Pd(II) in the complex [16, 18].

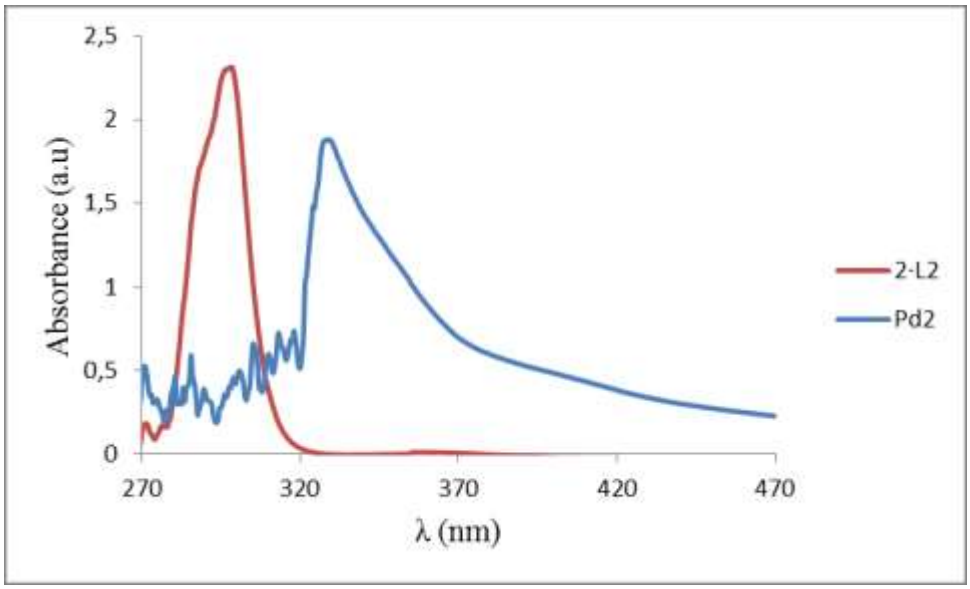

Figure 3.12: Electronic spectra of dibenzyl dithiocarbamate and Pd(II) complex

3.4.7. Electronic spectra of butyl dithiocarbamate and Pd(II) complex

The electronic spectra of the Pd(II) and the ligand is shown in Figure 3.15. Butyl dithiocarbamate has an absorption band at 291 nm assigned to the intraligand $\pi \rightarrow \pi^*$ transition. A broad band at 355 nm assigned to the MLCT is observed. There are strong charge transfer transitions present in palladium(II) complexes since they are diamagnetic, with no visible d-d transitions.

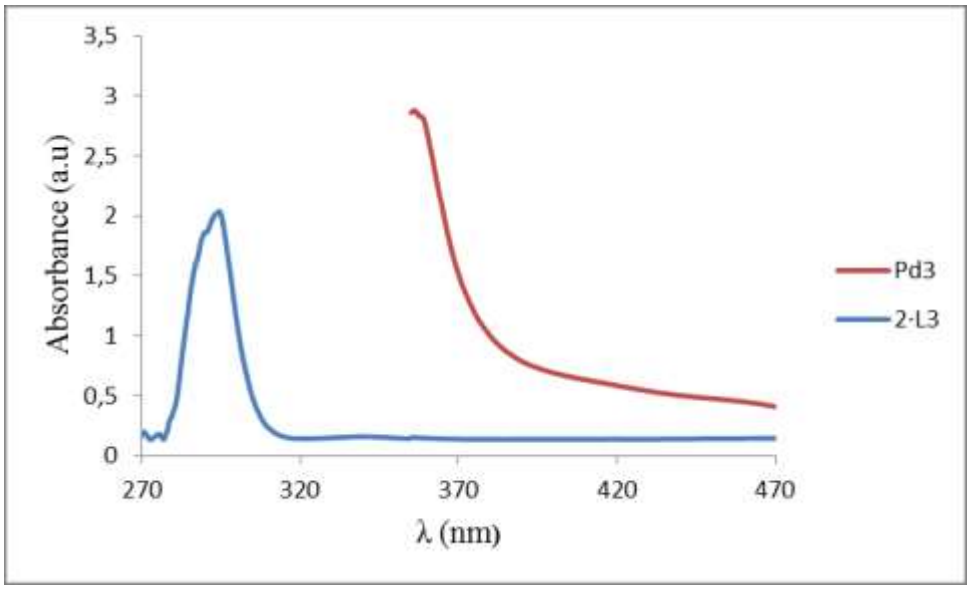

Figure 3.13: Electronic spectra of butyl dithiocarbamate and palladium complex

3.4.8. Electronic spectra of imidazolyl dithiocarbamate and Pd(II) complex

The electronic spectra of the ligand and Pd(II) complex is presented in Fig. 3.16. Imidazolyl dithiocarbamate has an absorption band at 297 nm for π→π* transitions of N-C-S and at 303 for n→π* bonding located on sulfur. Marov *et al*. reported three spin allowed singlets in diamagnetic palladium complexes and d-d transitions, but from the spectra shown in Figure 3.16 there is no d-d transition because the strong charge transfer transitions prevent the expected bands and show a strong band which is attributed to sulfur to metal charge transfer transitions [18].

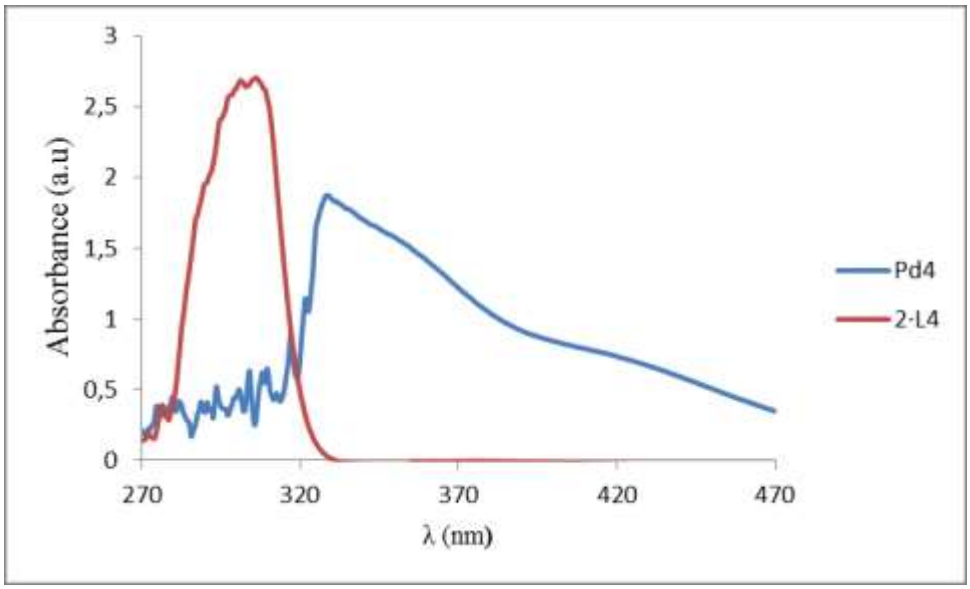

Figure 3.14: Electronic spectra of imidazolyl dithiocarbamate and palladium(II) complex (Pd4)

3.5 NMR spectra studies

^{1}H-NMR was done for ligands and palladium complexes because nickel is paramagnetic and it can spoil the machine.

3.5.1. ^{1}H-NMR of anisidine dithiocarbamate

^{1}H-NMR spectrum of anisidine dithiocarbamate displays doublets from 6.76-7.38 ppm (d, 2H) for =CH-CH= protons of the aromatic ring. A sharp singlet peak appeared at 2.5 ppm (s, 1H) =CH- of the ring and another singlet at 9.80 ppm (s, 1H) for N-H proton. These peaks confirm the formation of the ligand [19].

3.5.2. ^{1}H-NMR of dibenzyl dithiocarbamate

The ^{1}H-NMR of potassium dibenzyl dithiocarbamate displays a single sharp peak at 3.35 ppm is due to the solvent deuterated dimethyl sulfoxide (dmso-d_6) used. The multiplets peaks in the range of 7.23-7.21 ppm (m, 5H-C_6H_5) were from the aromatic ring protons (1,3H). At 5.30 ppm, there was a singlet peak (s, 2H- CH_2) due to the ethyl protons [20, 21].

3.5.3. ^{1}H-NMR of butyl dithiocarbamate

^{1}H-NMR of butyl dithiocarbamate ligand showed triplet at 0.87 ppm (t, 3H) of methyl protons. Multiplets were observed around 0.92 to 1.26 ppm (m, 4H) of the ethyl protons in the chain of butyl dithiocarbamate. At 7.8 ppm, there was a singlet peak (s, 1H) of the NH proton. The other peaks are due to the DMSO-d_6 solvent used.

3.5.4. ^{1}H-NMR of imidazolyl dithiocarbamate

^{1}H-NMR spectrum of imidazolyl dithiocarbamate displays one singlet peak at 2.5 ppm (s,2H) for the ethyl proton attached to nitrogen atoms. Two other singlet peaks which appeared at 7.03 ppm (s, 1H) and at 7.65 ppm (s,1H) for the CH proton attached to the nitrogen of the cyclic ring. The sharp peak observed at 3.1 ppm was due to the solvent used which was deuterated dimethyl sulfoxide, DMSO-d_6 [22].

3.5.5. ^{1}H-NMR of palladium(II) anisidine dithiocarbamate complex

^{1}H-NMR spectra of [Pd(L^1)$_2$] displays a singlet at 8.45 ppm (s, 1H) for N-H proton of anisidine dithiocarbamate. A downfield by δ 1.35 ppm as compared to the chemical shift of

the ligand was observed. It also displays multiplets from 7.41-6.91 ppm (m, 4H) for the aromatic ring protons from the ligand [20,22].

3.5.6. ^{1}H-NMR of palladium(II) dibenzyl dithiocarbamate complex

The ^{1}H-NMR signals of Pd(II) dibenzyl dithiocarbamate complex were carefully assigned, it displays a sharp singlet peak at 4.90 ppm (s, 2H) due to the ethyl protons attached to the aromatic ring. Multiplets appeared in the region 7.35-7.30 for the aromatic ring protons of the ligand. An upfield shift of about δ 0.12 ppm as compared to the chemical shift of the ligand was observed. A downfield by δ 0.4 ppm compared to the chemical shift of the dibenzyl dithiocarbamate was also observed in the complex [19].

3.5.7. ^{1}H-NMR of palladium(II) butyl dithiocarbamate complex

Palladium(II) butyl dithiocarbamate complex have its CH_3 protons split at a δ 0.98 ppm (t,3H) into a triplet by the adjacent CH_2 group. Both ethyl protons were split into multiplet by the neighbouring protons at 1.30 and 1.53 ppm. The δ of protons in the N-CH_2 occurred at 8.7 ppm [14].

3.5.8. ^{1}H-NMR of palladium(II) imidazolyl dithiocarbamate complex

^{1}H-NMR of Pd(II) imidazolyl complex displays a sharp singlet peak at 1.4 ppm (s, 1H) for N-H proton, a second singlet at 2.1 ppm (s, 1H) for NH proton of the cyclic ring from the ligand, another singlet peak at 3.7 ppm for NH proton of the cyclic ring again. A downfield by δ 1.0 ppm as compared to the chemical shift of the ligand was observed.

3.6 References

1. Dawood, Z.F.; Mohammed, T.J.; Sharif, M.R. New nickel(II) complexes with benzilbis (semicarbazone) and dithiocarbamate ligands. *Irish Vet J*., **2009**, 23, 135-141.

2. Hogarth, G.; Rainford-Brent, E-J.C-R.C.R.; Kabir, S.E.; Richards, I.; Wilton-Ely, J.D.E. T.; Zhang, Q. Functionalized dithiocarbamate complexes: Synthesis and molecular structures of 2-diethylaminoethyl and 3-dimethylaminopropyl dithiocarbamate complexes [M{$S_2CN(CH_2CH_2NEt_2)_{(2)}$}(n)] and [M{$S_2CN(CH_2CH_2CH_2NMe_2)$(n)] (n=2, M= Ni, Cu, Zn, Pd; n=3, M= Co). *Inorg*. *Chim*. *Acta*, **2009**, 362, 2020-2026.

3.Serano, A.; Ma, C.; Cristofori, P.; Venturini, M.B.; Giovagnini, L.; Fregona, D. Synthesis of a palladium(II)-dithiocarbamate complexes: Biological assay and nephrotoxicity in rats. *Arch*. *Toxicol*. **2002**, 76, 262-268.

4. Nabipouri, H.; Ghammamy, S.; Ashuri, S.; Aghbolag, Z.S. Synthesis of new dithiocarbamate compound and study of its biological properties. *Org*. *Chem*. *J*. **2010**, 2, 75-80.

5. Kanchi, S.; Singh, P.; Bisetty, K. Dithiocarbamates as hazardous remediation agent: A critical review progress in environmental chemistry for inorganic species studies of 20^{th} century. *Arab*. *J*. *Chem*. **2014**, 7, 11-25.

6. Ekennia, A.C. Antibacterial application of novel mixed ligand dithiocarbamate complexes of nickel(II). *J*. *Appl*. *Chem*. **2013**, 5, 36-39.

7. Tsuchida, E.; Oyaizu, K.; Ishii, Y.; Yamamoto, K. Synthesis and characterization of Nickel dithiocarbamate complexes bearing ferrocenyl subunits. *Chem*. *Eur*. *J*. **1999**, 5(11), 3193-3201.

8. Mansouri-Torshizi, H.; Khosravi, F.; Hassani, F.; Saeidifar, M.; Divslar, A.; Saboury, A. A. DNA binding and antitumor activity of α-diimineplatinum(II) and palladium(II) dithiocarbamate complexes. *Bioinorg*. *Chem*. *Appl*. **2011**, 394506, 1-12.

9. Khan, H.; Butler, I.S.; Badshah, A.; Murtaz, G.; Said, M.; Rehman, Z.; Neuhausen, C.; Todorova, M.; Jean-Claude, B. Synthesis, characterization and anticancer studies of mixed ligand dithiocarbamate palladium complexes. *Eur*. *J*. *Med*. *Chem*. **2011**, 46, 4071-4077.

10. Shi, Y.; Chu, W.; Wang, Y.; Du, J.; Li, S.; Zhou, G.; Qin, X.; Zhang, C.; Wang, J. Synthesis, characterization and cytotoxicity of the Au(III) complexes with cyclic amine-based dithiocarbamate ligands. *Inorg*. *Chem*. *Commun*. **2013**, 30, 178-181.

11. Vijayanthimala, V.; Gomathi, B.K.; Vijaya, M. Synthesis, characterization and study of biological application of simple mixed ligand complexes of nickel(II) with morphiline dithiocarbamate and amine such as ethylenediamine, diethylenetriamine and triethylenetetraamine. *Res*. *J*. *Pharm*. *Bio*. *Chem*. *Sci*. (RJPBCS), **2014**, 5(3), 1832-1837.

12. Odola, A.J.; Woods, J.A.O. Synthesis, characterization and antimicrobial activity studies of new nickel(II) mixed ligand complexes of disubstituted dithiocarbamates with ethylsalicylaldiminate. *Arc*. *Apl*. *Sci*. *Res*. **2011**, 3(4), 463-470.

13. Oliveira, M.R.L.; Diniz, R.; De Bellis, V.M.; Fernandes, N.G. Nickel(II) complexes of dithiocarbamates from sulphonamides: Synthesis and crystal structures. *Polyhedron*, **2003**, 22, 1561-1566.

14. Husarek, J.; Pastorek, R.; Malon, M; Sindalar, Z.; Pavlicek, M. Nickel(II) cyclohexylethyl dithiocarbamate complexes with monodentate P-donor ligands in the coordination sphere. *J*. *Serb*. *Chem*. *Soc*. **2004**, 69(12), 1053-1061.

15. Jenkins, R.M.; Singleton, M.L.; Almaraz, E.; Reibenspies, J.H.; Darensbourg, M.Y. Imidazole-containing (N_3S)-Ni^{II} complexes relating to nickel containing biomolecules. *Inorg*. *Chem*. **2009**, 48, 7280-7293.

16. Khan, H.; Badshah, A.; Rehman, Z.; Said, M.; Murtuza, G.; Shah, A.; Ahmed, S.l Butler, I.S.; Fontaine, F.G. New dimeric and supramolecular mixed ligand palladium(II) dithiocarbamates as potent DNA binders. *Polyhedron*, **2012**, 39, 1-8.

17. Baja, S.C.; Mishra, A. Synthesis and spectroscopic characterization of bis(N-alkyldithiocarbamato) nickel(II) complexes: Crystal structures of [$Ni(S_2CNH(n\text{-}Pr))_2$] and [$Ni(S_2CNH(i\text{-}Pr))_2$]. *J. Coord*. *Chem*. **2011**, 64(15), 2727-2734.

18. Manov, N.; Mishra, A. K.; Kaushik, N.K. Triphenylphosphine adducts of platinum(IV) and palladium(II) dithiocarbamate complexes: A spectral and in vitro study. *Spectrochim*. *Acta*. Part A, **2004**, 60, 3087.

19. Prakasam, B.A.; Ramalingam, K.; Bocelli, G.; Cantoni, A. NMR and fluorescence spectral studies on bisdithiocarbamates of divalent Zn, Cd and their nitrogenous adducts: Single crystal X-ray structure of (1,10-phenanthroline)bis(4-methylpiperazinecarbodithioato) zinc(II). *Polyhedron*. **2007**, 26, 4489–4493.

20. Tamizmani, M; Kankanala, R.; Sivasankar, C. Coordinated and uncoordinated anion dictated coordination mode of PN(Me)P ligand in Pd(II) complexes and their catalytic applications. *J. Organomet*. *Chem*. **2014**, 6(12), 763-764.

21. Akhtar, J.; Afzaal, M.; Vincent, M.A.; Burton, N.A.; Raftery, I.; Hillier, I.H.; O'Brien, P. Understanding the decomposition pathways of mixed sulphur/selenium lead phosphinato complexes explaining the formation of lead selenide. *J. Phys*. *Chem*. **2011**, 115(34), 16904-16909.

22. Trevisan, A.; Marzono, C.; Cristofori, P.; Venturini, M.B.; Giovagnini, L.; Fregona, D. Synthesis of a palladium(II)-dithiocarbamate complex: Biological assay and nephrotoxicity in rats. *Arch. Toxicol*. **2002**, 76, 262-268.

CHAPTER FOUR

SYNTHESIS AND STRUCTURAL STUDIES OF HDA-CAPPED NIS, PDS NANOPARTICLES AND STARCH NANOCOMPOSITES

4.0 Introduction

Different methods have been used for the preparation of metal sulfide nanoparticles but single source precursor method has been widely used to prepare metal sulfide nanoparticles and thin films since they have an advantage of forming in one-step synthesis with uniform size distribution [1, 2]. In the control of deposition of thin films, single source precursor plays the most important role [3]. The use of single source precursor method for the synthesis of nanoparticles is of great interest in the research industry [4]. Wang *et al*. reported the synthesis of CdS nanoparticles using single source precursor method, the results obtained from XRD showed hexagonal phase at high temperature and cubic phase at low temperature. TEM images showed roughly spherical nanoparticles with size ranging from 4-6 nm depending on the different precursors used in the synthesis. The photo catalyst properties of hexagonal phase were found to be better than those of cubic phase [4, 5].

Satyendra *et al*. [6] synthesised hexagonal HgS particles that were well-defined with narrow size distribution ranging from 5.8-15 nm using single source precursor method [6]. There are few factors that affect the particle size: Reaction time, temperature, concentration of capping agent, just to mention a few. An increase in molar concentration of capping agent leads to decrease in particle size [7, 8]. In this chapter, the use of the Ni(II) and Pd(II) complexes described in chapter 3 as single source precursors to prepare HDA-capped NiS and PdS nanoparticles are described. The metal sulfide nanoparticles were characterized by absorption and photoluminescence spectroscopy to determine their optical properties. XRD, TEM, SEM

and EDS were used to study the structural properties of the nanoparticles. The NiS and PdS were further used to synthesize metal sulfide/ starch nanocomposites that were structurally studied with SEM, and EDS

4.1 Chemicals and reagents

hexadecylamine (HDA), trioctylphosphine (TOP), toluene, methanol, potato starch, Ni(II) anisidine dithiocarbamae complex, Ni(II) dibenzyl dithiocarbamate complex, Ni(II) butyl dithiocarbamate complex, Ni(II) imidazolyl dithiocarbamate complex, Pd(II) anisidine dithiocarbamae complex, Pd(II) dibenzyl dithiocarbamate complex, Pd(II) butyl dithiocarbamate complex, Pd(II) imidazolyl dithiocarbamate complex,

4.2 Characterization techniques

4.2.1 UV-Vis spectroscopy

The optical absorption was measured using Elmer Lamda 25 spectrophotometer. About 2 mg of each nanoparticle was dissolved in 2 mL of toluene and then transferred into a quartz cell/ cuvettes and the optical absorption data was recorded as nanometres (nm). Toluene was also used as reference solvent. Band edges were determined from the obtained UV spectra and band gaps were calculated.

4.2.2 Photoluminescence emission

A very small amount of each nanoparticle was dissolved in toluene in test tubes. When they were completely dissolved, each solution was transferred into a quartz cell and inserted into a

Perkin Elmer Lamda 45 Fluorimeter. The PL data was recorded as wavelength (nm) versus intensity (a.u).

4.2.3 Powder X-ray Diffraction

The powder XRD spectra of metal sulfide nanoparticles were carried out on Bruker-D8 advance powder X-Ray diffractometer instrument operating at a voltage of 40 kV and a current of 30 mA with Cu kα radiation. The XRD samples were made by drop coating sample on a glass plate.

4.2.4 Transmission electron microscope

The TEM images were obtained using a ZEISS Libra 120 electron microscope operated at 120 kV. The samples were prepared by placing a drop of a solution of a sample in toluene on a carbon coated copper grid (300 mesh, agar). The excess solvent was wicked with a paper tip and the samples were dried over night at room temperature. TEM images were recorded on a mega view G2 camera using iTEM Olympus software.

4.2.5 Scanning electron microscope/Energy dispersive spectroscopy

The morphology of the synthesised nanoparticles was checked using scanning electron microscopy after coating with gold. SEM images were obtained from a Joel, JSM-6390 LV apparatus using accelerating voltage between 15-20 kV at different magnifications as indicated on the SEM images. The energy dispersive spectra were obtained using dispersive X-ray analysis (EDS) attached to the Joel JSM 6390 SEM.

4.3 Synthesis

4.3.1 Synthesis of NiS and PdS nanoparticles [5, 7]

0.2 g of each metal complex was dissolved in 2 mL of TOP, the solution was injected into a hot HAD (2 g) at 220 ºC, and the temperature was maintained for 1 hour. After an hour, when the temperature was cooled below 80 ºC, cold methanol was added to the product and centrifuged for about 15 minutes to precipitate the product. The methanol was decanted and another cold methanol was added to centrifuge again, this washing was done three times and the product obtained was kept in a fume cupboard to dry. The nickel sulfide nanoparticles prepared from $[Ni(L^1)_2]$ complex is labelled as NiS1, $[Ni(L^2)_2]$ is labelled as NiS2, $[Ni(L^3)_2]$ as NiS3, $[Ni(L^4)_2]$ as NiS4, $[Pd(L^1)_2]$ as PdS1, $[Pd(L^2)_2]$ as PdS2, $[Pd(L^3)_2]$ as PdS3 and $[Pd(L^4)_2]$ as PdS4.

4.3.2 Synthesis of polymer nanocomposites [9]

2 g potato starch polymer was dissolved in 10 mL THF followed by the addition of 0.4 g of metal sulfide nanoparticles dissolved in 10 mL toluene in a beaker. The mixture was heat and stirred vigorously for about 20 minutes until the solution become turbid (a certain colour of each metal sulfide) solution was obtained for each nanocomposite. The turbid solution was transferred into a glass plate or petri dish and dried.

4.4 Optical and structural studies of HDA-capped NiS nanoparticles

4.4.1 Absorption spectra studies of HDA-capped NiS nanoparticle

The absorption spectra of the NiS nanoparticles are presented in Figure 4.1. The band edges of the synthesised NiS nanoparticles were found to be 306 nm, 314, 271 and 310 nm for NiS1, NiS2, NiS3 and NiS4 respectively. These band edges were used to determine the band gaps (Eg) of the NiS nanoparticles using the following equation:

$Eg^* = hc/\lambda$ [10]

Where Eg = band gap, λ= cut off wavelength, h= Planks constant= 6.626×10^{-34} Joules sec, C= speed of light =3.0×10^8 ms^{-1}. The band gaps of all synthesised NiS nanoparticles were calculated and found to be 4.05, 3.95, 4.58 and 4.0 eV for NiS1, NiS2, NiS3, and NiS4 respectively. These were found to be blue shifted compared to the bulk of NiS [11]. This shows that NiS nanoparticles prepared have very small sizes, the increase in band gaps with decrease in particle size shows the quantum confinement effect [12].

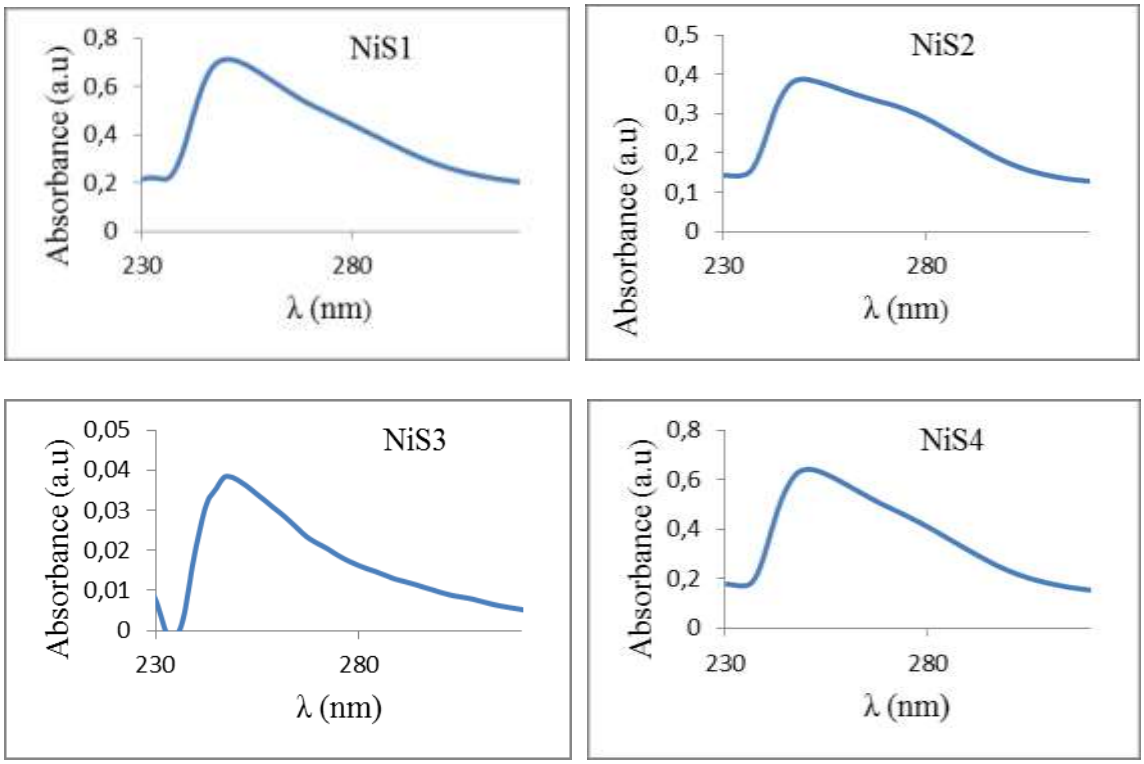

Figure 4.1: Absorption spectra of HDA-capped NiS nanoparticles at 220 °C

4.4.2 Photoluminescence spectra studies of NiS nanoparticles

PL spectra of HDA-capped NiS nanoparticles were recorded at excitation wavelength of 711 nm. The resulting spectra are shown in Figure 4.2. The spectra showed narrow emissions with emission maxima at 725, 720, 622 and 720 nm for NiS1, NiS2, NiS3 and NiS4 respectively. The emission maxima were found to be red shifted when compared to the optical absorption band edges. Size distribution caused the broadening of the emission peaks as shown in Figure 4.2 [11].

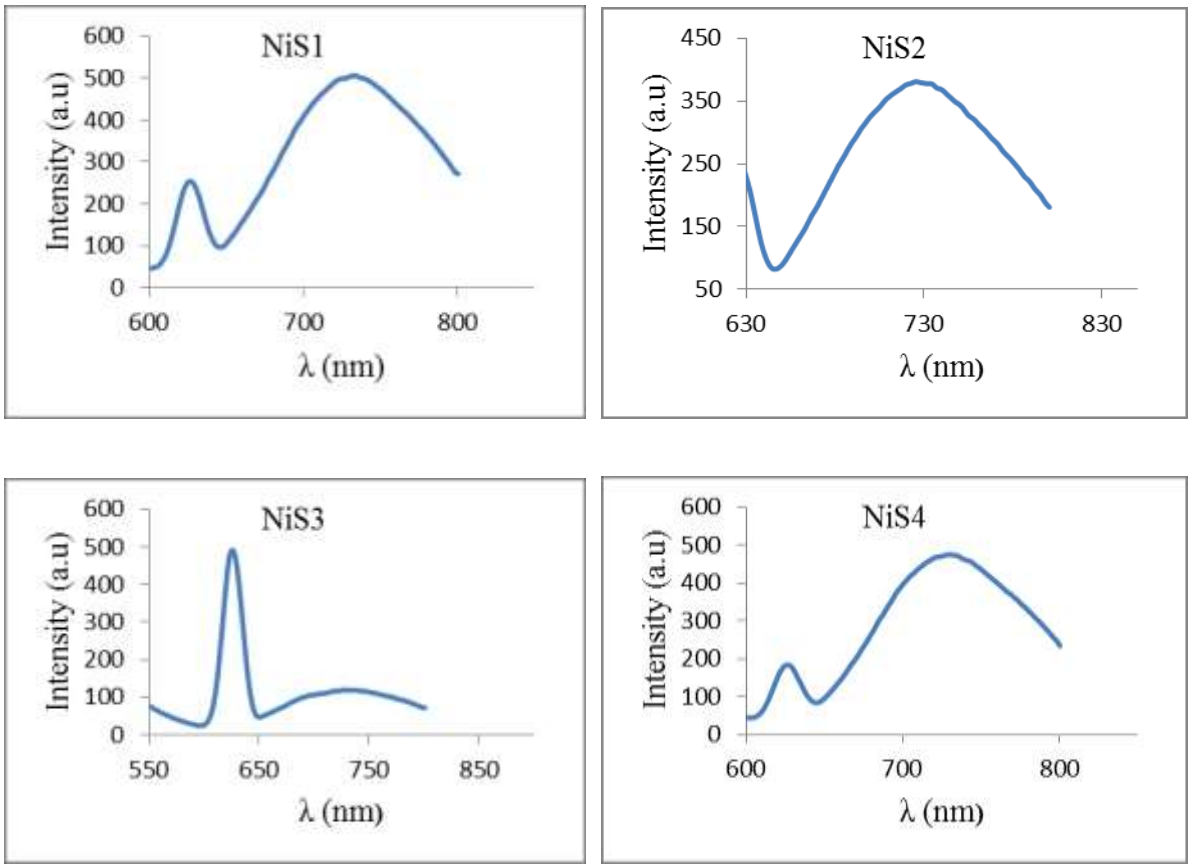

Figure 4.2: PL studies of HDA-capped NiS nanoparticles at 220 °C

4.4.3 XRD studies of the NiS nanoparticles

The XRD pattern was done to examine the composition of NiS nanoparticles. Figure 4.3.1 show the indexed cubic phase of nickel sulfide nanoparticles prepared from Ni(II) anisidine dithiocarbamate complex at 220 °C [12]. The crystalline phase of **NiS1** was observed at 2θ values of 21.2°, 22.5° and 40.7° which corresponds to (111), (220), and (311), Miller indices for cubic NiS nanoparticles respectively. Three peaks at 2θ values = 19.5°, 22.7°, and 39.8°, and 40.85 corresponding to (111), (220), and (311) planes of cubic phase of **NiS2** were observed [12].

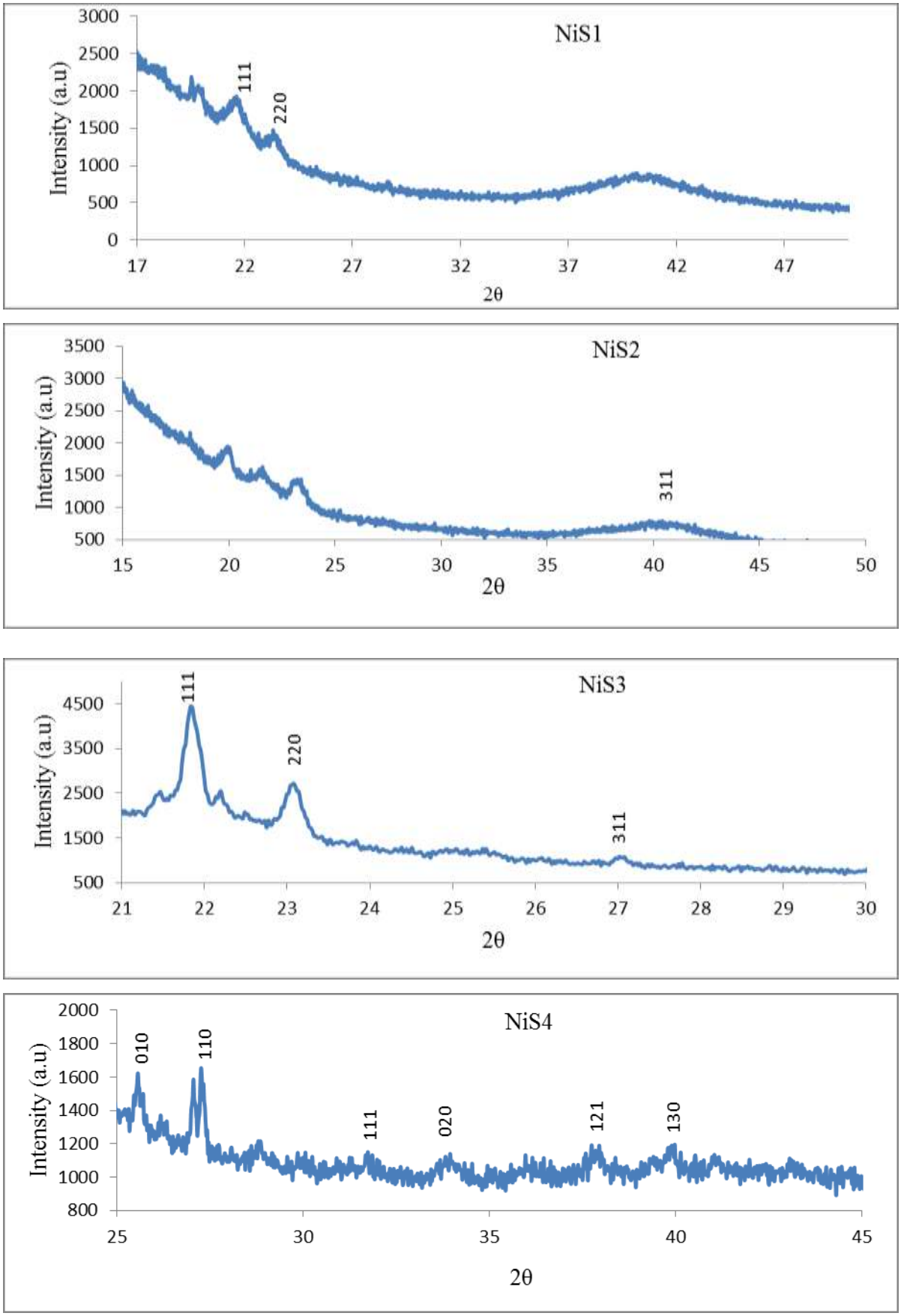

Figure 4.3: Powder XRD pattern of HDA-capped NiS nanoparticles

NiS3 has three peaks at 2θ values = 21.8°, 22.9° and 39.8° which corresponds to (111), (220) and (311) Miller indices for cubic NiS nanoparticles. The XRD patterns of **NiS4** shows six peaks at around 25.5º, 27.1º, 29.1º, 33.7º, 37.5º and 40.7º corresponding to (010), (110), (111), (020), (121) and (130) Miller indices of rhombohedral phase of NiS respectively [12, 13].

4.4.4 TEM studies of the NiS nanoparticles

The TEM images of the **NiS1** nanoparticles are shown in Figure 4.4.1. The **NiS1** nanoparticles have mixture of rod-like structures and close to spherical shapes. Some particles are elongated with crystallinity and agglomeration. Some particles are nearly spherical and triangular in shape. The size ranges from 12-38 nm with little agglomeration [14].

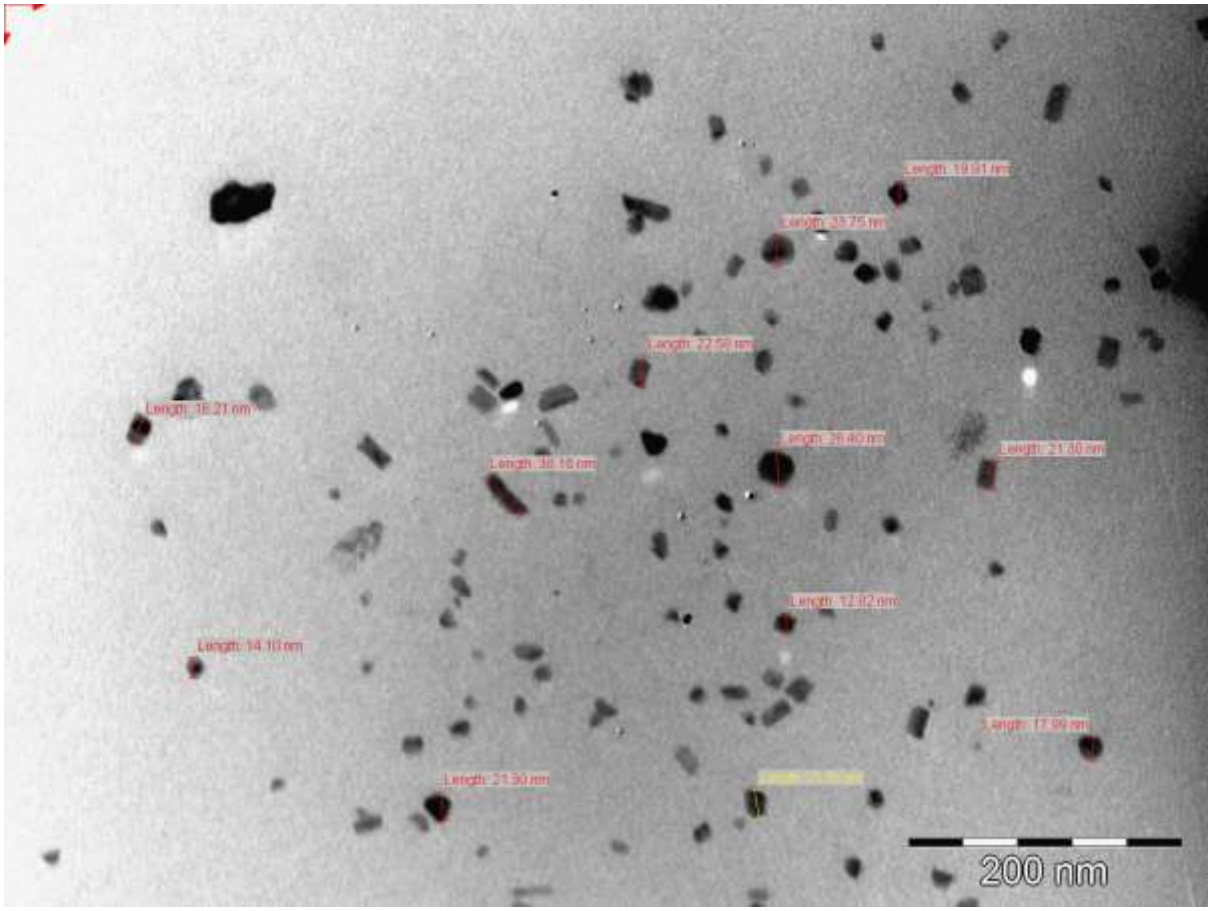

Figure 4.4.1: TEM image of HDA-capped NiS1 nanoparticles at 220 °C

The TEM image of **NiS2** nanoparticles are shown in Figure 4.4.2. The prepared nanoparticles have little agglomeration with particle size ranging from 8-11 nm, which is very small and is due to the quantum confinement effect. The particles are spherical in shape [15].

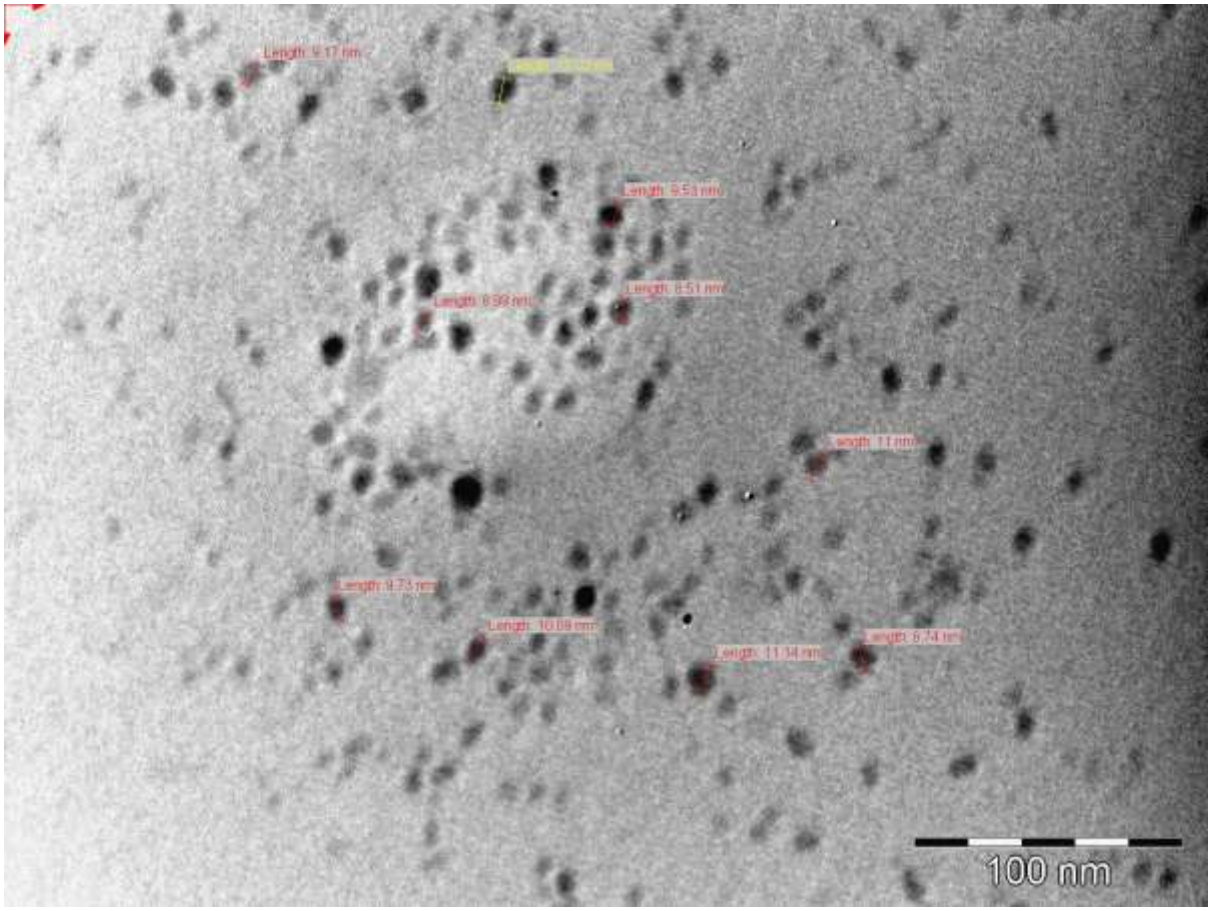

Figure 4.4.2: TEM image of HDA capped NiS2 nanoparticles at 220 °C

The TEM image of HDA-capped **NiS3** nanoparticles are shown in Figure 4.4.3. The prepared particles are spherical with little agglomeration in between particles. The particle size ranges from 9-16 nm.

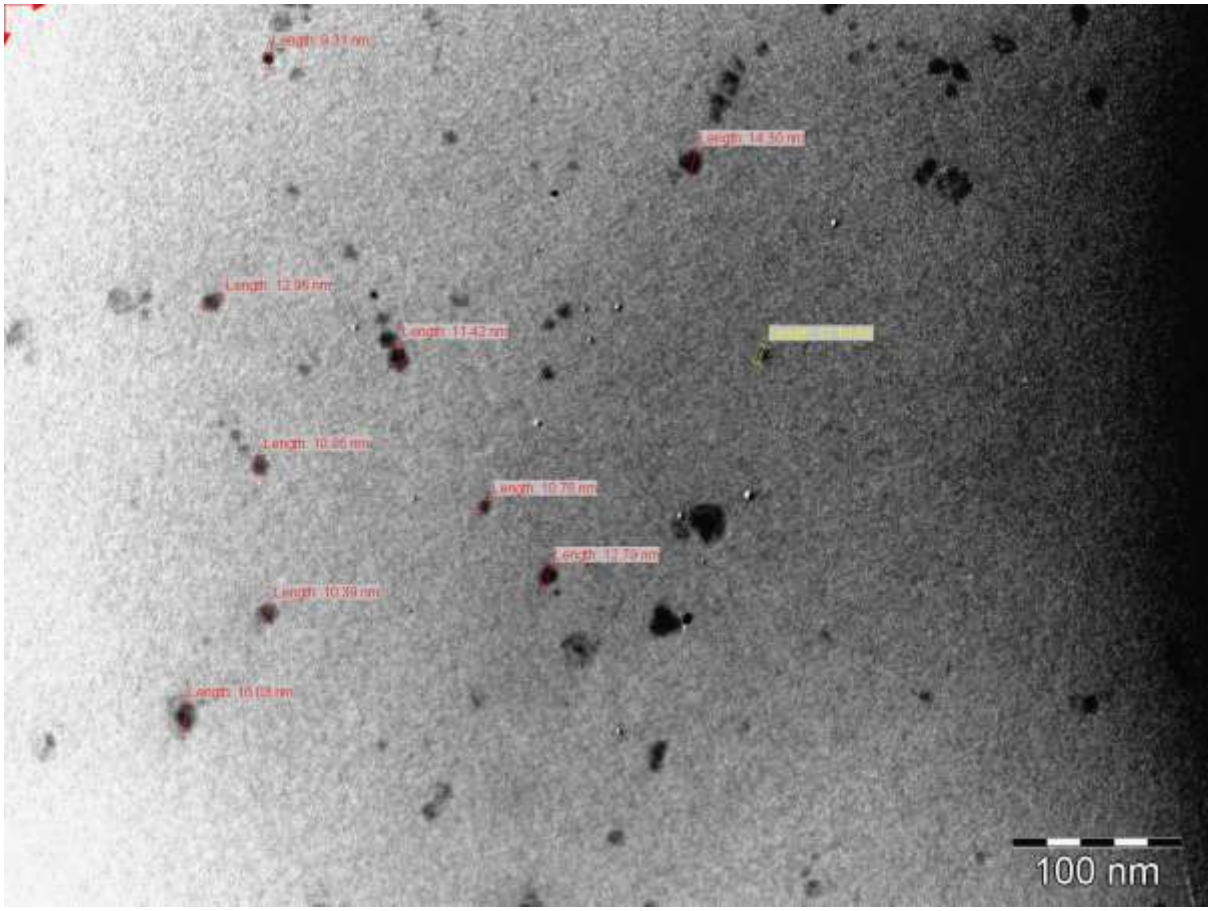

Figure 4.4.3: TEM image of HDA-capped NiS3 nanoparticles at 220 °C

The TEM image of **NiS4** nanoparticles are shown in Figure 4.4.4. The particle size ranges from 4-9 nm with few particles that agglomerate which might be due to the precursor not properly capped. These particles are spherical in shape and are close to one another.

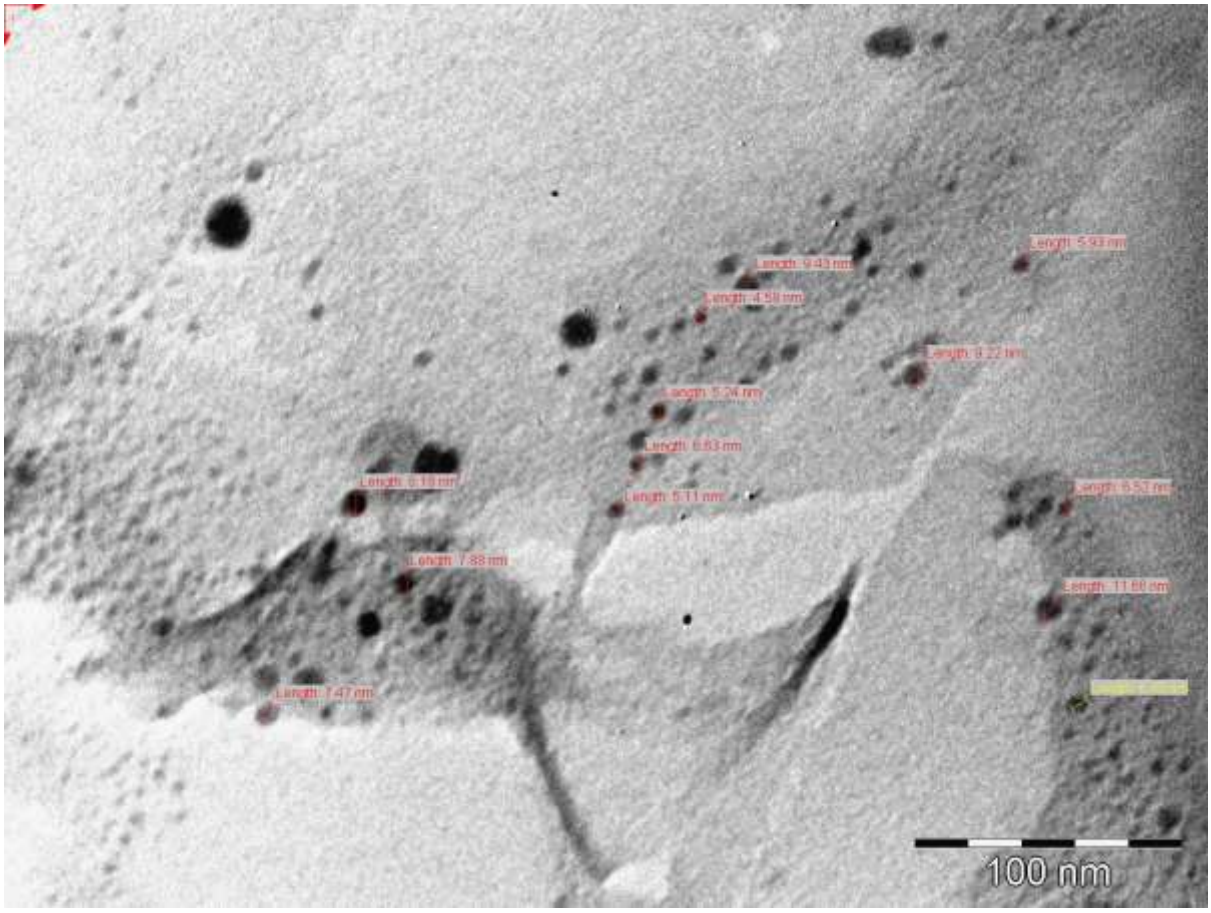

Figure 4.4.4: TEM image of HDA-capped NiS4 nanoparticles at 220 °C

4.4.5 SEM/EDS studies of NiS nanoparticles

The size, shape and morphology of the synthesized NiS and PdS nanoparticles were analysed using SEM. Figure 4.5 shows the SEM images of **NiS1** nanoparticles prepared from $[Ni(L^1)_2]$ complex. From the SEM images, it is clear that the agglomeration of particles is less since there are no lumps formed. These nanoparticles have uniform surface morphology. Elemental composition was confirmed using EDS and the spectrum showed that NiS was formed with the presence of Ni and S. Other traces of elements such as O, P and C are also observed. The observed P and O are due to trioctyl phosphine (TOP), C is attributed to the hexadecylamine (HDA) [16]. Figure 4.6 shows the SEM Images of HDA-capped **NiS2** nanoparticles prepared

from $[Ni(L^2)_2]$ precursor complex. They have uniform surface morphology both at low and high magnification. EDS reveal that the prepared nanoparticles are composed of Ni and S; other traces of elements are due to the capping agent used and TOP.

Figure 4.7 shows the SEM images of HDA-capped **NiS3** nanoparticles prepared from $[Ni(L^3)_2]$ complex. For both low and high magnification, they have homogeneous surface morphology with cauliflower like structure [17]. From the EDS analysis, it can be concluded that nickel sulfide nanoparticles were prepared due to the presence of S and Ni; other traces of elements are due to the capping agent used and TOP. SEM images of HDA-capped **NiS4** nanoparticles prepared from $[Ni(L^4)_2]$ precursor complex are shown in Figure 4.8. The surface morphology is uniform with quasi-spherical structures. They have uniform distribution on the surface of the particles [18]. EDS confirm the presence of Ni, S, C, P and O, and this proves that NiS nanoparticles were synthesised. Other elements such as C is due to the capping agent used (HDA), P and O can be attributed to trioctyl phosphine.

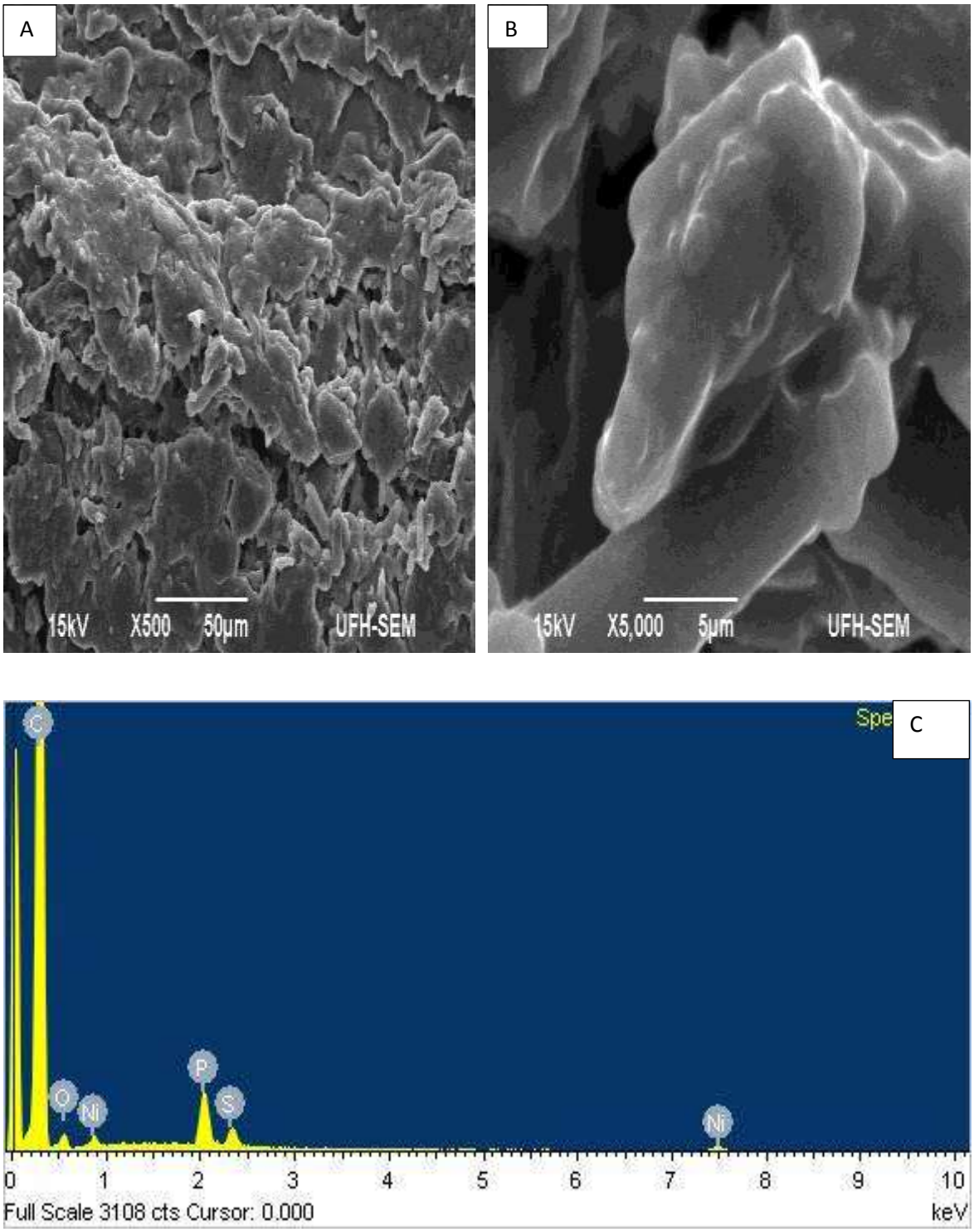

Figure 4.5: SEM images of NiS1 from $[Ni(L^1)_2]$ complex (A) low mag (B) high mag (C) EDS spectrum of the nanoparticle

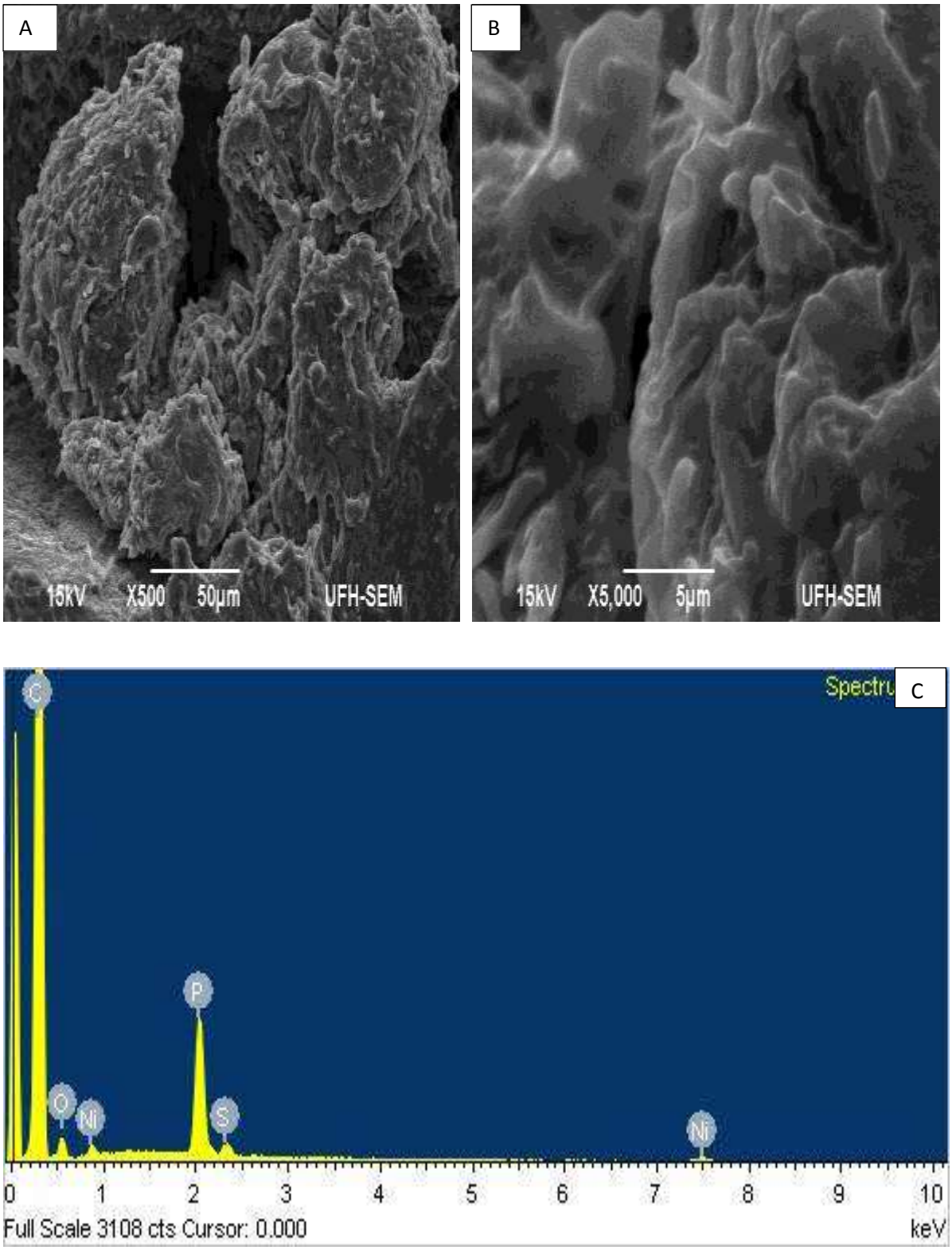

Figure 4.6: SEM images of Ni2 from $[Ni(L^2)_2]$ complex (A) low mag (B) high mag (C) EDS spectrum of the nanoparticle

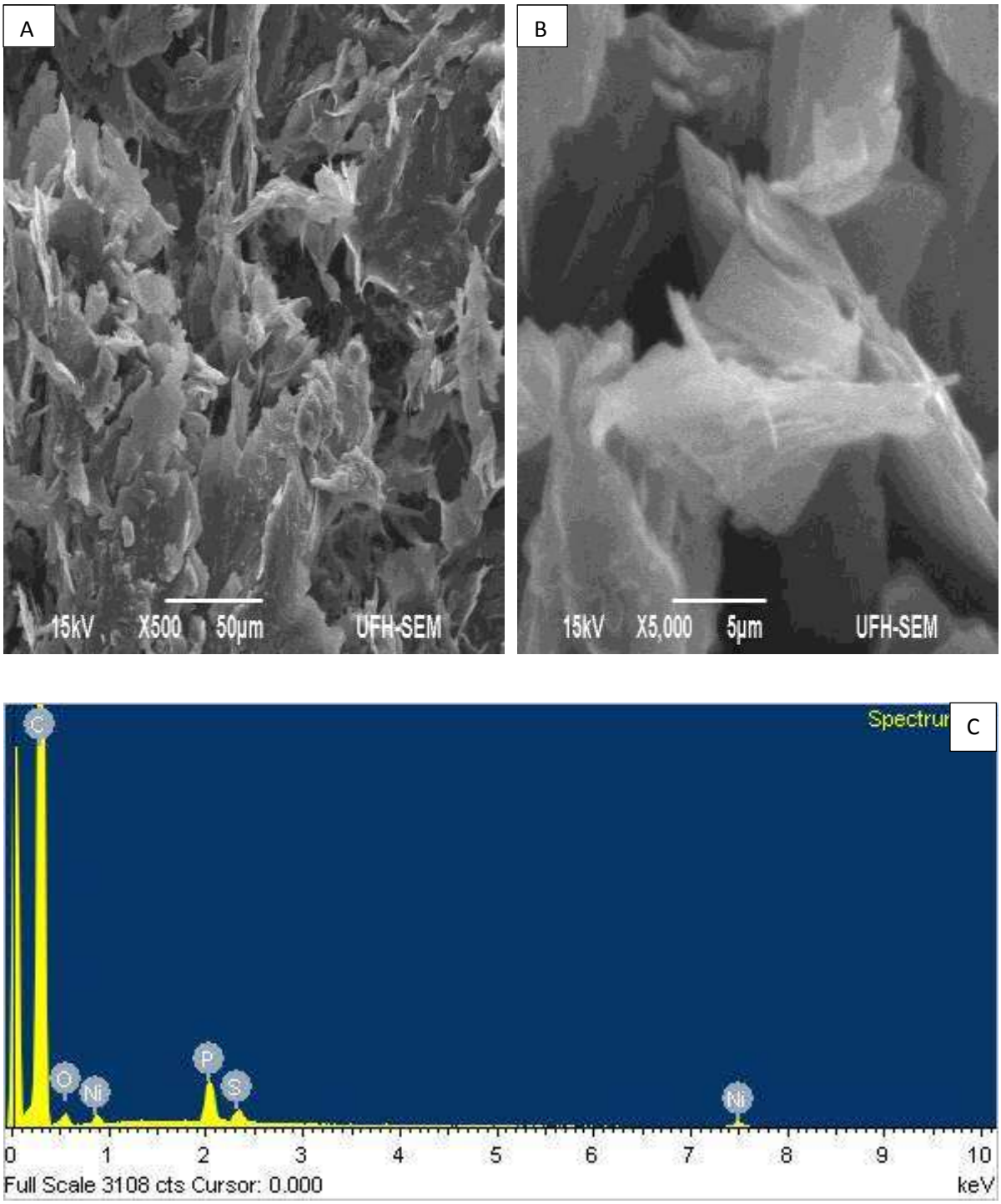

Figure 4.7: SEM images of NiS3 from $[Ni(L^3)_2]$ complex (A) low mag (B) high mag (C) EDS spectrum of the nanoparticle

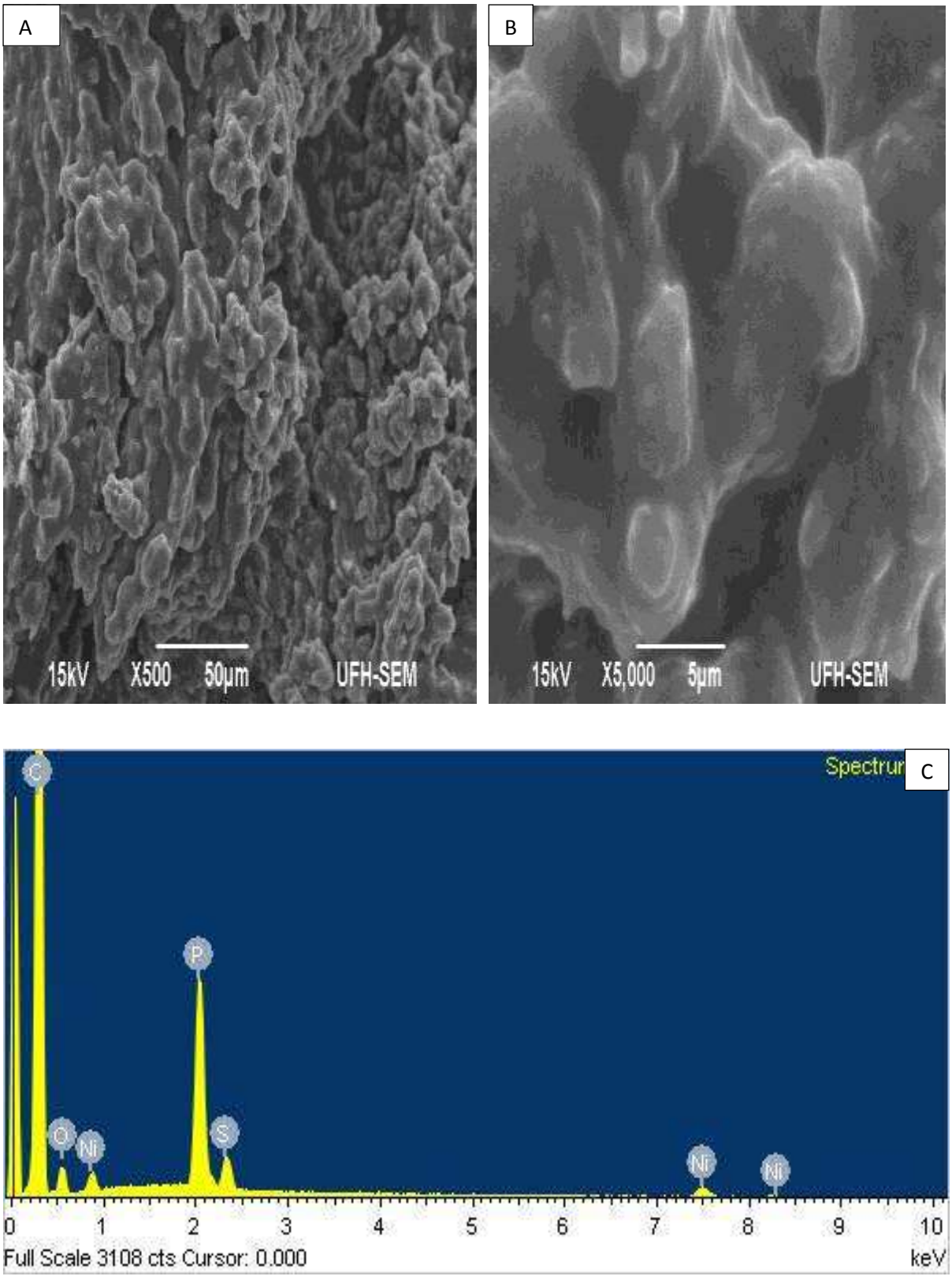

Figure 4.8: SEM images of NiS4 from $[Ni(L^4)_2]$ complex (A) low mag (B) high mag (C) EDS spectrum of the nanoparticle

4.5 Optical and structural studies of HDA-capped PdS nanoparticles

4.5.1 Absorption spectra of PdS nanoparticles

The absorption spectra of the PdS nanoparticles are shown in Figure 4.9. For PdS nanoparticles, the band edges were found to be 324, 318, 326 and 321 nm for **PdS1**, **PdS2**, **PdS3** and **PdS4** respectively and their calculated band gaps were found to be 3.87, 3.94, 3.84 and 3.90 eV. These were blue shifted relative to the bulk (2.0 eV) and shows they have small particle size due to the quantum confinement effect [19].

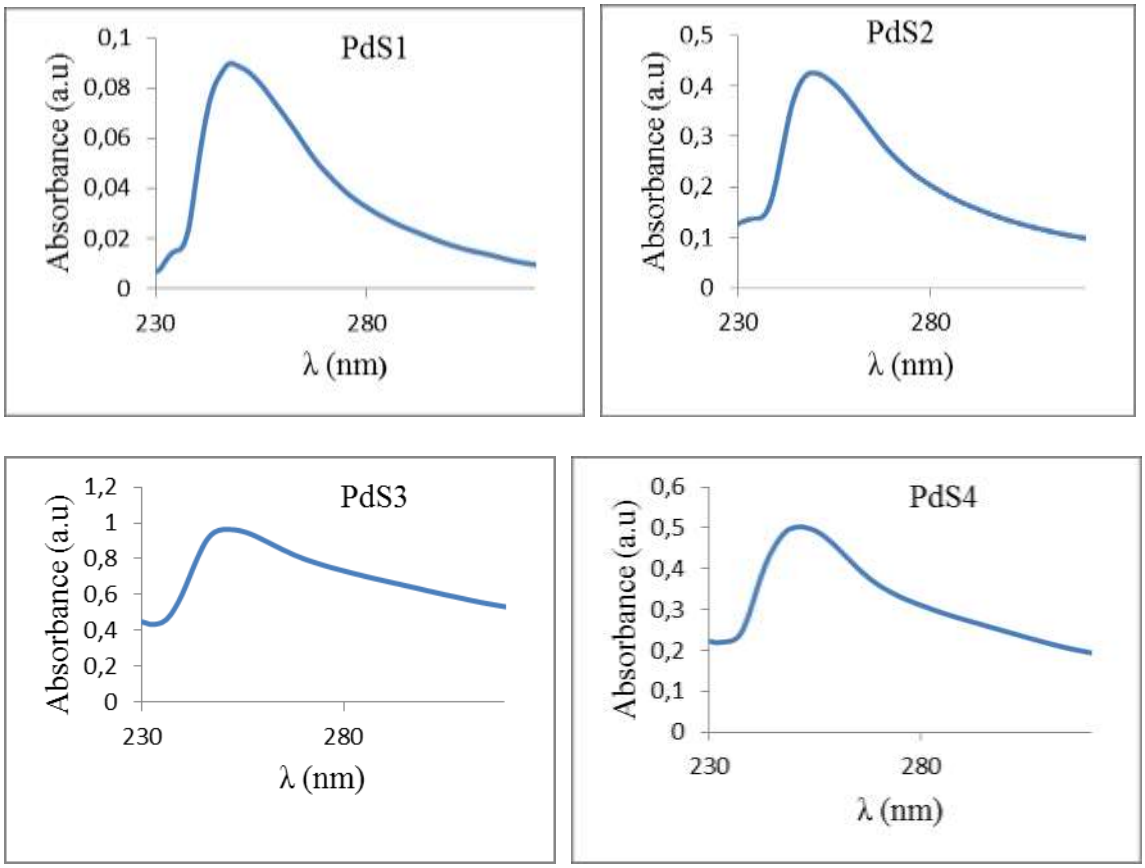

Figure 4.9: Absorption spectra of HDA-capped PdS nanoparticles at 220 °C

4.5.2 Photoluminescence studies of PdS nanoparticles

Palladium sulfide nanoparticles have PL peaks at 710, 714, 377 and 623 nm for **PdS1**, **PdS2**, **PdS3** and **PdS4** respectively. The emission maxima of the HDA-capped PdS nanoparticles were found to be red shifted relative to the optical absorption band edges. The broadening of the peaks as shown in Figure 4.10 is caused by size distribution. PdS4 have less broadness exitonic peak which might be attributed to good confinement and good narrow distribution [20].

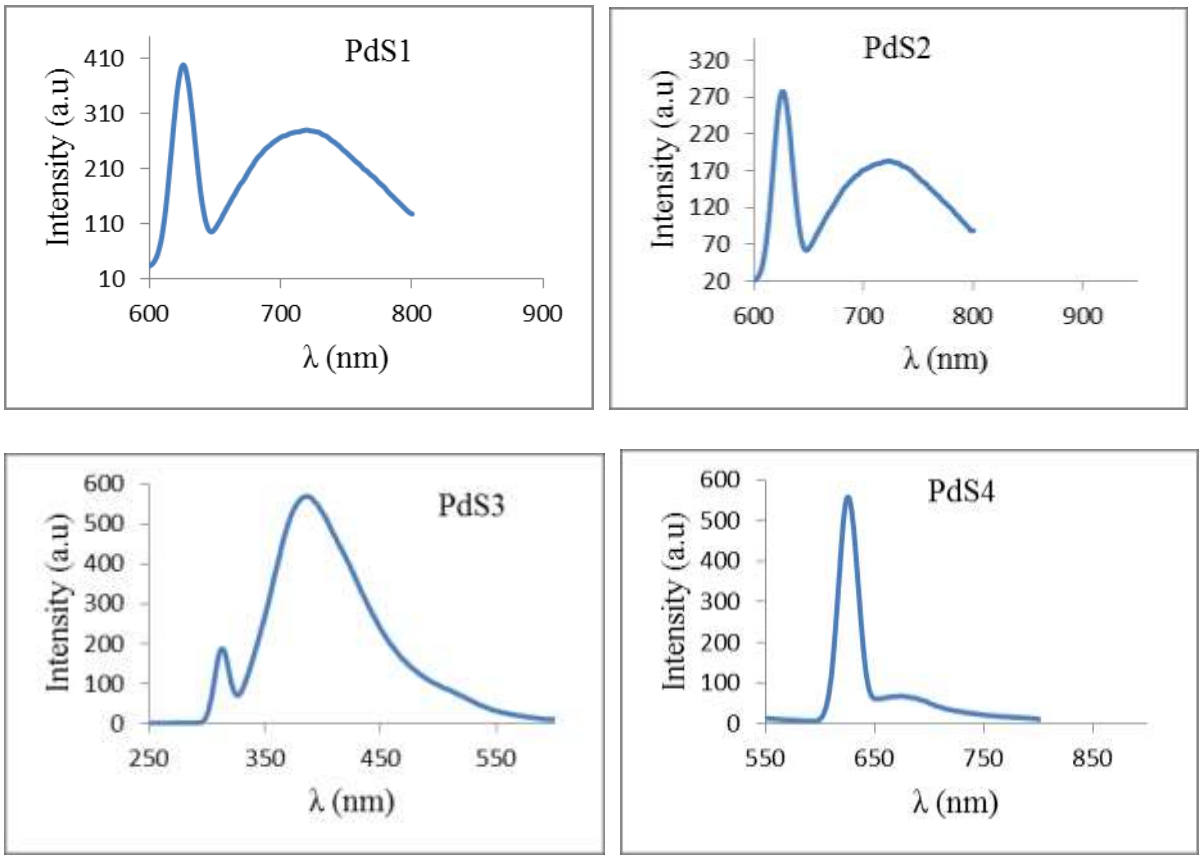

Figure 4.10: PL studies of HDA-capped PdS nanoparticles at 220 °C

4.5.3 XRD studies of PdS nanoparticles

The XRD pattern of **PdS1** shows three peaks at 2θ values around 19.9, 21.7 and 23.1 which corresponds to (002), (100) and (110) Miller indices for cubic PdS nanoparticles. **PdS4** shows four XRD peaks at around 19.7°, 21.7°, 23.2° and 40.3°. The broadness of the peaks is the indication of small particle size. The elongation of the XRD pattern is the confirmation that an organic capping agent (HDA) was used in the synthesis of the nanoparticles [21, 22].

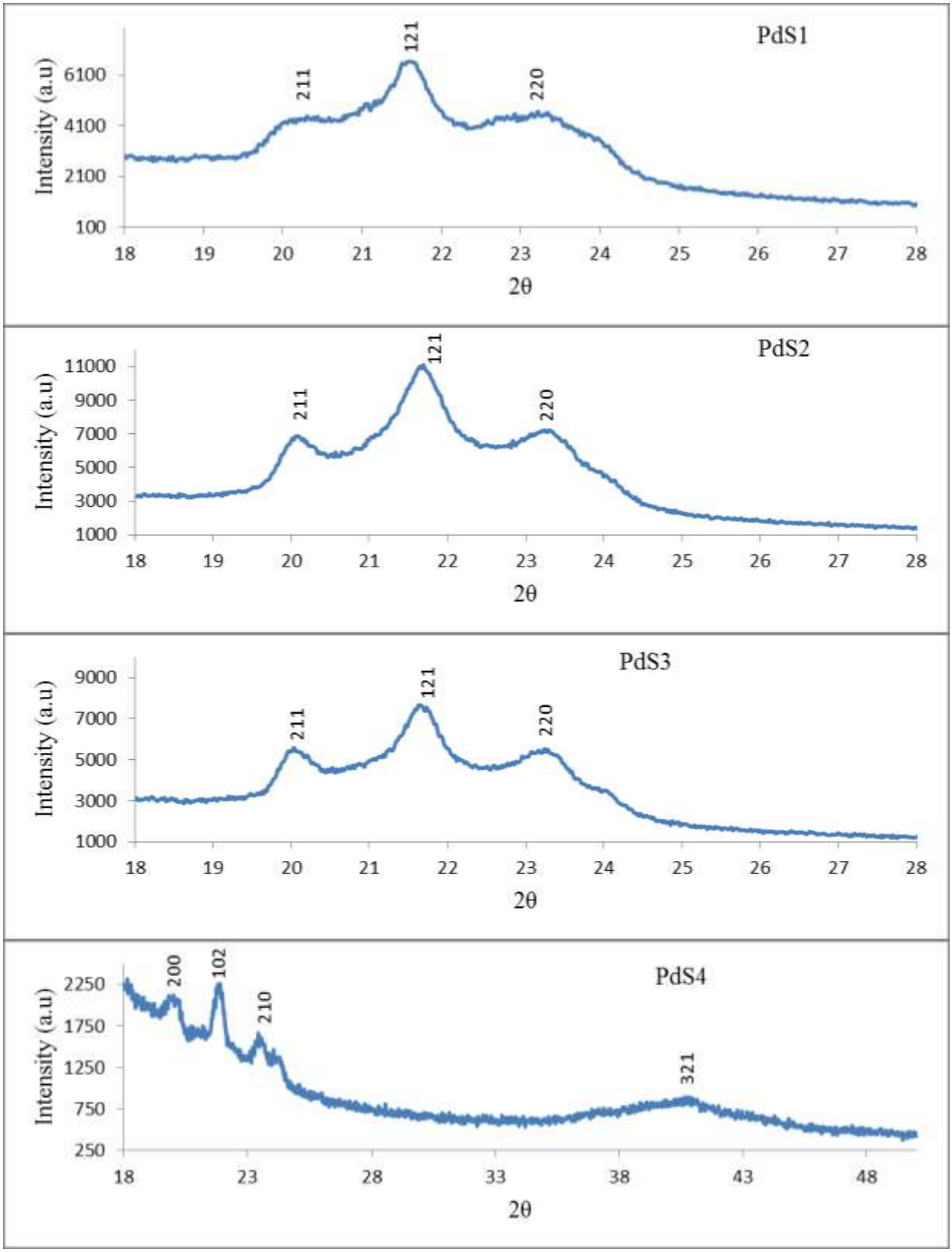

Figure 4.11: RXD pattern of HDA-capped PdS nanoparticles

4.5.4 TEM studies of PdS nanoparticles

Figure 4.12 shows TEM images of HDA-capped PdS1 nanoparticles prepared at 220 °C. They have spherical shapes with very small size ranging from 6.94-9.62 nm. There is no agglomeration of particles because the precursor was perfectly capped with HDA. PdS2 nanoparticles show close to spherical shape with uniform size distribution. Figure 4.12.3 shows PdS3 nanoparticles with spherical shape and size distribution of 7.15nm to 16.46 nm. PdS4 shows mixture of cubic and spherical shapes with sizes ranging from 10.65-16.23 nm [23]. The particles are well dispersed and there is no aggregation.

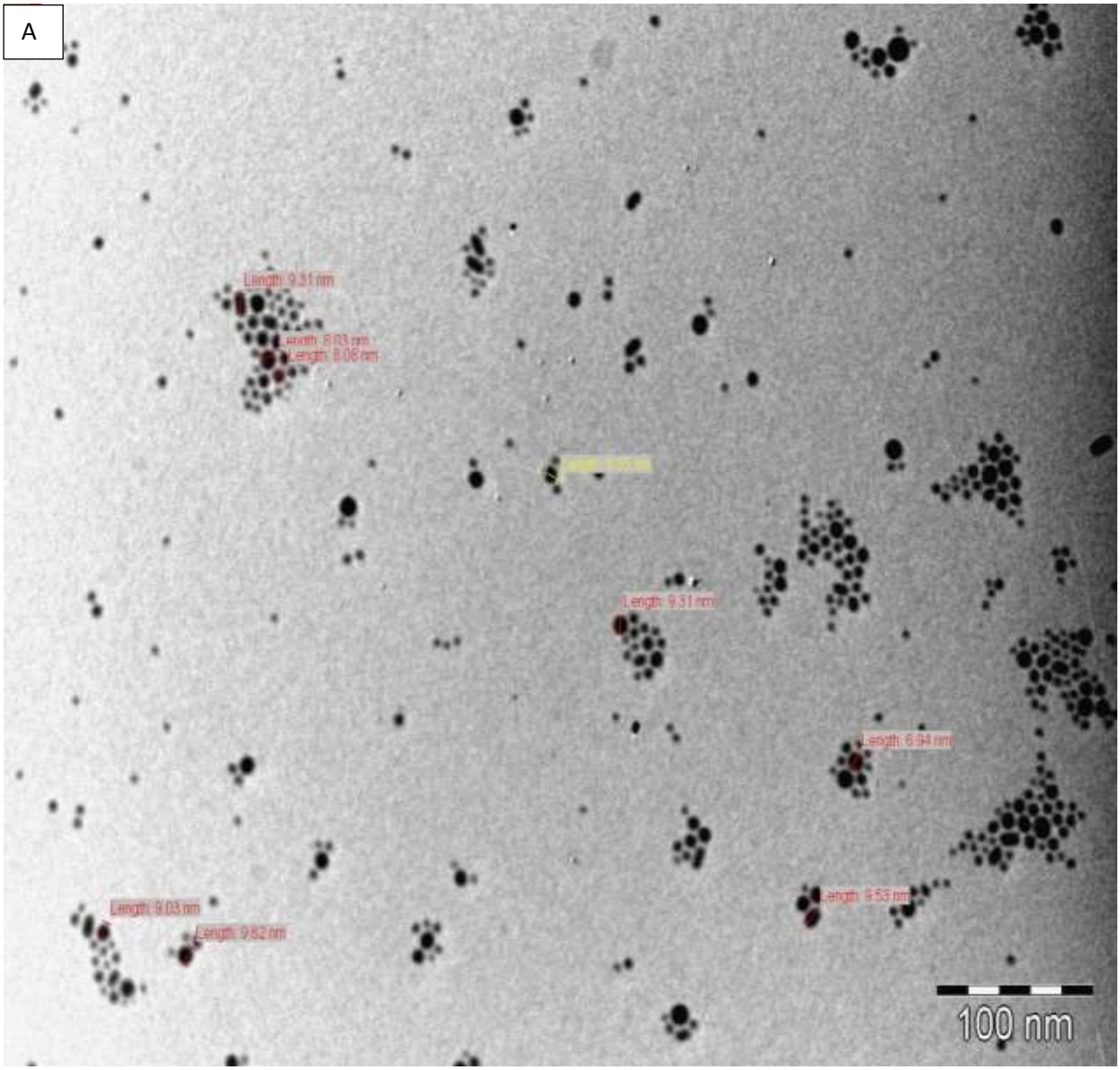

Figure 4.12.1: TEM image of HDA-capped PdS1 nanoparticles at 220 °C

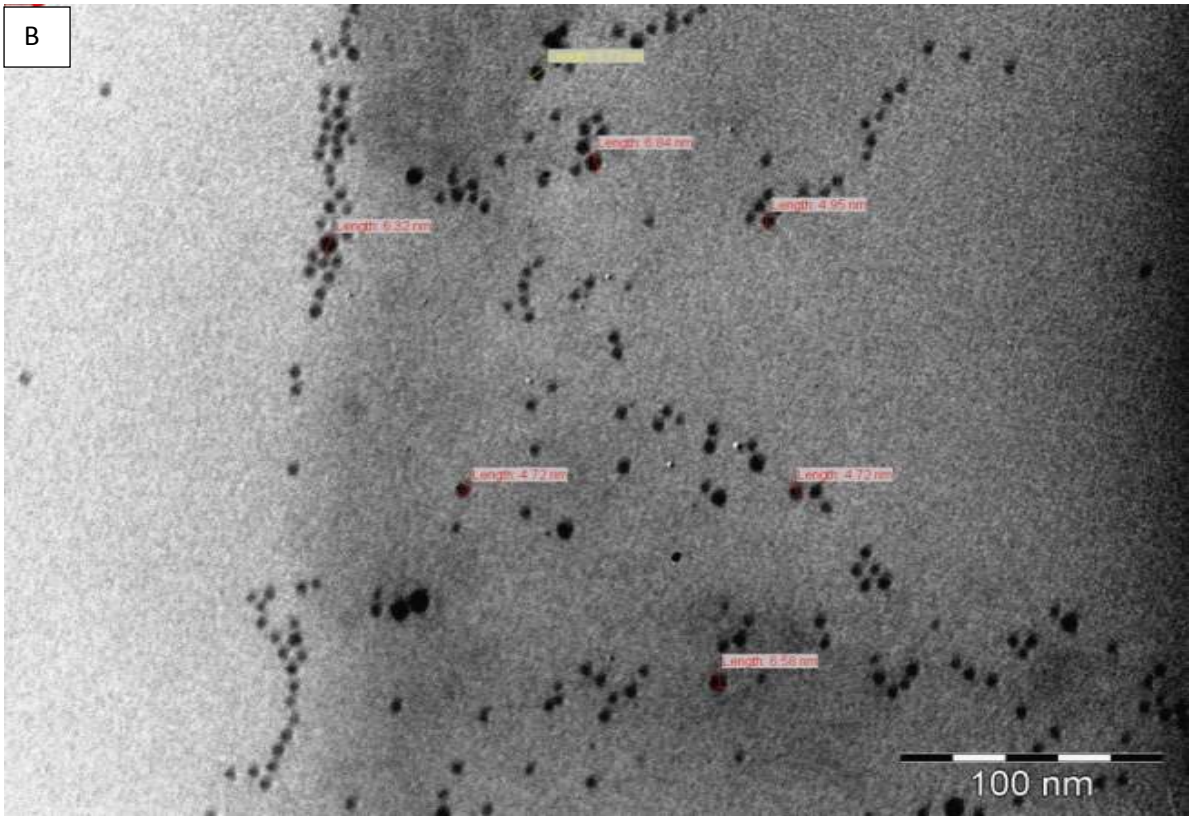

Figure 4.12.2: TEM image of HDA-capped PdS2 nanoparticles at 220 °C

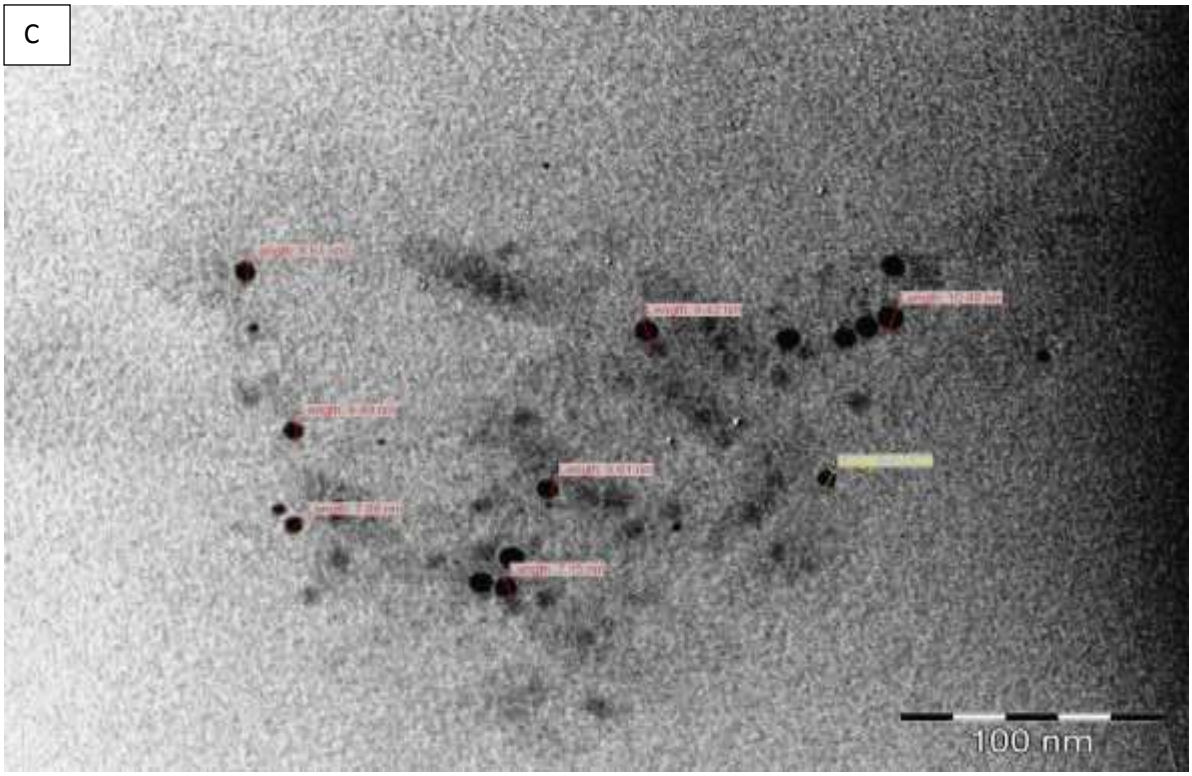

Figure 4.12.3: TEM image of PdS3 nanoparticles at 220 °C

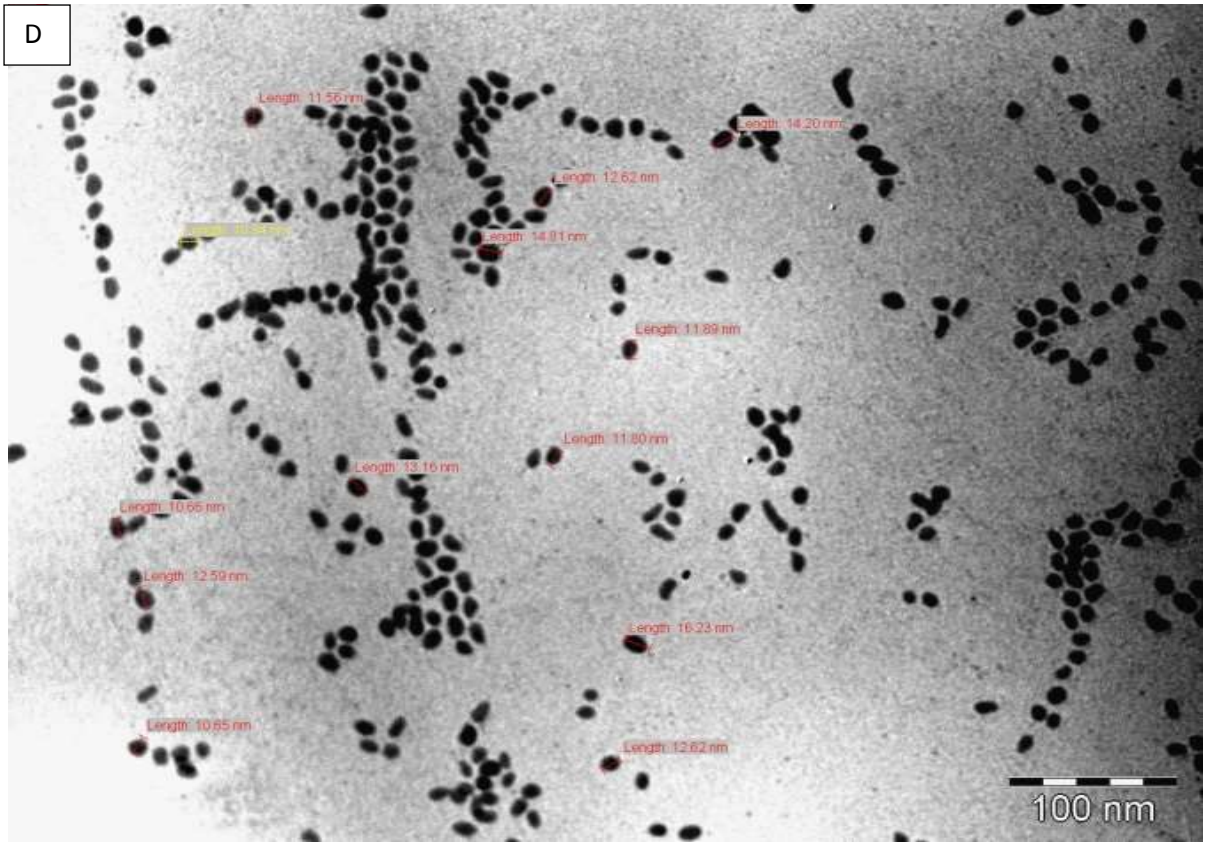

Figure 4.12.4: TEM image of HDA-capped PdS4 nanoparticles at 220 °C

4.5.5 SEM/EDS studies of PdS nanoparticles

The SEM images of the synthesized HDA-capped PdS nanoparticles are shown in Figure 4.13 labelled A (low magnification) and B (high magnification). The results show that **PdS1** has homogeneous surface morphology and is smooth. In both high and low magnification, they have pores in between particles and these nanoparticles do not aggregate [24]. EDS for the analysis of elemental composition was done and the spectrum is labelled C. From the obtained results from EDS, Pd and S are present and this confirms the formation of PdS nanoparticles. Other traces of elements such as C, O, and P are also observed. The observed C is attributed to carbon of the capping agent (HDA), P is due to TOP, and O might be due to

the oxidation of sulfur to oxygen atoms [25]. SEM images of **PdS2** nanoparticles prepared from $[Pd(L^2)_2]$ precursor complex are shown on Figure 4.14 with the same surface morphology and close to spherical shape. Figure 4.4.6 show EDS spectrum with both Pd and S present. P is due to TOP and C is due to the capping agent (HDA).

SEM images of **PdS3** nanoparticles are shown in Figure 4.15. The surface is rougher with hollow like structures [26]. These nanoparticles have uniform surface morphology and there are no lumps. From the EDS analysis, both elements are present and P is due to the TOP used, C can be attributed to the capping agent (HDA). Figure 4.16 shows SEM images of HDA-capped **PdS4** nanoparticles prepared from $[Pd(L^4)_2]$ precursor complex. The surface of the shape is rough with homogeneous morphology. EDS shows the presence of Pd and S elements, P and C are due to TOP and the capping agent used [27].

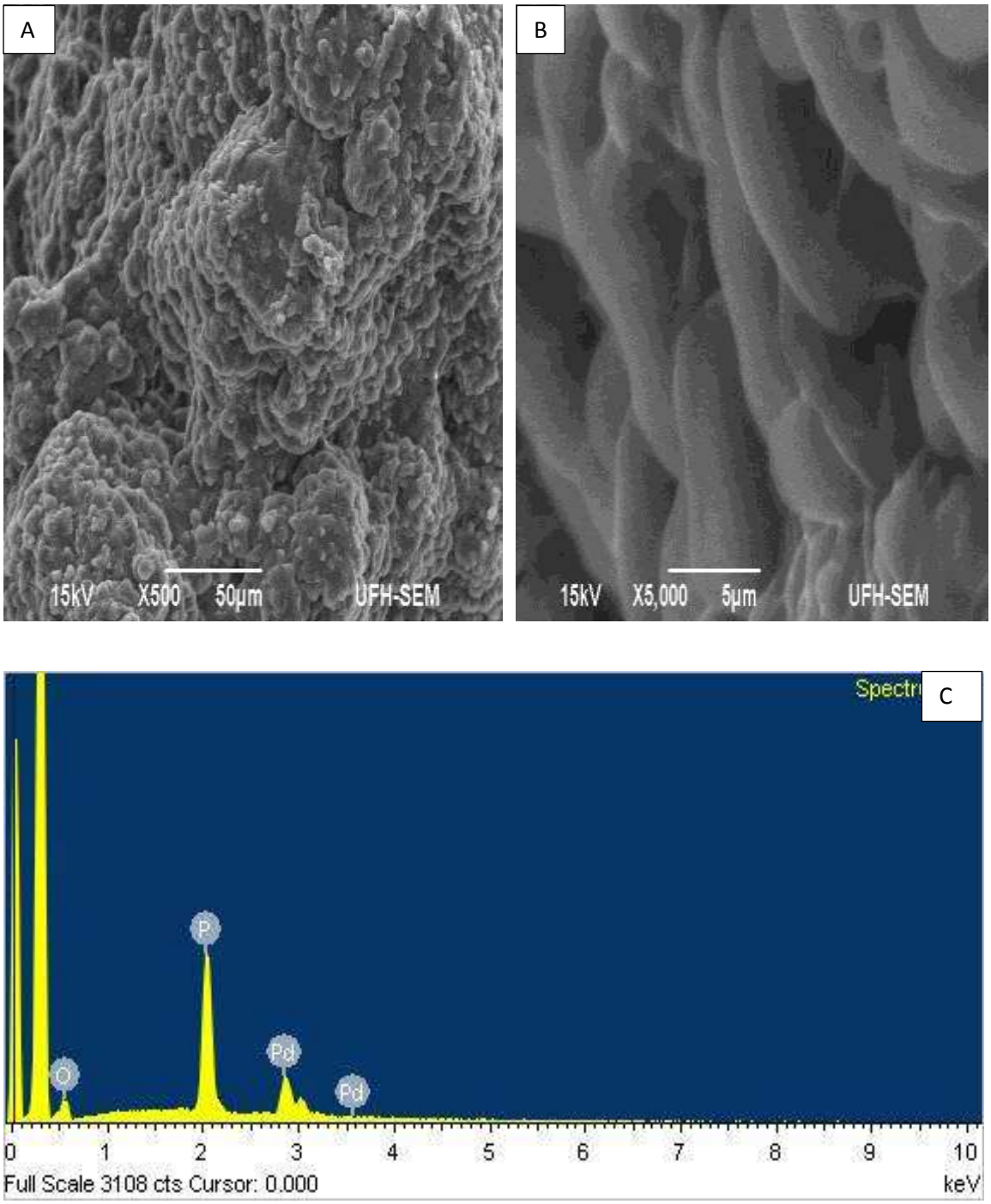

Figure 4.13: SEM images of PdS1 from $[Pd(L^1)_2]$ complex (A) low mag (B) high mag (C) EDS spectrum of the sample

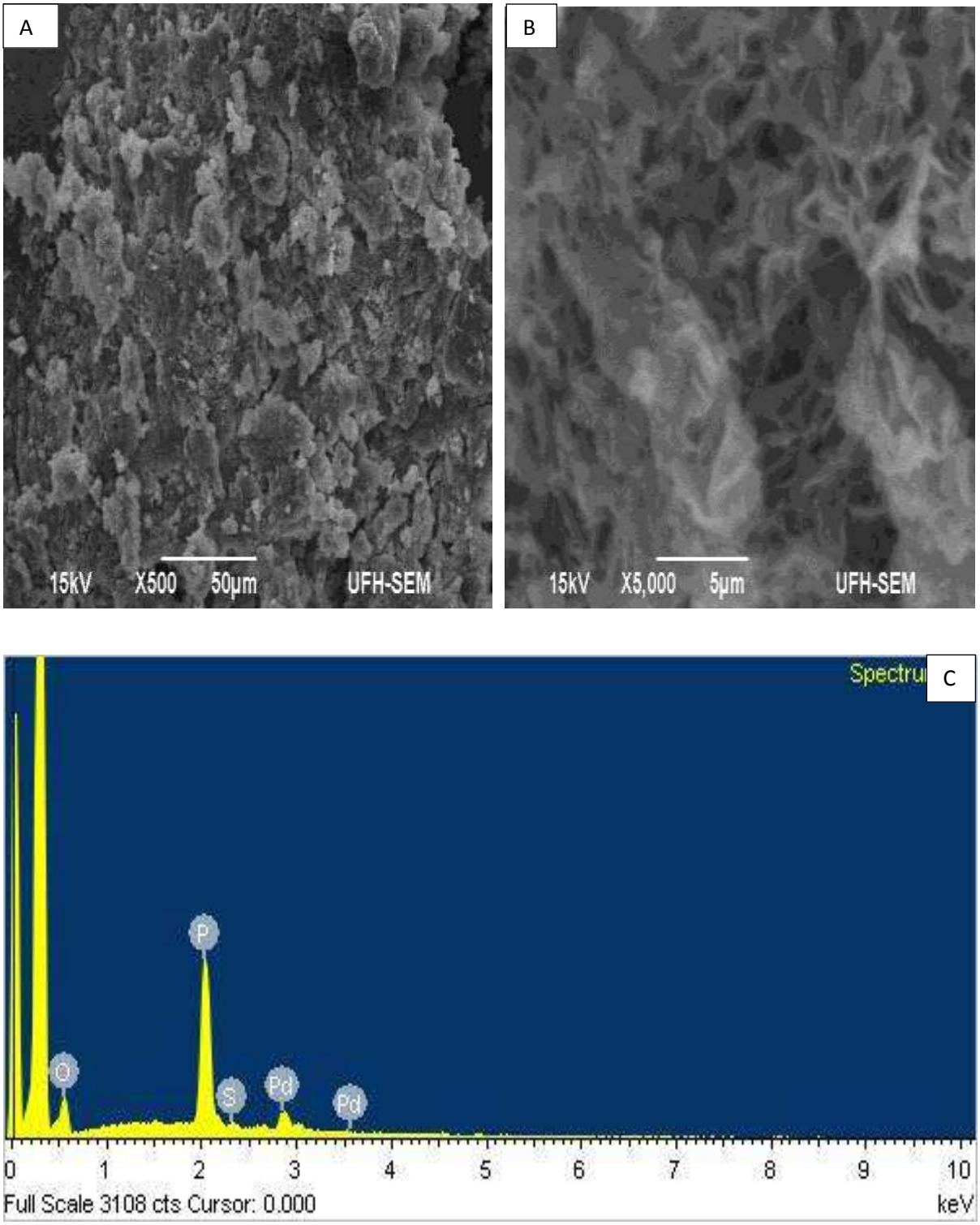

Figure 4.14.: SEM images of PdS2 from $[Pd(L^2)_2]$ complex (A) low mag (B) high mag (C) EDS spectrum of the sample

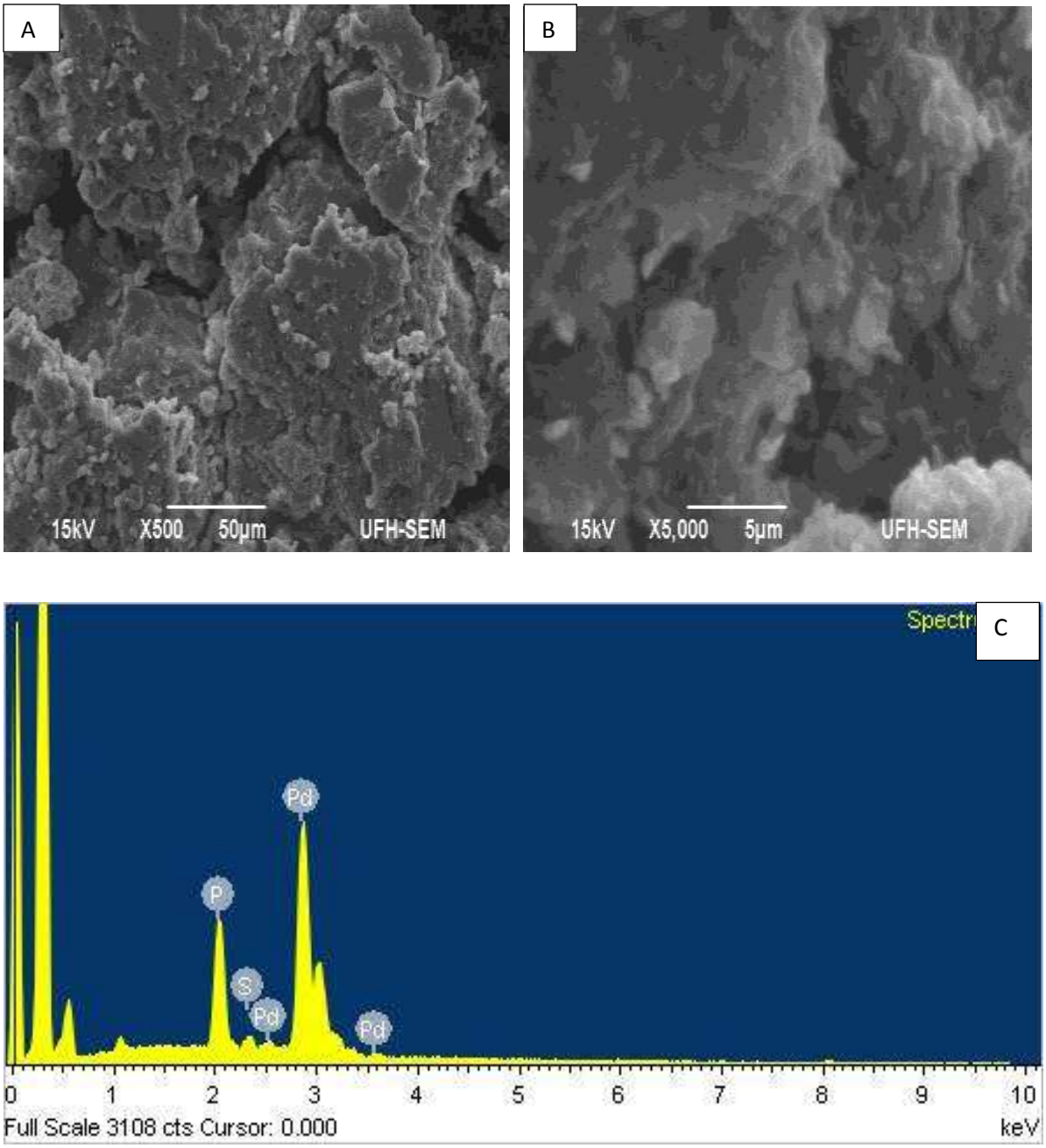

Figure 4.15: SEM images of PdS3 from $[Pd(L^3)_2]$ complex (A) low mag (B) high mag (C) EDS spectrum of the sample

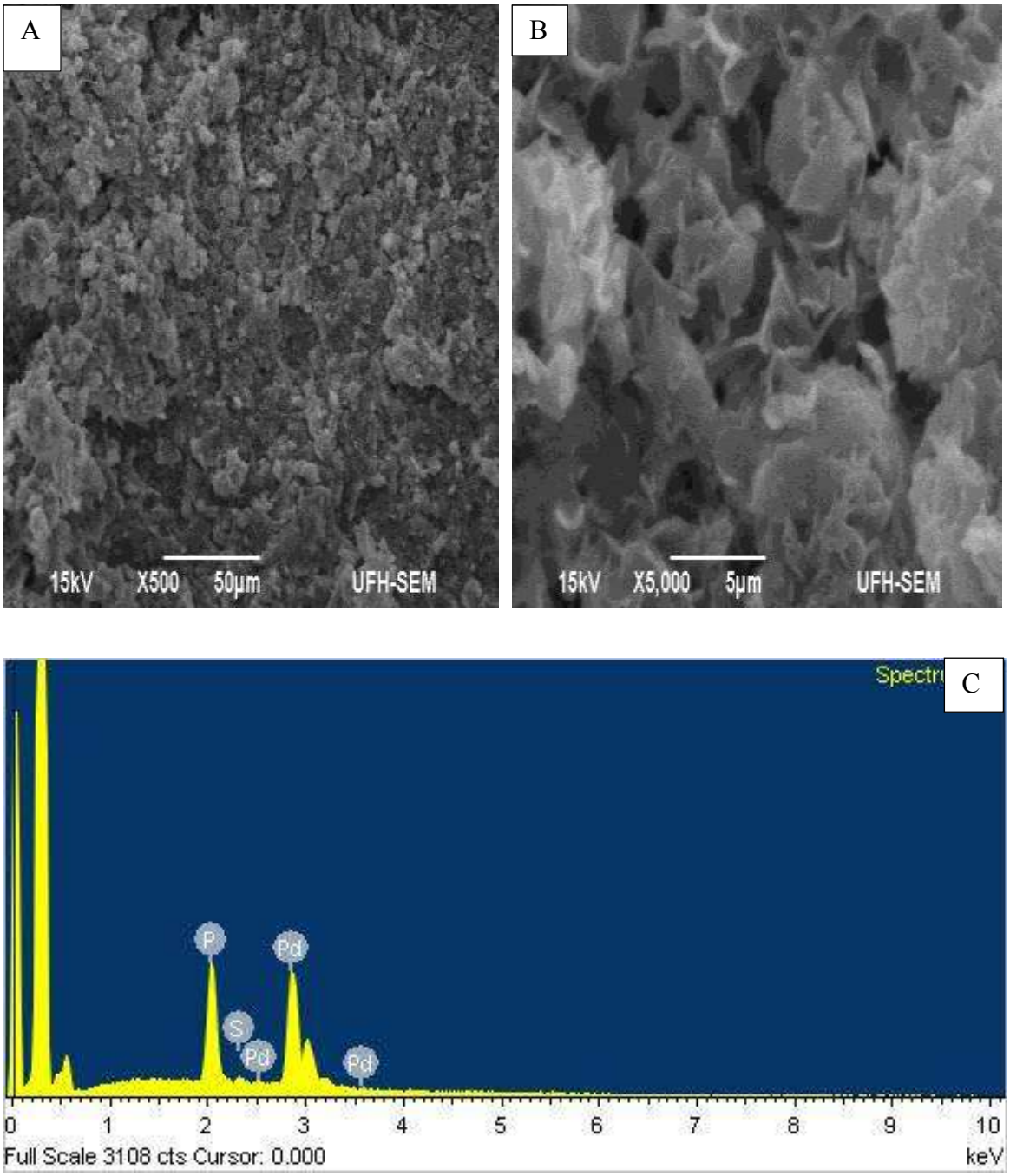

Figure 4.16: SEM images of PdS4 from $[Pd(L^4)_2]$ complex (A) low mag (B) high mag (C) EDS spectrum of the sample

4.6 Structural studies of metal sulfide starch nanocomposites

Potato starch polymer nanocomposites

Scanning electron microscope was used to check the surface morphology of the nanocomposites. Figure 4.17 (A and B) shows SEM images of **NiS1**/starch nanocomposites at different magnifications. From the SEM images, it can be seen that there are NiS nanoparticles dispersed in the matrix of potato starch [28, 29]. The potato starch polymer also played a role of preventing agglomeration of the particles because the starch is adsorbed into different planes of NiS nuclei [30]. The shape is not very clear but they have homogeneous surface morphology. Figure 4.17 (C) shows EDS spectrum which confirm the presence of Ni and S in the NiS1/starch nanocomposites.

SEM images of **NiS2**/starch polymer nanocomposites are shown in Figure 4.18 (A and B) at low and high magnification. The surface morphology is rough with particles close to spherical in shape. EDS reveal that the prepared nanocomposites are composed of Ni and S, which confirms the presence of NiS nanoparticles in the matrix of the polymer [32]. Figure 4.19 shows SEM images and EDS spectrum of **NiS3**/starch polymer nanocomposites. There are few dispersed nanoparticles on the matrix of potato starch polymer; this is due to the small ratio of nanoparticles used. EDS show peaks for Ni, S which confirm the presence of NiS nanoparticles. Other traces of elements were also observed such as P which can be attributed to the TOP that was used, C is due to the capping agent used (HDA). SEM images of **NiS4**/starch polymer nanocomposites are shown on Figure 4.20 with increase in surface smoothness of the particles in between the pores of the polymer. There were small peaks of Ni and S observed from the EDS spectrum because the ratio of nanoparticles used was small.

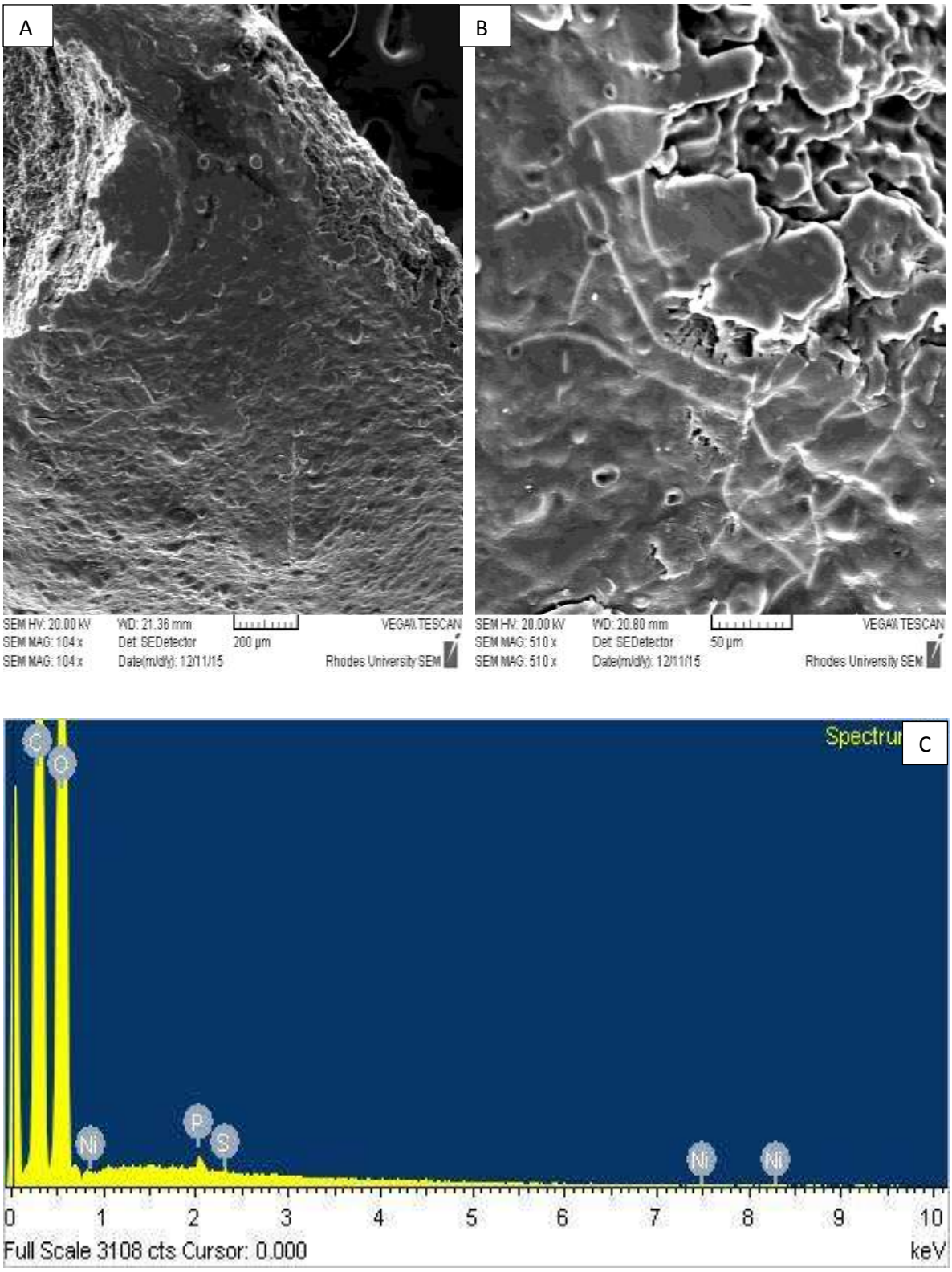

Figure 4.17: (A) and (B) are SEM images of NiS1/potato starch nanocomposites. (C) EDS spectrum of the nanocomposites

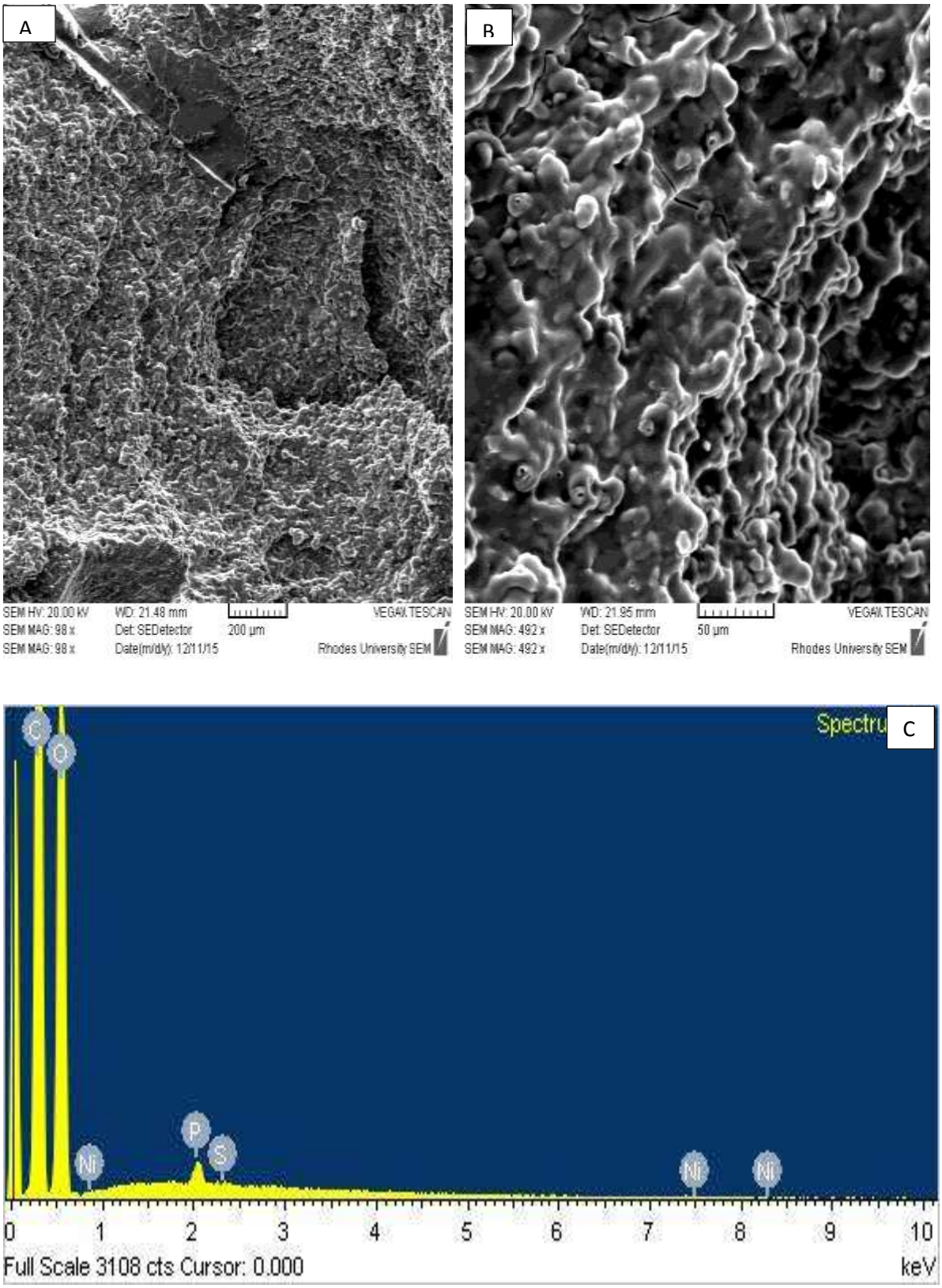

Figure 4.18: (A) and (B) are SEM images of NiS2/potato starch nanocomposites. (C) EDS spectrum of the nanocomposites

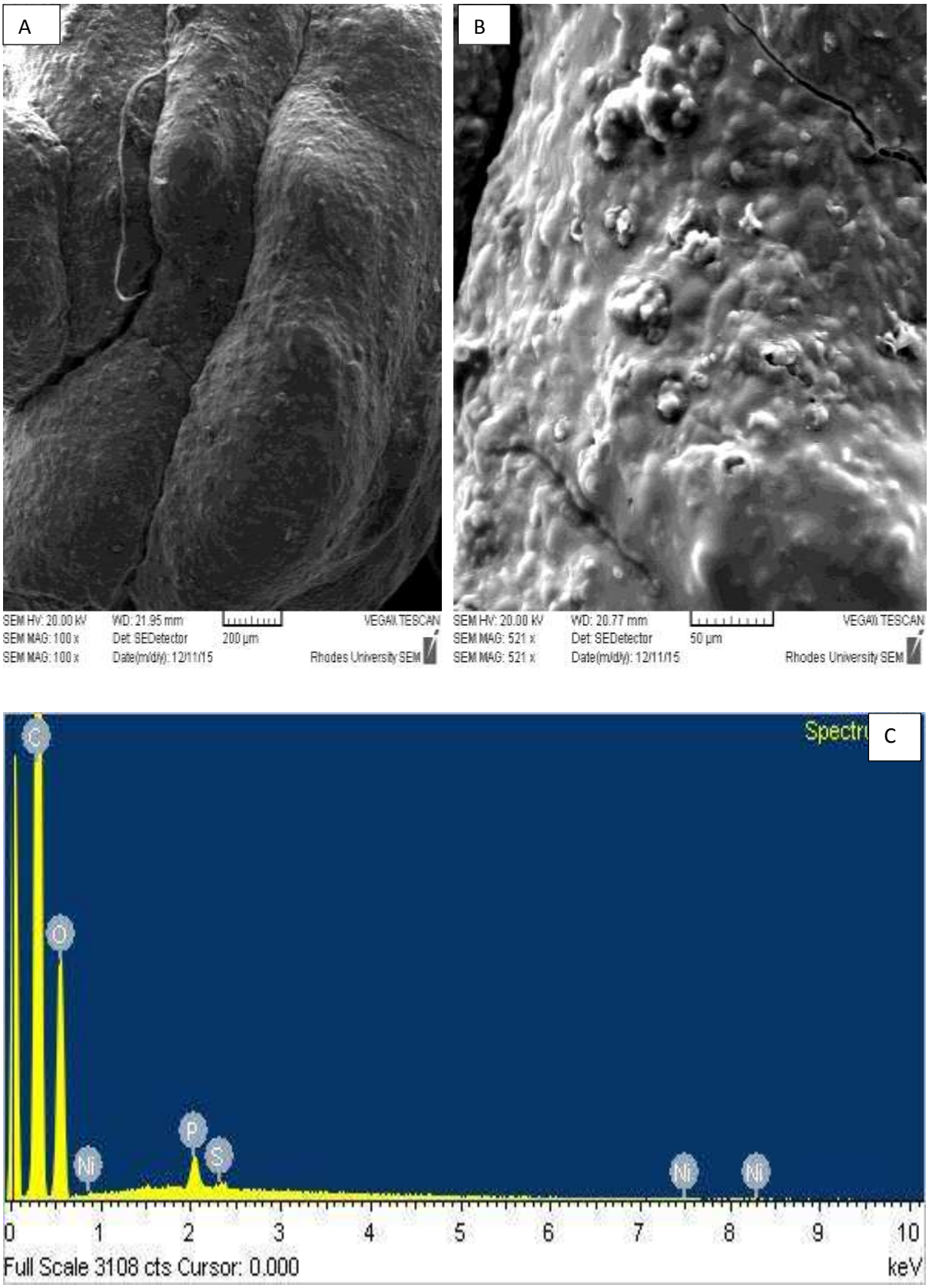

Figure 4.19: (A) and (B) are SEM images of NiS3/potato starch nanocomposites. (C) EDS spectrum of the nanocomposites

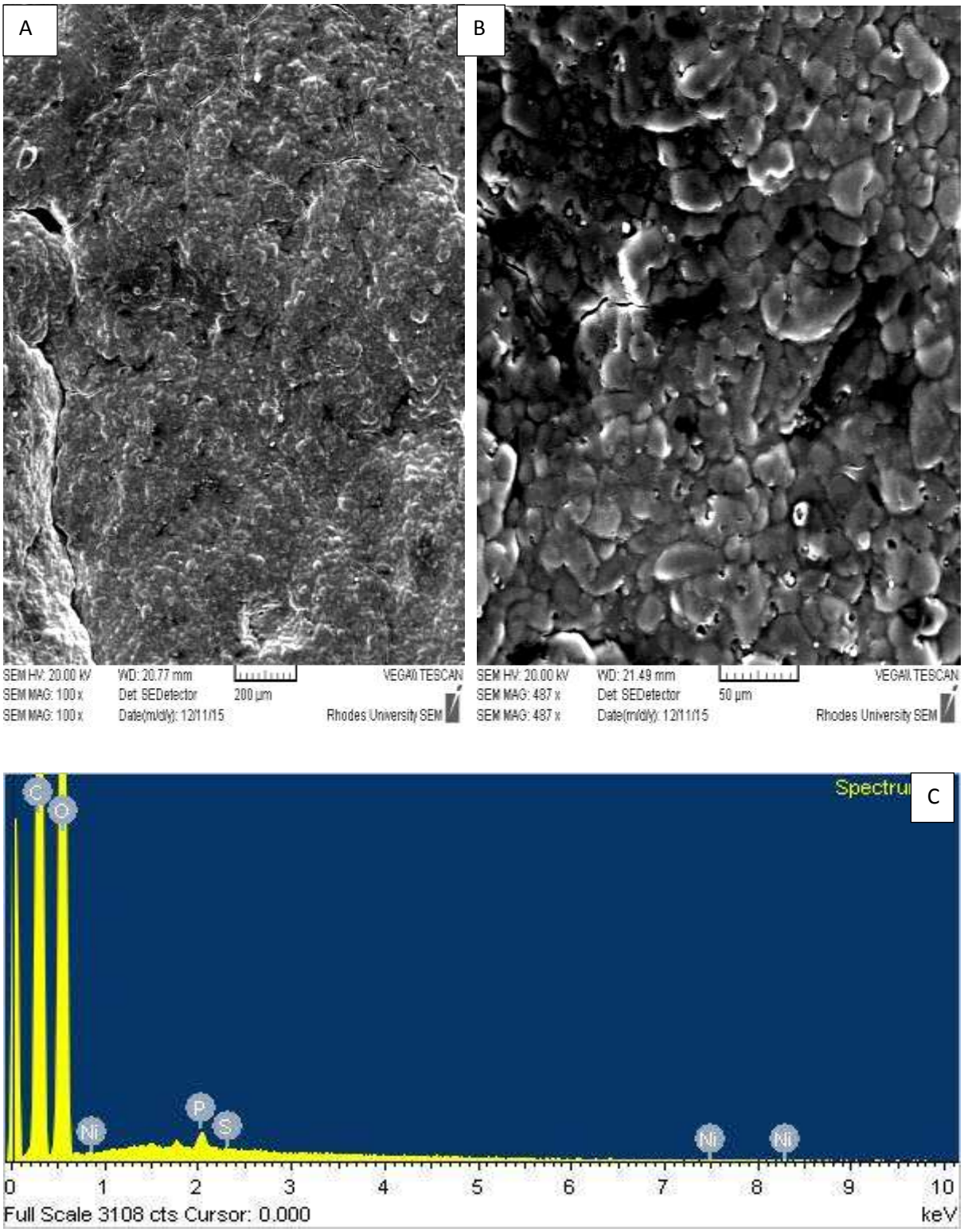

Figure 4.20: (A) and (B) are SEM images of NiS4/potato starch nanocomposites. (C) EDS spectrum of the nanocomposites

4.6.2 Structural studies of PdS/starch nanocomposites

SEM images of PdS1/starch polymer nanocomposites are shown on Figure 4.21 (A) low magnification and (B) high magnification. Image A show dispersed nanoparticles that are on the surface of potato starch polymer. There is an increase in the surface roughness of the particles [33]. Figure 4.22 shows the SEM/EDS of PdS2/starch composites. SEM images show nanocomposites with increase in the roughness of surface morphology. PdS nanoparticles are well dispersed into the matrix of the starch. EDS shows peaks of Pd and S which is the confirmation for the presence of nanoparticles.

Figure 4.23 shows the SEM/EDS of PdS3/starch nanocomposites. The SEM images at low and high magnification show smooth composites with very few particles present. The EDS spectrun confirm the presence of metal sulfide nanoparticles with the presence of Pd and S elements. Figure 4.24 shows the SEM/EDS of PdS4/starch nanocomposites. The SEM images shows smooth nanocomposites with few nanoparticles dispersed in the matrix of potato starch [34]. They have homogeneous surface morphology with close to spherical shapes. The EDS spectrum confirm the presence of PdS nanoparticles by peaks of Pd and S.

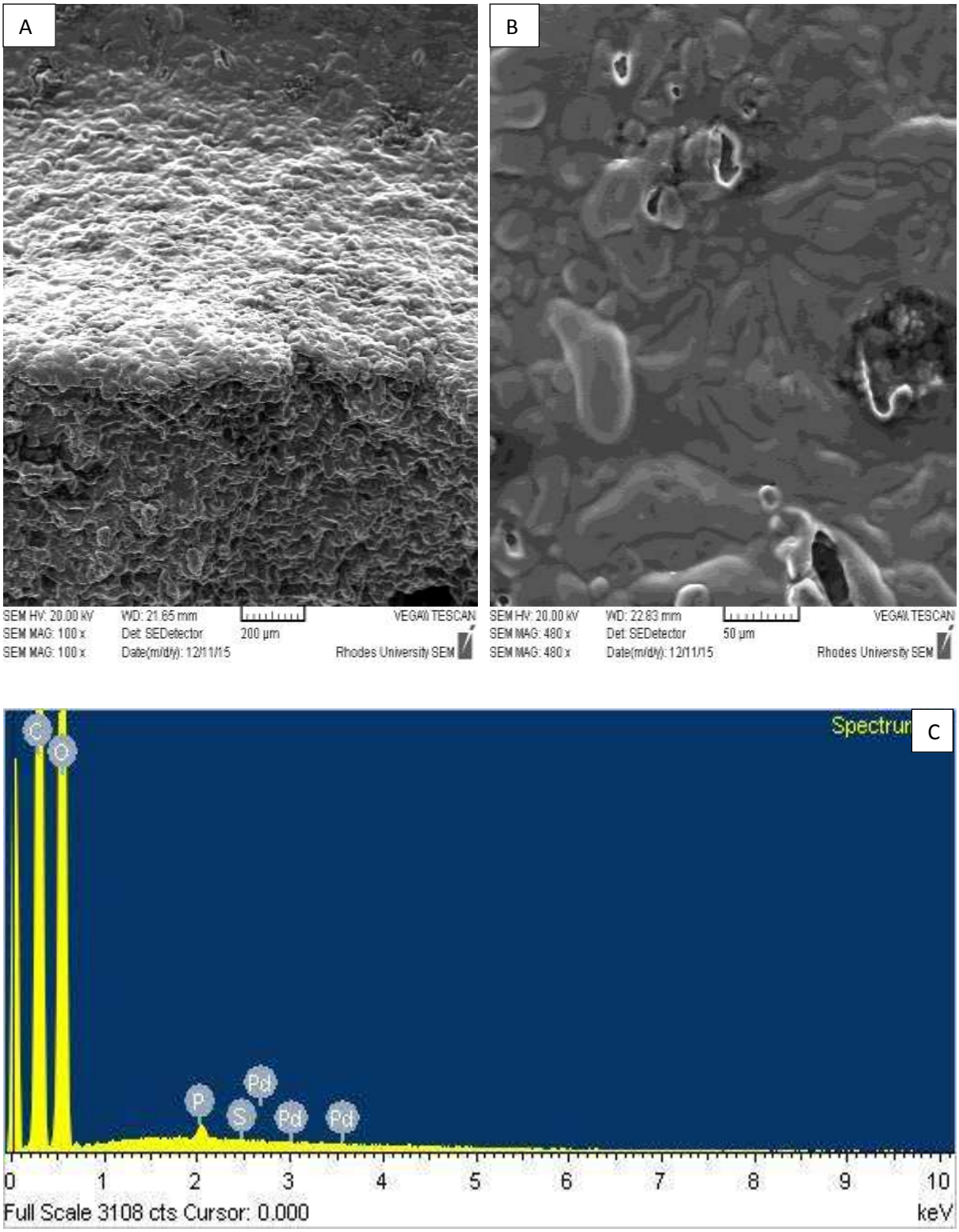

Figure 4.21: (A) and (B) are SEM images of PdS1/potato starch nanocomposites. (C) EDS spectrum of the nanocomposites

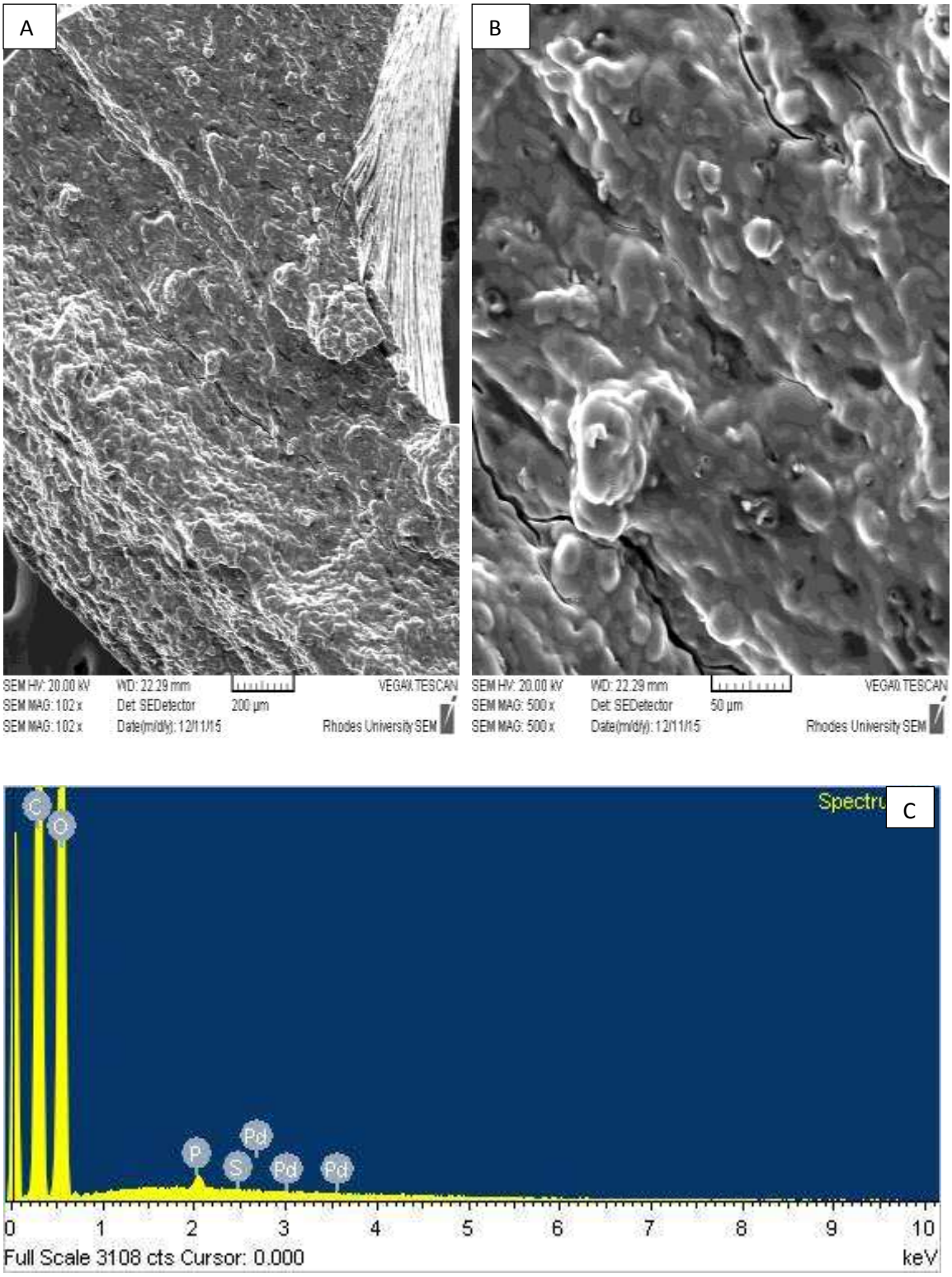

Figure 4.22: (A) and (B) are SEM images of PdS2/starch nanocomposites. (C) EDS spectrum of the nanocomposites

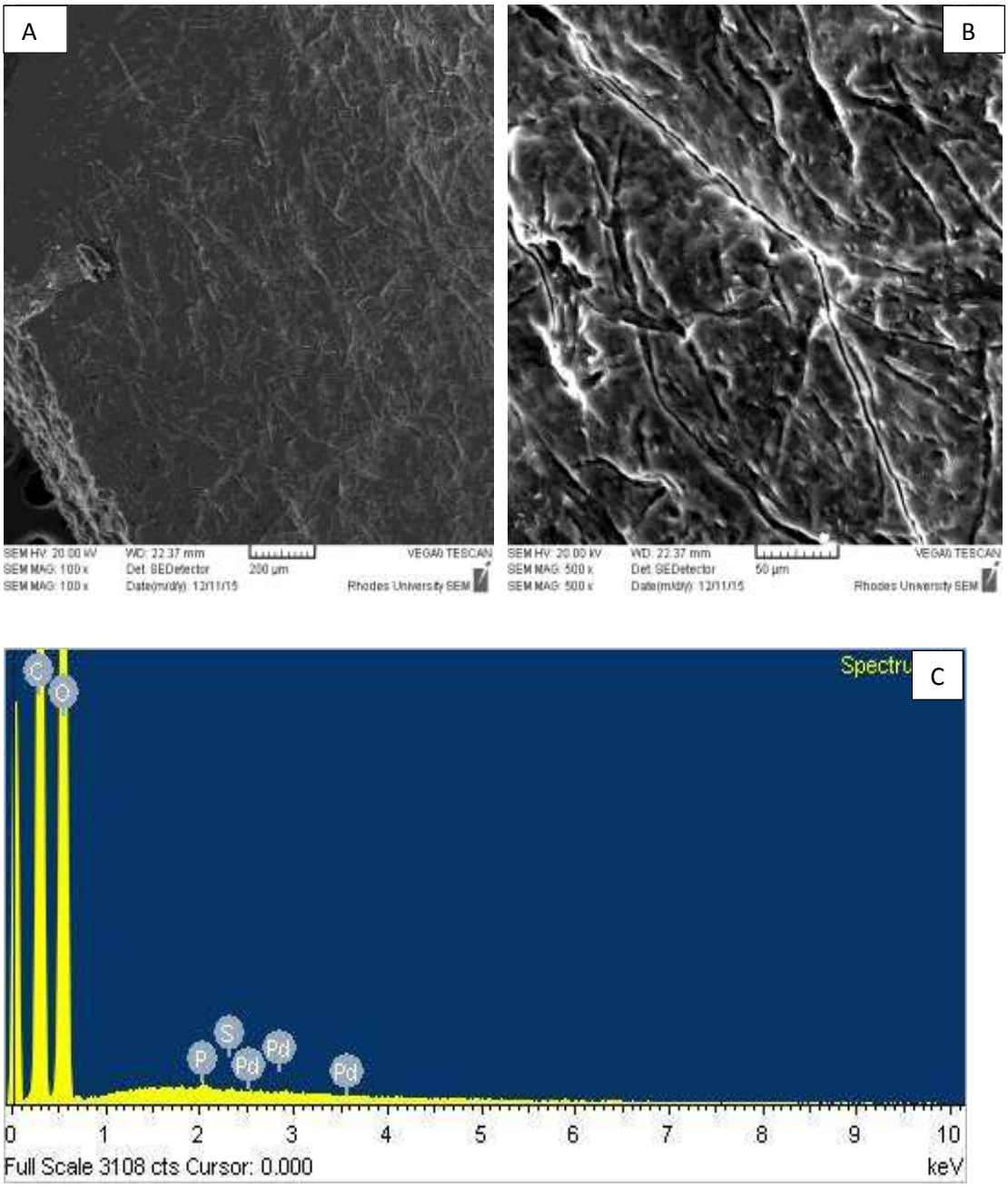

Figure 4.23: (A) and (B) are SEM images of PdS3/potato starch nanocomposites. (C) EDS spectrum of the nanocomposites

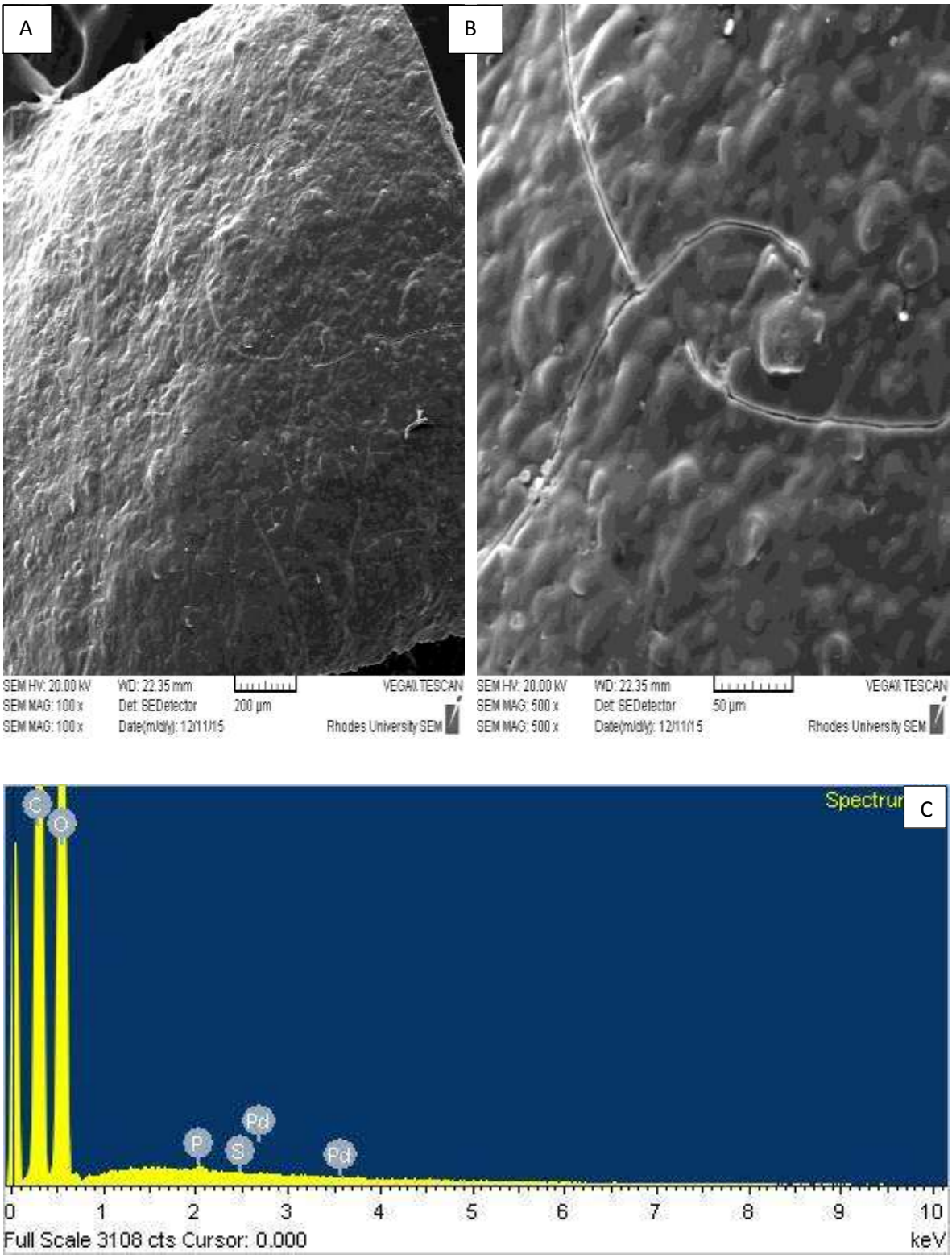

Figure 4.24: (A) and (B) are SEM images of PdS4/potato starch nanocomposites. (C) is the EDS spectrum of the nanocomposites

4.6.3 FTIR spectra studies of NiS and PdS/starch nanocomposites

The FTIR spectra of all NiS/potato starch nanocomposites and potato starch are identical due to the metal sulfide nanoparticles present in the pores of the starch networks without disturbing the network of the starch [36, 38]. The peaks observed in the starch are also observed in the nanocomposites but they are more intens, which might be due to the coordination of the nanocomposites with the polymer (potato starch). The absence of Ni-S vibration in the range of 250-500 cm^{-1} is due to the extent of the measurement used starting from 500-3500 cm^{-1}. Around 800 cm^{-1} there are deformation vibration peaks which are due to bending vibration of C-H [37].

The FTIR spectrum of PdS/potato starch nanocomposite shows impurities that might be due to the precursor used in the synthesis of PdS/potato starch nanocomposites. The broad peak at 3200 cm^{-1} can be ascribed to H_2O in the nanocomposites. Peaks around 1300 cm^{-1} are due to O-H deformation and C-C stretching of the ring. At 1000 cm^{-1} there is a sharp peak which can be attributed to O-C, C-C, and C-O deformations [38]. Around 1100 cm^{-1} there is a peak of C-O-C and C-C stretching. The peak around 2900 cm^{-1} is small in the starch, but in the spectrum of nanocomposites it is prominent because of the coordination of starch with nanoparticles [39].

References

1. Zainala, N.A.; Shukor, S.R.A.; Wabb, H.A.A.; Razak, K.A. Study on the effect of synthesis parameters of silica nanoparticles entrapped with rifampicin. *Chem*. *Eng*. *Trans*. **2013**, 32, 2245-2250.

2. Tack Ng, M.; Boothroyd, C.; Vittal, J.J. Shape and size control of Ag_2Se nanocrystals from a single source precursor $[(Ph_3P)_3Ag_2(Se\{O\}Ph_2)]$.

3. Singhal, A.; Dutta, D. P.; Tyagi, A. K.; Mobin, S. M.; Muthur, P.; Lieberwith, I. Palladium(II)/ allypalladium(II) complexes with xanthate ligands: Single source precursors for the generation of palladium sulfide nanocrystals. *J*. *Organomet*. *Chem*. **2007**,692, 5285-5294.

4. Wang, W.M.; Sun, Z.X.; Hao, W.; Su, D.W.; Vaughan, D.J. Synthesis of size tuneable cadmium sulfide nanoparticles from single source precursor using ammonia as solvent. *Mater*. *Res*. *Bullet*. **2011**, 46, 2266-2270.

5. Cumberland, S.L.; Hanif, K.M.; Javier, A.; Khitrovig, A.; Strouse, G.F.; Woessner, S.M.; Yun, C.S. Inorganic cluster as single source precursors for preparation of CdSe, ZnSe, and CdSe/ZnS nanomaterials. *Chem*. *Mater*. **2002**, 14, 1576-1584.

6. Satyendra, N. Shukla, S.N.; Gaur, P.; Rai, N. Complexes of tetraethylthiuram disulfide with group 12 metals: Single-source precursor in metal sulfide nanoparticles' synthesis. *Appl*. *Nanosci*. **2015**, 5, 583–593.

7. Yang, Z.; Smetana, A. B.; Sorensen, C. M.; Klabunde, K. J. Synthesis and characterization of a new tiara Pd(II) thiolate complex $[Pd(SC_{12}H_{25})_2]_6$, and its solution-phase thermolysis to prepare nearly monodispersed palladium sulfide nanoparticle. *Inorg*. *Chem*. **2007**, 46, 2427-2431.

8. Al-Rasoul, K.; Abbas, N.K.; Shanan, Z.J. Structural and optical characterization of Cu and Ni doped ZnS nanoparticles. *Int*. *J*. *Electrochem*. *Sci*. **2013**, 8, 5594-5604.

9. Zhao, O.; Samulski, E.T. A comparative study of poly(mthyl methacrylate) and polystyrene/clay nanocomposites prepared in supercritical carbon dioxide. *Polymers*, **2006**, 47, 663-671.

10. Abdo, M.M.; Elham, G.; Nayereh, S.; Mahmoud, W.M.Y.; Elias, S. Structural, optical and electrical properties of PVA/PANI/Nickel nanocomposites synthesized by gamma radio lytic method. *Polymers* **2014**, 6, 2435-2450

11. Banerjee, M.; Chongad, L.; Sharma, A. Structural and optical properties of pure and copper doped NiS nanoparticles. *Res*. *J*. *Recent*. Sci. **2013**, 2, 326-329.

12. Sahiner, N.; Sel, K.; Meral, K.; Onganer, Y.; Butun, S.; Ozay, O.; Silan, C. Hydrogel template CdS quantum dots synthesis and their characterization. *Col*. *Surf*. *A*: *Physiochem*. *Eng*. *Aspects*. **2011**, 389, 6-11.

13. Languna, M.A.; Paillard, V.; Kohn, B.; Ehbrecht, M.; Huisken, F; Ledoux, G.; Papoular, R.; Hofmeister, H. Optical properties of nanocrystalline silicon thin films produced by size-selected cluster beam deposition. *J*. *Lumin*. **1999**, 80, 223-228.

14. Pouretedal, H.R.; Momenzadeh, Synthesis, characterization and study of photocatalytic activity of nanocomposites of oxides and sulphides of Ni(II) and Ni(III). *Bulgar*. *Chem*. *Commun*. **2015**, 11, 59-65.

15. Yang, Z.; Smetana, B. A.; Sorensen, C, M.; Klabunde, K.J. Synthesis and characterization of a new tiara Pd(II) thiolate complex $[Pd(C_{12}H_{25})_2]_6$; and its solution-phase thermolysis to prepare nearly monodispersed palladium sulfide nanoparticles. *Inorg*. *Chem*. **2007**, 46, 2427-2431.

16. Fazli, Y.; Pourmortazavi, S.M.; Kohsari, I.; Sadeghpur, M. Electrochemical synthesis and structure characterization of nickel sulfide nanoparticles. *Mat*. *Sci*. *Semi*. *Process*, **2014**, 27, 362-367.

17. Torkes-Nieto, J.; Arevalo, A.; Garcia, J.J. Catalytic desulfurization of dibenzothiophene with palladium nanoparticles. *Inorg*. *Chem*. **2008**, 47, 11429-11434.

18. Kumara, K.S.; Divyaa, A.; Reddya, P.S.; Uthannaa, S.; Martinsb, R.; Elangovanb, E. Structural and Optical Behaviour of Ni Doped CdS Nanoparticles Synthesized by Chemical Co-Precipitation Method. *Acta Physica Polonica* A, **2011**, 120, 52-54.

19. Wang, S.; An, C.; Yuan, J. Synthetic fabrication of nanoscale MoS_2-based transition metal sulfide. *Materials*, **2010**, 3, 401-433.

20. Salavati-Niasari, M.; Davar, F.; Emadi, H. Hierarchical nanostructured nickel sulfide architectures through simple hydrothermal method in the presence of thioglycolic acid. *Chalcog*. *Lett*. **2010**. 7(12), 647-655.

21. Dey, S.; Jain, V.K.; Platinum group metal chalcogenides: Their synthesis and application in catalysis and materials science. *Plat*. *Met*. *Rev*. **2004**, 48(1), 16-29.

22. O'Brien, P.; Waters, P. Deposition of Ni and Pd sulfide thin films via aerosol-assisted CVD. *Chem*. *Vap*. *Deposition*. **2006**, 12, 620-626.

23. Boey, H.T.; Tan, W.L.; Abu Bakar, N.H.H.; Abu Bakar, M.; Ismail, J. Formation and morphology of colloidal chitosan-stabilized copper sulphides. *J*. *Phys*. *Sci*. **2007**, 18(1), 87–101.

24. Masala, O.; Seshadri, R. Synthesis routes for large volumes of nanoparticles. *Annu*. *Rev*. *Mater*. *Res*. **2004**, 34, 41–81.

25. Tong, M.C.; Chen, W.; Sun, J.; Ghosh, D.; Chen, S. Dithiocarbamate-Capped Silver Nanoparticles. *J. Phys. Chem.* B. **2006**, 110, 19238-19242.

26. Morsy, S.M.I. Role of surfactants in nanotechnology and their applications. *Int. J. Curr. Microbiol. App. Sci* **2014**, 3(5), 237-260.

27. Sartale, S.D.; Lokhande, C.D. Preparation and characterization of nickel sulfide thin films using successive ionic layer adsorption and reaction (SILAR) method. *Mat. Chem. Phys.* **2001**, 72, 101-104.

28. Vickers, M.S.; Beer, P.D.; Cookson, J.; Bishop, P.J.; Thiebaut, B. Dithiocarbamate ligand stabilised gold nanoparticles. *J. Mater. Chem.* **2006**, 16, 209-215.

29. Alonso, F.; Riente, P.; Sirvent, J. A.; Yus, M. Nickel nanoparticles in hydrogen-transfer reductions: Characterization and nature of the catalyst. *Appl. Catal.* A: Gen **2010**. APCATA-12428; No. of Pages 10.

30. Jeon, Y.; Baek, J. Nanocomposites derived from polymers and inorganic nanoparticles. *Materials*, **2010**, 3, 3654-3674.

31. Osorio, M.A.; Restrepo, D.; Velásquez-Cock, J.A.; Zuluaga, R.O.; Montoya, U.; Rojas, O.; Gañán, P.F.; Marind, D.; Castro, C.I. Synthesis of thermoplastic starch-bacterial cellulose nanocomposites via in situ fermentation. *J. Braz. Chem. Soc.* **2014**, 25 (9), 1607-1613.

32. Srithongkham, S.; Vivitchanont, L.; Krongtaew, C. Starch/cellulose biocomposites prepared by high-shear homogenization/compression moulding. *J. Mat. Sci. Engineer. B*, **2012**, 2 (4), 213-22.

33. Prakobna, K.; Galland, S.; Berglund, L.A. High-performance and moisture-stable cellulose−starch nanocomposites based on bioinspired core−shell nanofibers. *J. Amer. Chem. Soc.* **2015**, 16, 904−912.

34. Kamellia, N.; Rezvanh, Z. Preparation and magnetic properties of nano size nickel ferrite particles using hydrothermal method, *Chem*. *Centr*. *J*. **2012**, 6-23.

35. Ganachari, S.V.; Bhat, R.; Deshpande, R.; Venkataraman, A. Synthesis and characterization of nickel oxide nanoparticles by self-propagation low temperature combustion method. *Rec*. *Res*. *Sci*. *Tech*, **2012**, 4(4), 50-53.

36. Hou, Y.; Kondoh, H.; Ohta, T.; Gao, S. Size-controlled synthesis of nickel nanoparticles. *Appl*. *Surf*. *Sci*. **2005**, 241, 218-222.

37. Salavati-Niasari, M.; Davar, F.; Emadi, H. Hierarchical nanostructured nickel sulfide architectures through simple hydrothermal method in the presence of thioglycolic acid. 2010, 7(12), 647-655.

38. Osorio, M.A.; Restrepo, D.; Velásquez-Cock, J.A.; Zuluaga, R.O.; Ursula Montoya, U.; Rojas, O.; Gañán, P.F.; Marind, D.; Castroe, C.I. Synthesis of thermoplastic starch-Bacterial cellulose nanocomposites via in situ fermentation. J. Braz. Chem. Soc.2014, 25(9), 1607-1613.

39. Gipson, K.; Stevens, K.; Brown, P.; Ballato, J. Infrared spectroscopic characterization of photo luminescent polymer nanocomposites. Journal of Spectroscopy Volume 2015, Article ID 489162, 9 pages

CHAPTER FIVE

5.0 SUMMARY OF RESULTS, CONCLUSIONS AND RECOMMENDATIONS

5.1 Summary of results

In this study, Ni(II) and Pd(II) dithiocarbamate complexes were synthesized and characterized by elemental analysis and spectroscopic techniques. The compounds were used as single source precursors for the synthesis of NiS and PdS nanoparticles and metal sulfide starch nanocomposites. The introduction of the study in chapter one focuses on nanomaterial, properties of nanoparticles that make them useful in different areas such as data storage, antibacterial agent, and catalysis among others. The chapter also contained a brief introduction on methods used to synthesize nanoparticles with emphasis on single source precursor method and lastly, dithiocarbamates and metal complexes of dithiocarbamates. Chapter two contains detailed experimental procedures, the synthesis of dithiocarbamate ligands and their corresponding complexes. Analytical and spectroscopic techniques used to characterize all synthesised ligands and complexes. The techniques include: UV-Vis spectroscopy (UV), Elemental analysis, Fourier Transform Infrared spectroscopy (FTIR) and Nuclear Magnetic Resonance spectroscopy (NMR). The complexes were obtained in powder form and are air and moisture stable at room temperature with the yield ranging from 44-67%.

The physicochemical and spectroscopic studies of the dithiocarbamates ligands and corresponding Ni(II) and Pd(II) complexes were presented in Chapter three. Electronic spectra studies showed that the complexes are all 4-coordinate square planar geometry. The Ni(II) complexes shows d-d transitions confirming the proposed square planar geometry and Pd(II) complexes shows strong metal to ligand charge transfer transitions. The FTIR spectra

studies confirmed the coordination of the dithiocarbamate ligands with the metal ions. The νNi-S stretching vibration was observed in the region 375-543 cm^{-1} and νPd-S stretching vibrations in the range 529-545 cm^{-1}. From the FTIR spectra studies, the υ(C-S) stretching vibrations that appeared as two peaks in ligands shifted to single sharp bands in the metal complexes. This thus confirmed that the dithiocarbamate acted as bidentate chelating ligands through the sulfur atoms. The dithiocarbamate ligands and the Pd(II) complexes were further characterized using ^{1}H-NMR spectroscopy. The results further confirm the coordination of the ligands to the Pd^{2+} ion.

The metal complexes were used as single source precursors and thermolysed in hexadecylamine (HDA) at 220 °C to prepare four HDA-capped NiS and four HDA-capped PdS nanoparticles. The as-prepared NiS and PdS nanoparticles were further dispersed in potato starch to prepare NiS/potato starch and PdS/potato starch nanocomposites. The optical properties of the nanoparticles were studied using electronic absorption and emission spectroscopy. Powder X-ray diffraction, transmission electron microscopy, scanning electron microscopy and energy dispersive X-ray spectroscopy were used to examine the structural properties of the as-prepared nanoparticles. The results showed that the absorption spectra of the NiS and PdS nanoparticles are blue shifted compared to their corresponding bulk materials indicating that the nanoparticles are quantum confined due to their small crystallite sizes while the photoluminescence spectra show narrow emissions that are red-shifted.

The XRD patterns confirmed the formation of cubic and rhombohedral phase for NiS nanoparticles and cubic phase for PdS nanoparticles. The TEM images indicates that the individual NiS nanoparticles are almost nearly spherical in shape with crystallite sizes of 12-

38 nm for **NiS1**, 8-11 nm for **NiS2**, 9-16 nm for **NiS3** and 5.11-11.66 nm for **NiS4** nanoparticles with some agglomeration. TEM images of PdS showed monodisperse nanocrystal with average crystallite sizes of 6.94-9.62 nm for **PdS1**, 4.94-6.52 for **PdS2**, 7-10.43 for **PdS3** and 10.65-14.20 nm for **PdS4** and the individual PdS nanocrystals are well separated without any agglomeration. The SEM images showed uniform surface morphology of NiS and PdS nanoparticles with different shapes, while EDS confirms the presence of Ni and S from the prepared HDA-capped NiS nanoparticles and Pd and S for HDA-capped PdS nanoparticles respectively. SEM images and EDS of the NiS/potato starch and PdS/potato starch nanocomposites confirmed the dispersion of the nanoparticles in starch matrices and their FTIR further confirms the formation of the nanocomposites.

5.2 Conclusions for the study

Four dithiocarbamate ligands were successfully synthesized and characterized by UV-Vis, FTIR, NMR and elemental analysis. Their corresponding N(II) and Pd(II) complexes were synthesised and characterized by analytical and spectroscopic techniques. The complexes were formulated as four coordinate square planar in which the dithiocarbamate act as bidentate chelating ligands. Electronic spectra studies confirm the proposed geometry. FTIR indicates the dithiocarbamate ligand act as chelating ligands. The splitting signals of ^{1}H-NMR for both ligands and palladium(II) complexes corresponded with the proposed structures, it can then be concluded that all compounds were truly synthesised.

Four NiS and four PdS nanoparticles have been successfully synthesised using the individual metal complexes as single source precursors at 220 °C. Absorption spectra showed that all prepared metal sulfide nanoparticles were blue shifted relative to the bulk with small sizes

and exhibit quantum confinement effects. PL spectra showed that metal sulfide nanoparticles were red shifted compared to the absorption band edges. XRD patterns reveal the crystallinity of particles varies. SEM showed close to spherical shape and EDS confirmed the presence of the metal sulfide nanoparticles. TEM images showed spherical and close to spherical shapes with uniform and narrow size distributions. SEM images and EDS of polymer nanocomposites showed that there were small NiS and PdS nanoparticles dispersed in the matrices of the potato starch.

5.3 Recommendations and suggestions for future studies

In this study, several attempts to grow single crystals suitable for X-ray crystallography have been unsuccessful. There is the need to grow crystals of the metal complexes to ultimately confirm their coordination geometry. The future direction of this research work is to be able to use the metal sulfide nanoparticles and polymer nanocomposites in catalysis. There is need to study the effect of temperature, effect of precursor concentrations, effect of time and the effect of capping agents on the crystallite sizes of the nanoparticles. This will enable the researcher to determine the optimum condition necessary for the synthesis of the nanoparticles to give monodisperse nanoparticles with small crystallite sizes or quantum dots that might lead to better catalysts that can be used in catalysis reactions for industrial transformation.

This is necessary because it has been established that changing the reaction condition in the course of nanoparticles synthesis using single source precursor methods occurred through two possible mechanisms. It could be a growth dominated route or a nucleation driven process that produces nanoparticles whose sizes are temperature dependent. Thus, there is a

need to carry out thermolysis in at least three different temperatures. Even though the thermolysis is carried out for one hour, there is a need to monitor the growth of the nanoparticles every 15 minutes by taken samples and checking their electronic absorption and emission in order to establish the optimum time necessary to get the required crystallite size for the nanoparticles.

It is also necessary to explore the use of other carriers for the nanoparticles such as dendrimers. This might result in getting nanoparticles that have large surface area with small particle sizes which can be used in hydrogenation catalysis or alkene polymerization. In the synthesis of polymer nanocomposites, different polymers from synthetic to natural polymers should be consider for further studies. This might give insights into the best polymer for the potential catalytic applications. The %w of nanoparticles to be impregnated on the matrix of polymer should vary at 0-5 intervals to prevent agglomeration and to give better results of SEM/EDS.

APPENDIX

AC1	FTIR spectrum of NiS1/potato starch nanocomposites
AC2	FTIR spectrum of NiS2/potato starch nanocomposites
AC3	FTIR spectrum of NiS3/potato starch nanocomposites
AC4	FTIR spectrum of NiS4/potato starch nanocomposites
AC5	FTIR spectrum of PdS1/potato starch nanocomposites
AC6	FTIR spectrum of PdS2/potato starch nanocomposites
AC7	FTIR spectrum of PdS3/potato starch nanocomposites
AC8	FTIR spectrum of Pd4/potato starch nanocomposites
AC9	FTIR spectrum of potato starch
L^1	NMR spectrum of anisidine dithiocarbamate
L^2	NMR spectrum of dibenzyl dithiocarbamate
L^3	NMR spectrum of butyl dithiocarbamate
L^4	NMR spectrum of imidazolyl dithiocarbamate
$[Pd(L^1)_2]$	NMR spectrum of Pd(II) anisidine dithiocarbamate complex
$[Pd(L^2)_2]$	NMR spectrum of Pd(II) dibenzyl dithiocarbamate complex
$[Pd(L^3)_2]$	NMR spectrum of Pd(II) butyl dithiocarbamate complex
$[Pd(L^4)_2]$	NMR spectrum of Pd(II) imidazolyl dithiocarbamate complex

L^1

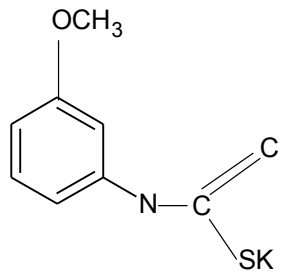

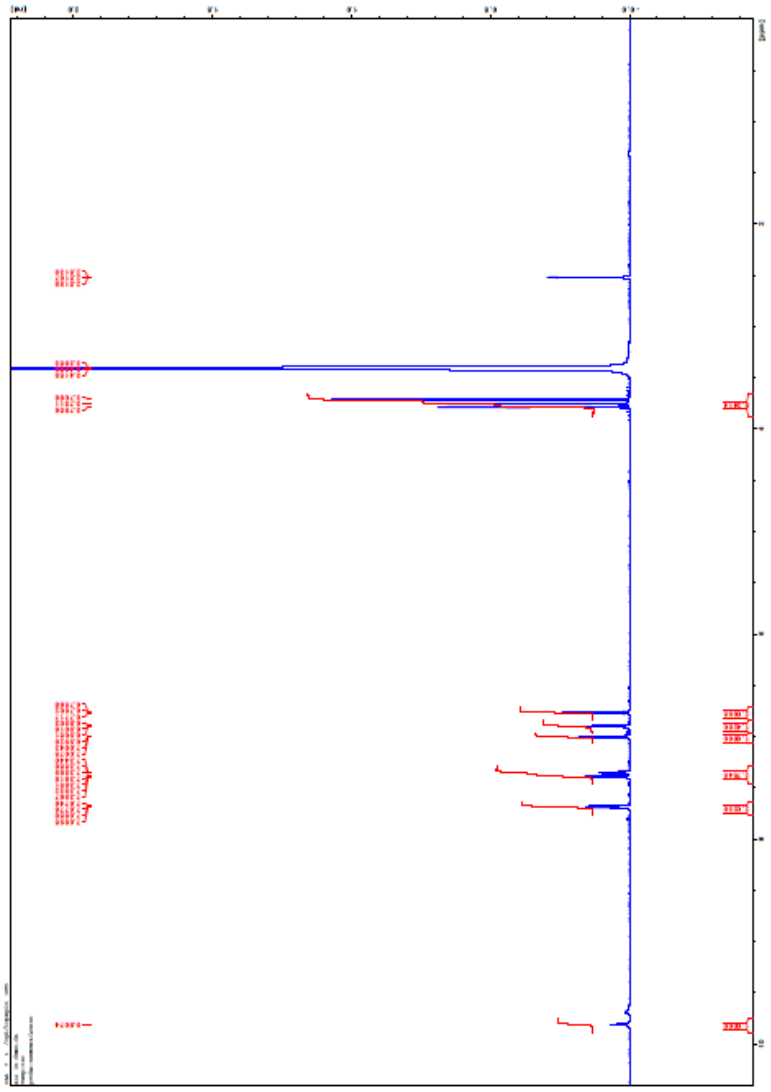

L^2

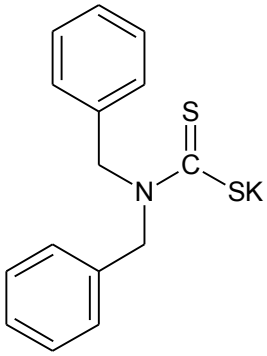

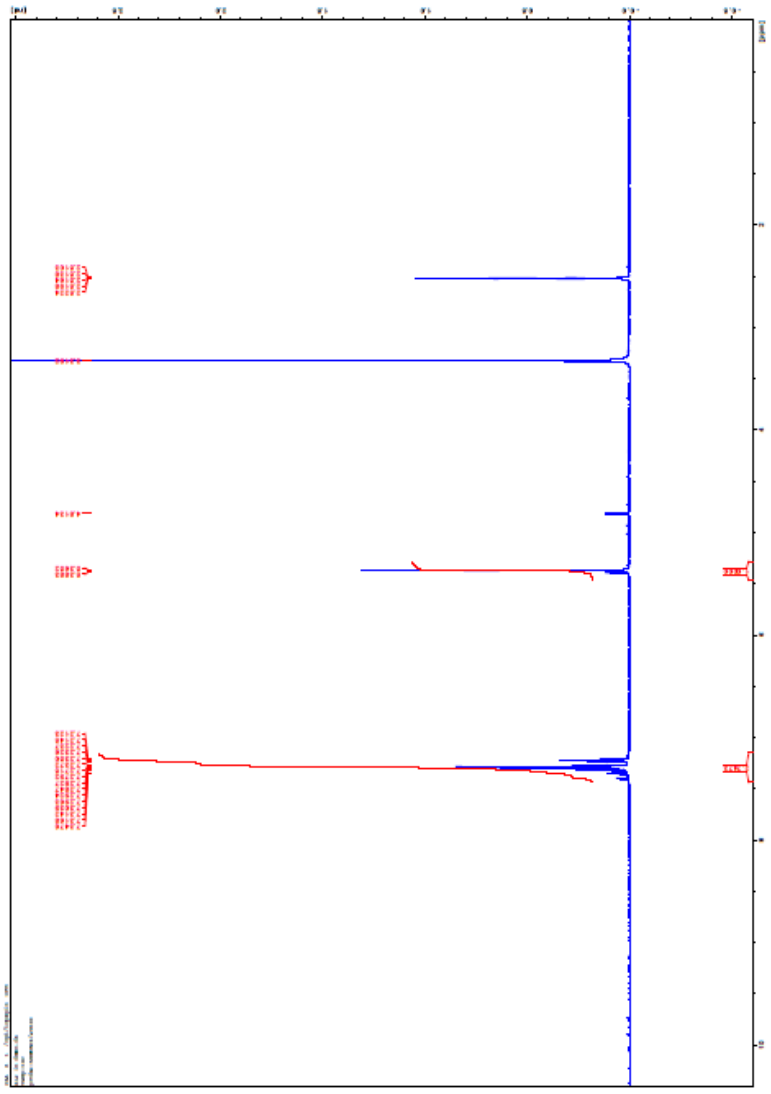

L^3

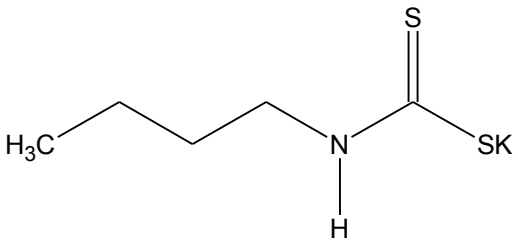

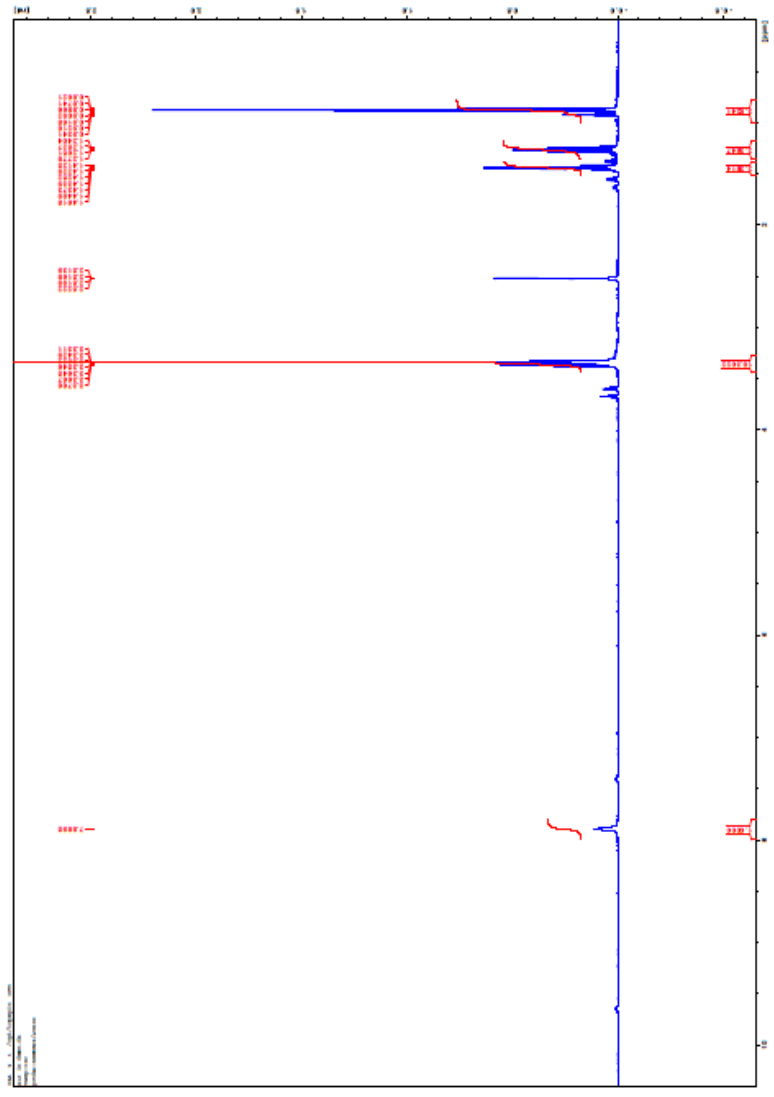

L^4

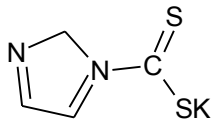

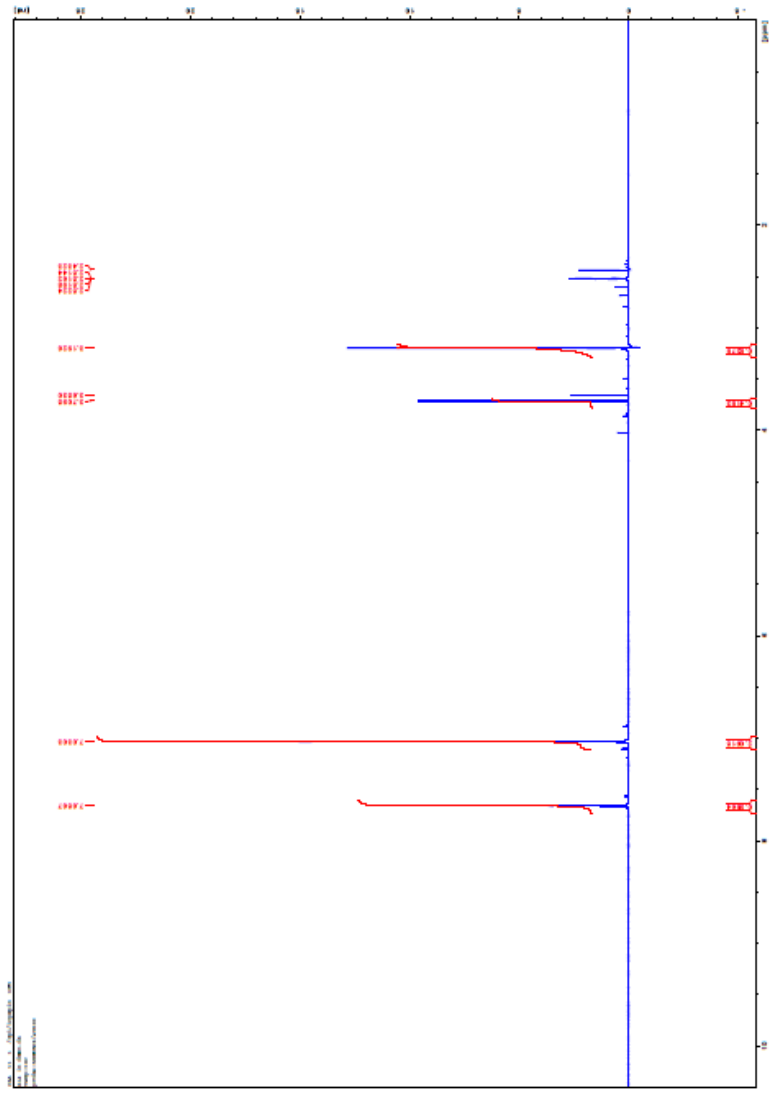

$[Pd(L^1)_2]$

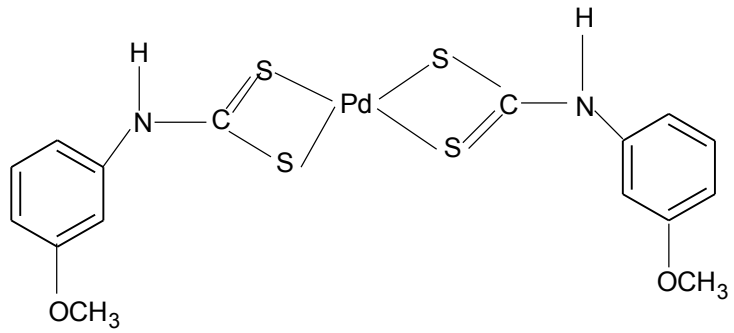

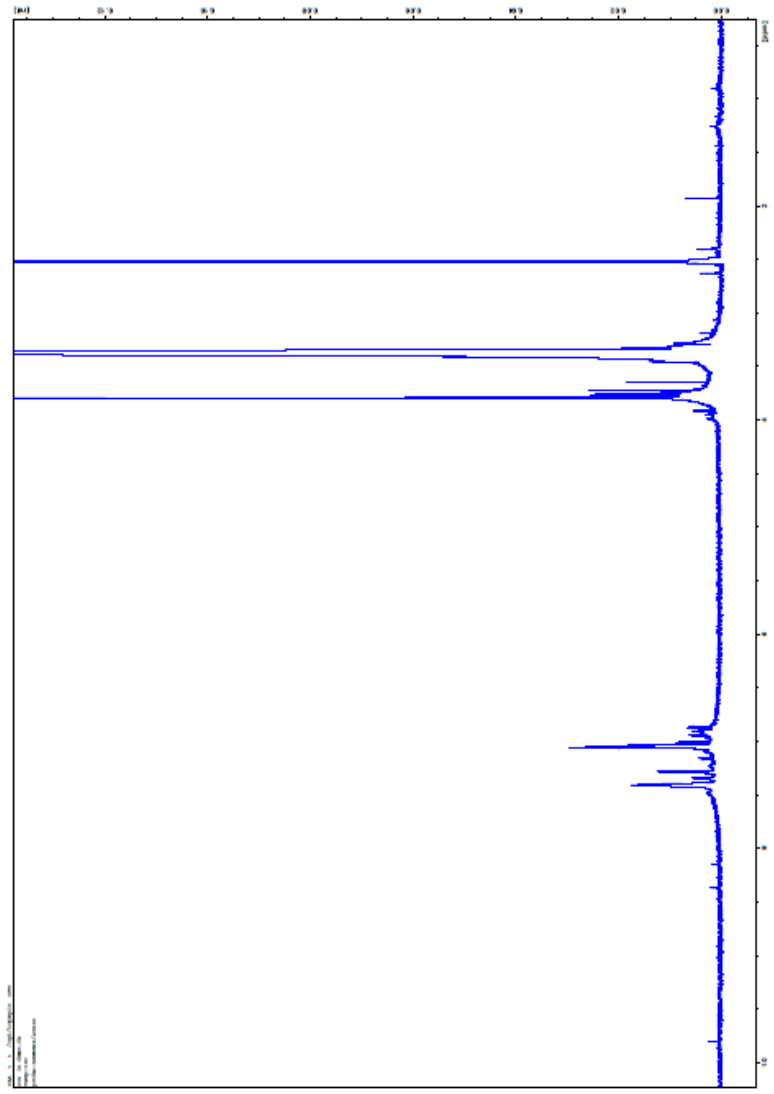

$[Pd(L^2)_2]$

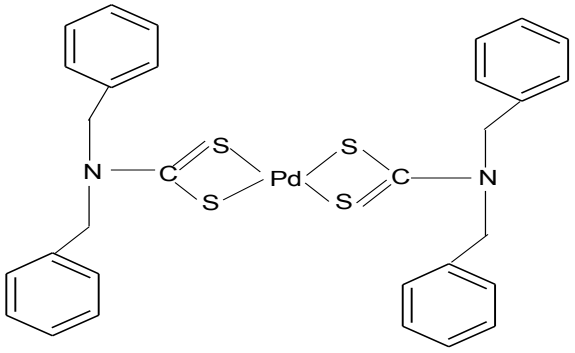

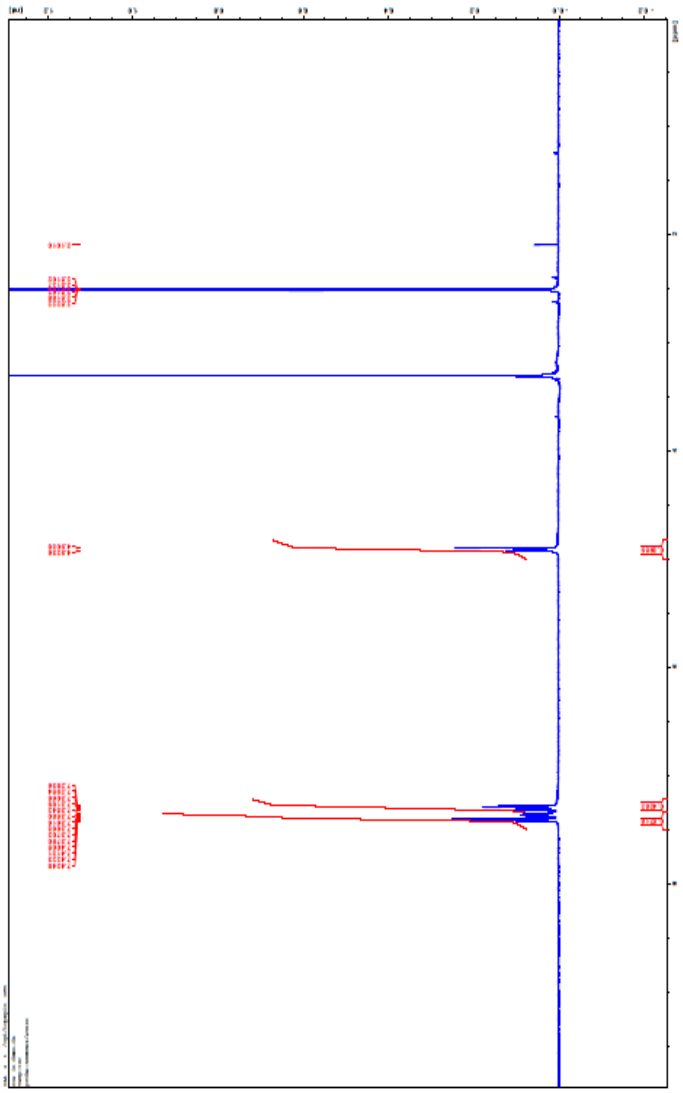

$[Pd(L^3)_2]$

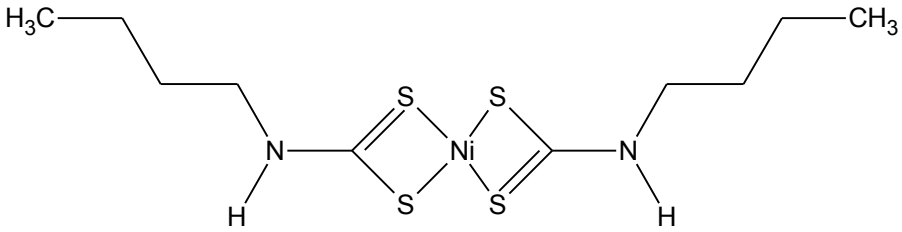

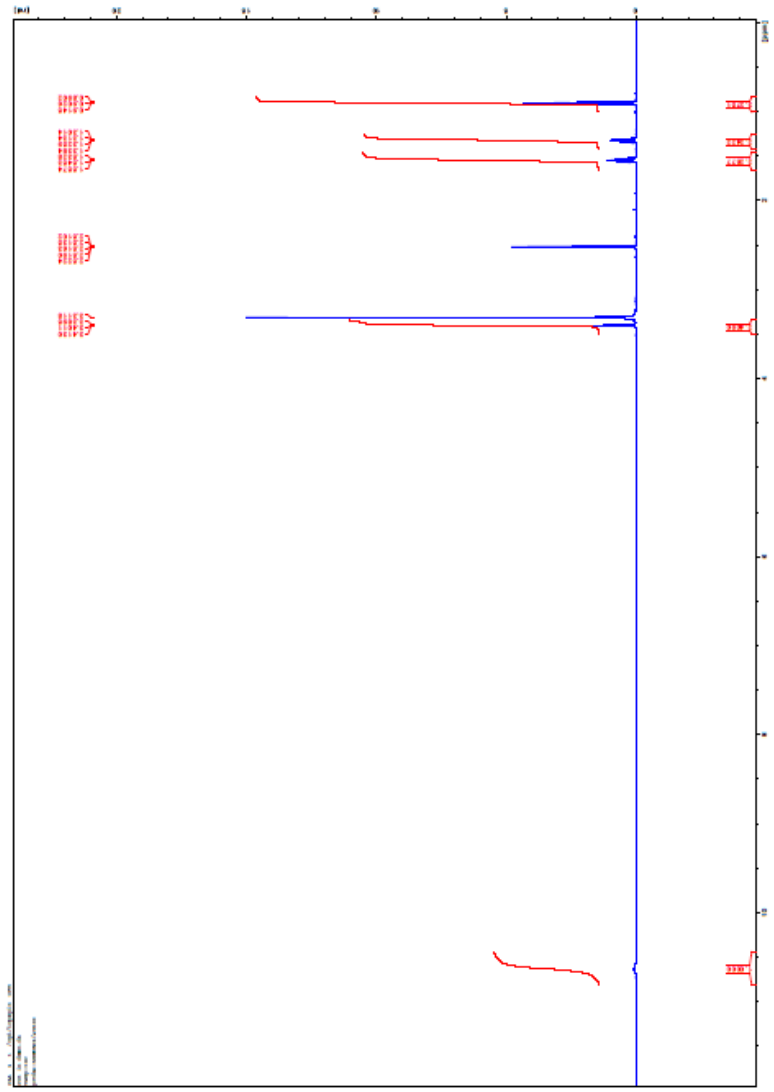

$[Pd(L^4)_2]$